Appendix for
A New Approach to Identifying the Real Effects of Uncertainty Shocks

This version: May 6, 2018

There are five sections in this appendix.

- Section A details how we compute the posterior distributions of the impulse response functions.
- Section B describes the algorithms to compute the impulse response functions.
- Section C discusses further empirical results from our two models in the empirical section.
- Section D describes an event study exercise detailing the relationship between financial uncertainty and the macroeconomy and also describes theoretical and empirical exercises that support our spread identification assumption in the main text.
- Section E discusses an exercise using our sign restrictions methodology on data simulated from a DSGE model.

A Posterior distribution of IRFs

In this section, we describe how to obtain quantities that are reported in our empirical exercises. Our inference is based on the following posterior distribution for ψ and Q,

$$P(\psi, Q|Y) \propto p(Y|\psi)p(\psi)1\{\psi \in \mathbb{P}(\mathcal{R})\}p(Q|\psi) \tag{A.1}$$

where the first approach (Full Bayesian approach) assumes that the prior for Q is conditionally flat on $\mathbb{Q}(\psi, \mathcal{R})$, which is the admissible set for Q at the parameter ψ and sign restrictions $\mathcal{R}$. The second approach considers a set of all proper prior distributions for Q on $\mathbb{Q}(\psi, \mathcal{R})$.

The marginal prior distribution for ψ is specified as

$$\widetilde{p}(\psi) = \frac{1}{vol(\mathbb{P}(\mathcal{R}))}1\{\psi \in \mathbb{P}(\mathcal{R})\}p(\psi), \quad vol(\mathbb{P}(\mathcal{R})) = \int_{\{\psi: p(\psi)>0\}} 1\{\psi \in \mathbb{P}(\mathcal{R})\}p(\psi)d\psi \tag{A.2}$$

where the initial proper prior distribution for ψ, $p(\psi)$, is truncated to the region $\mathbb{P}(\mathcal{R})$, which is the set of ψ that $\mathbb{Q}(\psi, \mathcal{R})$ is non-empty. The choice of $p(\psi)$ is model and application specific. So, we leave the discussion about the prior distribution for ψ to section C.1.3 in this appendix for the CAIW model and section C.2.1 for the model of Carriero et al. (2017).

A.1 Fully Bayesian approach with a flat prior

Let $IRF(Q, \psi)$ be a collection of $IRF(y_{i,t+s}|v_t^* = e_j, Q, \psi)$ for all $i = 1, 2, ..., k$, $j = 1, 2, ..., J$, and $J < k$, and $s = 0, 1, ..., S$. We approximate the posterior moments of IRFs using the following steps

Posterior sampling for IRFs with a flat prior (Uhlig, 2005)

1. Generate $\psi^{(m_1)}$ from $p(\psi|Y)$ for $m_1 = 1, 2, ..., M_1$ and store them.

2. For each $m_1 = 1, 2, ..., M_1$, iterate the following steps for $m_2 = 1, 2, ...M_2$:

   (a) Generate Q^* uniformly from $\mathcal{O}(k)$.

   (b) Compute $IRF(Q^*, \psi^{(m_1)})$.

   (c) Set $IRF(Q^{(m_2,m_1)}, \psi^{(m_1)}) = IRF(Q^*, \psi^{(m_1)})$ and store it if $Q^* \in \mathbb{Q}(\psi, \mathcal{R})$.

After this algorithm, we have posterior draws of $IRF(\psi^{(m)}, Q^{(m)})$ for $m = 1, 2, ..., M$.[1]

The algorithm is based on the following decomposition

$$p(\psi, Q|Y) = \underbrace{p(Q|\psi)1\{\psi \in \mathbb{P}(\mathcal{R})\}/vol(\mathbb{P}(\mathcal{R}))}_{\text{step 2}} \times \underbrace{p(Y|\psi)p(\psi)/P(Y)}_{\text{step 1,} \equiv p(\psi|Y)} \tag{A.3}$$

The first step is to generate ψ from its posterior distribution with non-truncated prior distribution and it is model specific. In our empirical exercises, we use the particle Gibbs sampler. The second step aims to generate draws from $Q^{(m_2,m_1)}$ from $p\left(Q|\psi^{(m_1)}\right)$ using the reject/accept sampling. Step 2-(a) can be done by QR algorithm of Rubio-Ramirez et al. (2010). Step 2-(b) is done by simulation-based approximation (Section B.1 in this appendix). Step 2-(c) is simply to check whether $IRF(\psi^{(m_1)}, Q^*)$ satisfies the sign restrictions.

We present posterior moments of interest such as pointwise median and quantiles for each s-step-ahead horizon response of the ith variable to the jth uncertainty shock.

Point estimator. We report measures of central tendency using the pointwise posterior median as well as the median target method of Fry and Pagan (2007). For the median target method, we first compute the posterior median for each s-step-ahead horizon response of the ith variable to the jth uncertainty shock. Then, we report the impulse response function that is the most closest to this pointwise median among $\{IRF(\psi^{(m_1)}, Q^{(m_2,m_1)}) : \text{for all } m_1, m_2\}$

[1] For notational convenience, we re-index posterior samples so that we transform $(m_1, (m_1, m_2))$ into (m). Then, M is the number of kept $IRFs$ from this algorithm.

in L_2 norm. That is, for each variable (i) and shock of interest (j), we find m_1 and m_2 that minimize the following:

$$\sum_{s=0}^{S} \left(IRF(y_{i,t+s}|v_t^* = e_j, Q^{(m_2,m_1)}, \psi^{(m_1)}) - \widehat{IRF(y)} \right)^2. \tag{A.4}$$

In this way, we preserve the dynamics in IRF over the horizons, which is potentially missing in the pointwise posterior medians. In our application, reported point estimates and pointwise posterior medians are very close to each other (see section C.1.9).

Interval estimator. We report pointwise equal-tailed $\alpha\%$ credible regions for the IRFs. We approximate upper and lower quantiles based on the posterior draws from the above algorithm.

A.2 Robust Bayesian approach

In the empirical illustration, we compute and robust credible sets and the robust posterior mean bounds for sign-restricted IRFs based on the following algorithm:

Posterior sampling for IRFs (Algorithm 4.1 of Giacomini and Kitagawa, 2015)

1. Generate $\psi^{(m_1)}$ from $p(\psi|Y)$ for $m_1 = 1, 2, ..., M_1$ and store them.
2. For each $m_1 = 1, 2, ..., M_1$, iterate the following steps for M_2 times:
   (a) Generate Q^* uniformly from $\mathcal{O}(k)$.
   (b) Compute $IRF(\psi^{(m_1)}, Q^*)$.
   (c) Set $IRF(Q^{(m_2^{(m_1)},m_1)}, \psi^{(m_1)}) = IRF(Q^*, \psi^{(m_1)})$ and store it if $Q^* \in \mathbb{Q}(\psi, \mathcal{R})$. Increase $m_2^{(m_1)}$ by 1.

3. Approximate pointwise lower and upper bound of s-period-ahead impulse response of ith variable to jth shock at m_1th draw by

$$\begin{aligned} l^{(m_1)}(i,j,s) &= \min_{m\in\{1,2,\ldots,m_2^{(m_1)}\}} IRF(y_{i,t+s}|v_t^* = e_j, Q^{(m,m_1)}, \psi^{(m_1)}) \\ u^{(m_1)}(i,j,s) &= \max_{m\in\{1,2,\ldots,m_2^{(m_1)}\}} IRF(y_{i,t+s}|v_t^* = e_j, Q^{(m,m_1)}, \psi^{(m_1)}). \end{aligned} \tag{A.5}$$

4. Posterior mean bound for s-period-ahead impulse response of the ith variable to the jth shock is approximated by

$$\left(\frac{1}{M_1}\sum_{m_1=1}^{M_1} l^{(m_1)}(i,j,s),\ \frac{1}{M_1}\sum_{m_1=1}^{M_1} u^{(m_1)}(i,j,s)\right) \tag{A.6}$$

5. α%-robustified credible interval for the s-period-ahead impulse response of ith variable to jth shock is approximated by $[r_\alpha^* - \hat{z}_\alpha(r_\alpha^*),\ r_\alpha^* + \hat{z}_\alpha(r_\alpha^*)]$ with $r_\alpha^* \in \arg\min_r \hat{z}_\alpha(r)$ where $\hat{z}_\alpha(r)$ is the sample αth quantile of $\max\{|r - l^{(m_1)}(i,j,s)|, |r - u^{(m_1)}(i,j,s)|\}$.

This is based on Giacomini and Kitagawa (2015). A more efficient implementation is possible for these objects with a class of linear VAR models (Amir-Ahmadi and Drautzburg, 2017).

B Computation of IRFs

In this section, we describe steps to compute the impulse response functions of various objects to uncertainty shocks. The first part of this section works with the general form of the model (equations 1, 2, and 3). Then, we discuss cases in which the stated algorithm is simplified.

B.1 General algorithm

We define the impulse response functions as

$$IRF[y_{i,t+s}; v_t^* = e_j, Q, \psi] = E[y_{i,t+s}|v_t^* = e_j; R_t, \psi] - E[y_{i,t+s}|v_t^* = 0; R_t, \psi] \tag{A.7}$$

where $R_t = chol(\Omega(w_{t-1}; \omega))Q$. We explicitly state the dependency of Q.

Here is the steps to approximate IRFs using the right-hand-side term in the above equation given R_t and ψ.

Algorithm to compute IRFs. Set $m = 1$ (m is the index of the simulation number, with total simulations as M) and follow steps below.

1. Consider one standard deviation increase of an element in v_t^*

$$v_t^{*,1} = e_j \quad \text{versus} \quad v_t^{*,0} = 0_{k\times 1} \tag{A.8}$$

   where e_j is a $k \times 1$ column vector with a 1 in the jth element and zeros elsewhere and $0_{k\times 1}$ is a vector of zeros.

2. Form reduced-form shocks in the initial period v_t^1 and v_t^0. Note that as the jth shock is operative, only the jth column of R_t must be identified.

$$v_t^1 = R_t e_j \quad \text{versus} \quad v_t^0 = 0_{k\times 1}. \tag{A.9}$$

3. Simulate two volatility and observable paths indexed by (m), using equations 1, 2, and 3, conditional on R_t and ψ,

$$\{h_\tau^{(m)}(v_\tau^1)\}_{\tau=t,t+1,\ldots,t+s} \quad \text{versus} \quad \{h_\tau^{(m)}(v_\tau^0)\}_{\tau=t,t+1,\ldots,t+s}, \tag{A.10}$$

and

$$\{\Sigma_\tau^{(m)}(v_\tau^1)\}_{\tau=t,t+1,\ldots,t+s} \quad \text{versus} \quad \{\Sigma_\tau^{(m)}(v_\tau^0)\}_{\tau=t,t+1,\ldots,t+s}. \tag{A.11}$$

and

$$\{y_\tau^{(m)}(v_\tau^1)\}_{\tau=t,t+1,\ldots,t+s} \quad \text{versus} \quad \{y_\tau^{(m)}(v_\tau^0)\}_{\tau=t,t+1,\ldots,t+s}. \tag{A.12}$$

Go to step 4 with $m = m + 1$ if $m < M$; otherwise go to step 4.

4. Form $(\tau - t)$-horizon impulse response of ith variable to jth uncertainty shock by integrating out simulated shocks, $\{v_\tau, \epsilon_\tau\}_{\tau=t+1,t+2,\ldots,s}$ and ϵ_t,

$$\begin{aligned}
IRF[y_{i,\tau-t}; v_t^* = e_j, Q, \psi] &= \frac{1}{M}\sum_{m=1}^{M} y_{i,\tau}^{(m)}(v_t^1) - \frac{1}{M}\sum_{m=1}^{M} y_{i,\tau}^{(m)}(v_t^0) \\
IRF_s[\Sigma_{ii,\tau-t}; v_t^* = e_j, Q, \psi] &= \frac{1}{M}\sum_{m=1}^{M} \Sigma_{ii,\tau}^{(m)}(v_t^1) - \frac{1}{M}\sum_{m=1}^{M} \Sigma_{ii,\tau}^{(m)}(v_t^0) \\
IRF_s[h_{i,\tau-t}; v_t^* = e_j, Q, \psi] &= \frac{1}{M}\sum_{m=1}^{M} h_{i,\tau}^{(m)}(v_t^1) - \frac{1}{M}\sum_{m=1}^{M} h_{i,\tau}^{(m)}(v_t^0)
\end{aligned} \tag{A.13}$$

and the impulse response of $(\tau - t + 1)$-step-ahead forecast error variance is computed as

$$\frac{1}{M}\sum_{m=1}^{M}\left(y_{i,\tau}(v_t^1) - \frac{1}{M}\sum_{m=1}^{M} y_{i,\tau}^{(m)}(v_t^1)\right)^2 - \frac{1}{M}\sum_{m=1}^{M}\left(y_{i,\tau}(v_t^0) - \frac{1}{M}\sum_{m=1}^{M} y_{i,\tau}^{(m)}(v_t^0)\right)^2. \tag{A.14}$$

B.2 Discussion

In its most general form, as is generally the case with nonlinear impulse response functions, the linear relationship between volatility shocks (v_t) and uncertainty shocks (v_t^*) are path dependent via $\Omega_t = \Omega(h_{t-1}, \omega)$, making the IRFs also path dependent. However, for many existing models in the form of equations 1, 2, 3, there is no path dependence. Moreover, if the model is specified in a way that object of interest is linear in v_t, then our definition of the IRFs coincides with the traditional IRFs, which does not require any stochastic simulation. Cholesky volatility specification in section 3.1 is such a case. The IRFs for h_t is then

$$IRF(h_{.,t+s}|v_t^* = e_j, Q, \psi) = \left(\prod_{\tau=0}^{s} \Phi^\tau\right) chol(\Omega)Q. \tag{A.15}$$

If we assume that $g^y(\Sigma_t) = f^{-1}(\Sigma_t; A) = h_t$ (as in our second application and Carriero et al. (2017) but with $B^h = 0$), then the first moment response function is

$$IRF(y_{.,t+s}|v_t^* = e_j, Q, \psi) = B^y \left(\prod_{\tau=0}^{s} \Phi^\tau\right) chol(\Omega)Q. \tag{A.16}$$

When there is path dependent in IRFs, there are two options on the table: 1) present IRFs conditional on a specific path; 2) integrate out the path dependency using its invariant distribution or integrate out the posterior distribution of object that approximates this path dependency.

For CAIW model, the IRFs depend on Σ_{t-1} at time t. More specifically, Ω_t is a function of Σ_{t-1}, $\Omega_t = \Omega(\Sigma_{t-1}; \omega)$ where $\Omega()$ is a deterministic function of Σ_{t-1} and $\omega = \nu, A, C$. In our empirical application, we take the second approach and integrate Σ_{t-1} out using its invariant distribution.[2] Then, for example, ith element of the left expectation in equation

[2] We thank the referee for this suggestion.

A.7 is defined as

$$E[y_{i,t+s}|v_t^* = e_j; R_*, \psi] \equiv \int E[y_{i,t+s}|v_t^* = e_j; chol(\Omega(\Sigma_0))Q, \psi] p_*(\Sigma_0|\psi)\, d\Sigma_0 \tag{A.17}$$

where $p_*(\Sigma_0|\psi)$ is an invariant distribution of Σ_{t-1} at parameter ψ. In computing this IRF, we further truncate the joint prior distribution of ψ and Σ_0 to the region $\mathbb{P}(\mathcal{R})$, which is the set of ψ and Σ_0 that there is at least one Q^* in $\mathcal{O}(k)$ that $IRF[y_{.,t+s}|chol(\Omega(\Sigma_0))Q^*, \psi]$ satisfies $\mathcal{R}$.

There are alternative ways to integrate the path dependency. One way would be:

$$E[y_{i,t+s}|v_t^* = e_j; R_*, \psi] \equiv E[y_{i,t+s}|v_t^* = e_j; chol(\Omega(\Sigma_*))Q, \psi] \tag{A.18}$$

where Σ_* = the long run mean of Σ_t. The long run mean of Σ_t is a known function of other model paratmers, Φ, C, ν. So, we write $\Sigma_* = g_{\Sigma_*}(\Phi, C, \nu)$. Then, for example, the posterior mean of these IRFs can be computed using posterior draws from the algorithm in section A.1:

$$\begin{aligned}\int E[y_{i,t+s}|v_t^* = e_j; &chol(\Omega(g_{\Sigma_*}(\Phi, C, \nu)))Q, \psi]\; p(Q, \psi|Y) dQ d\psi \\ &= \frac{1}{M}\sum_{m=1}^{M} E[y_{i,t+s}|v_t^* = e_j; chol(\Omega(g_{\Sigma_*}(\Phi^{(m)}, C^{(m)}, \nu^{(m)})))Q^{(m)}, \psi^{(m)}]\end{aligned} \tag{A.19}$$

where $\Phi^{(m)}, C^{(m)}, \nu^{(m)}$ are in $\psi^{(m)}$.

Another alternative way is to define:

$$E[y_{i,t+s}|v_t^* = e_j; R_*, \psi] \equiv E[y_{i,t+s}|v_t^* = e_j; chol(\Omega(\Sigma_{**}))Q, \psi] \tag{A.20}$$

where $\Sigma_{**} = \frac{1}{T}\sum_{t=1}^{T} \Sigma_t$ (the sample average of Σ_t). Then, for example, the posterior mean

of these IRFs can be computed using posterior draws from the algorithm in section A.1:

$$\begin{aligned}\int E[y_{i,t+s}|v_t^* = e_j; chol(\Omega(\Sigma_{**}))Q, \psi]\; p(Q, \psi|Y) dQ d\psi \\ = \frac{1}{M}\sum_{m=1}^{M} E[y_{i,t+s}|v_t^* = e_j; chol(\Omega(\Sigma_{**}^{(m)}))Q^{(m)}, \psi^{(m)}]\end{aligned} \tag{A.21}$$

where $\Sigma_{**}^{(m)} = \frac{1}{T}\sum_{t=1}^{T}\Sigma_t^{(m)}$ and $\Sigma_{1:T} \in \psi$.

Finally, we want to mention that all three approaches are different in the way they approximate the long-run aspect of Σ_t, but they all lead to quite similar posterior distribution in our application. For example in Figure A-1, we report the response of the IP to financial uncertainty shocks (left) and macro uncertainty shocks (right) based on these three approaches.

Figure A-1 Response of the IP to financial uncertainty shocks (left) and macro uncertainty shocks (right). Based on different integration schemes to average the state dependency out.

Based on equation A.17

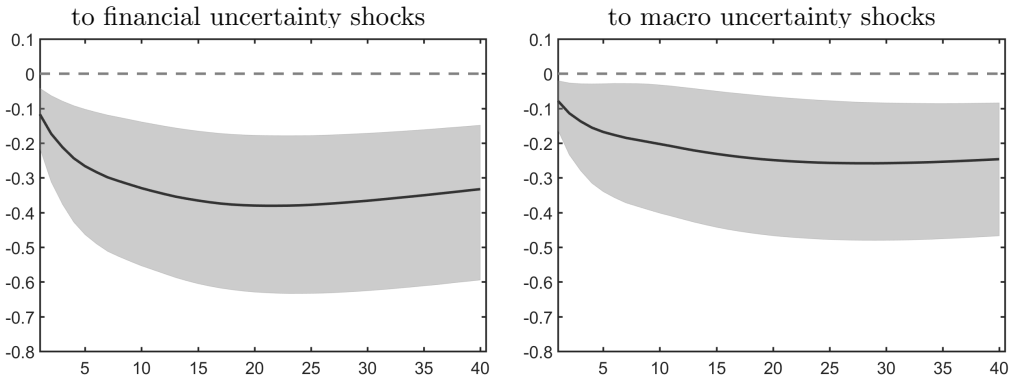

Based on equation A.19

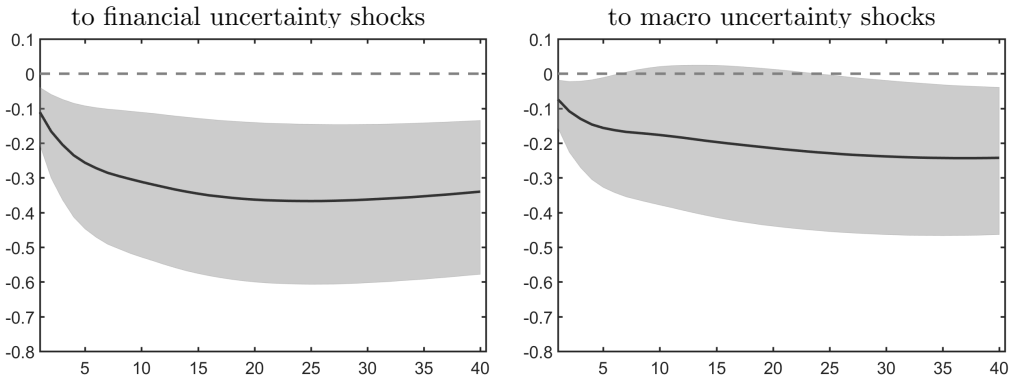

Based on equation A.21

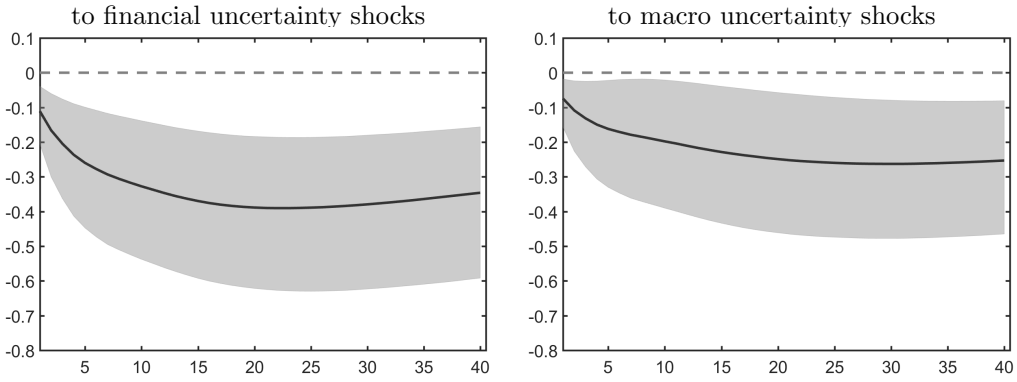

C Details of the empirical section

C.1 Example 1: Small-scale VAR

C.1.1 Model

The CAIW(1)-in-VAR(12) model we considered in the empirical exercise is

$$\begin{aligned} y_t &= \mu^y + \sum_{p=1}^{12} \Phi_p^y y_{t-p} + B^y log(diag(\Sigma_t)) + \epsilon_t, \quad \epsilon_t|\mathcal{F}_{t-1} \sim N(0, \Sigma_t) \\ \Sigma_t|\Sigma_{t-1} &\sim IW((\nu - n - 1)(C + \Phi\Sigma_{t-1}\Phi'), \nu) \end{aligned} \tag{A.22}$$

Note that the process is formulated in a way that the conditional mean of the volatility matrix has the following simple form

$$E[\Sigma_t|\mathcal{F}_{t-1}] = C + \Phi\Sigma_{t-1}\Phi' \tag{A.23}$$

and

$$Cov(\Sigma_{ij,t},\ \Sigma_{lm,t}|\mathcal{F}_{t-1}) = \frac{2\Psi_{ij,t}\Psi_{lm,t} + (\nu - n + 1)(\Psi_{il,t}\Psi_{jm,t} + \Psi_{im,t}\Psi_{lj,t})}{(\nu - n)(\nu - n - 3)} \tag{A.24}$$

where $\Psi_t = C + \Phi\Sigma_{t-1}\Phi'$. This delivers a convenient linear representation for the multivariate volatility process with innovations that are martingale difference sequences. This leads to the VAR representation of volatility process[3],

$$h_t = \mu^h + \Phi^h h_{t-1} + v_t, \quad E[v_t|\mathcal{F}_{t-1}] = 0, \quad \text{and} \quad E[v_t v_s'|\mathcal{F}_{t-1}] = 0, \quad \forall s \neq t, \tag{A.25}$$

where $h_t = vech(\Sigma_t)$, $\mu^h = vech(C)$, $\Phi^h = L_n(\Phi \otimes \Phi)D_n$ with $D_n vec(x) = vech(x)$ and $vech(x) = L_n vec(x)$. The covariance matrix of v_t, Ω_t, is a deterministic function of Σ_{t-1}, Φ,

[3]The VAR form of the volatility process proves key to deriving unconditional moments and giving stationarity conditions, as discussed in Golosnoy et al. (2012).

C and ν, and its formula is given by the equation A.24.

C.1.2 Data

We estimate the model on industrial production, CPI, federal funds rate, and the excess bond premium. We plot in figure A-2 the four monthly series used in our estimation of the model.

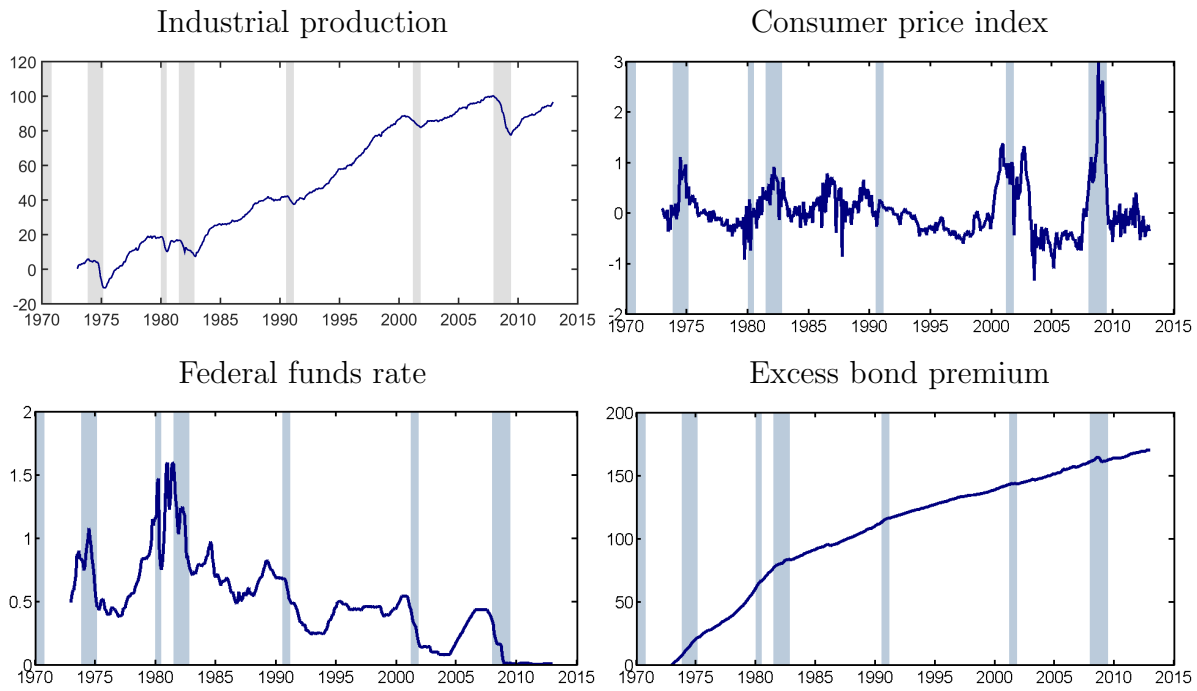

Figure A-2 (Clockwise from top) Monthly log industrial production of the manufacturing sector, log consumer price index, federal funds rate, and excess bond premium (bottom) $1973M1 - 2012M12$. Blue bars indicate NBER recession dates. We obtained the macroeconomic data from the Federal Reserve Bank of St. Louis FRED and the excess bond premium data from Simon Gilchrist's website.

C.1.3 Prior specification

In setting up the prior, we divide up the parameters into three categories:

- VAR conditional mean parameters : $\{\mu^y, \Phi^y(L)\}$
- Volatility process parameters: $\{C, \Phi, \nu\}$
- Volatility-in-mean parameter: B^y
- Rotation matrix: Q

In this section, we begin by discussing our initial proper prior distributions over the reduced-form parameters $p(\psi)$ and the conditional prior of $p(Q|\psi)$. As was discussed in the main text, given the set of sign restrictions $\mathcal{R}$, we must then truncate this joint prior distribution over ψ and Q to only take into account parameters that lead to IRFs in the identified set.

VAR conditional mean parameters For the standard VAR conditional mean parameters μ^y and Φ^y, we use a Minnesota prior. We center the mean of the prior over all elements of μ^y around 0 with a variance of 1000. For the Φ^y parameters, we center all terms around 0, except for the diagonal elements of $\Phi^y(1)$, which are centered around 1. The variances of the values are set at $\left(\frac{\theta}{l}\frac{\sigma_i}{\sigma_j}\right)^2$ for variable j in equation i. We set $\theta = 0.2$. σ_i is the standard deviation of the innovation term estimated from a $VAR(12)$ model using OLS.

Volatility process parameters The inverse Wishart volatility process is fairly new to the macro literature. We attempt to choose priors for its parameters that lead to similar implications for the volatility processes when compared to the literature.

We choose an independent normal prior over the elements Φ that centers around a fair amount of persistence in the volatilities and no cross-term interaction between the elements of the variance covariance matrix (prior mean of Φ that is diagonal with elements 0.9 with prior variance of 0.01). We truncate this prior to only consider Φ^h draws that

lead to stationarity. We choose an inverse Wishart prior for C with precision matrix $(15 - ndim - 1)\, diag\left([0.085, 0.009, 0.039, 0.011]\right)$ with degrees of freedom of 15. As we need to ensure the positive definiteness of the C matrix, we find it easier to place a prior directly over C instead of over the long-run mean of volatility. We choose values of the prior over the precision matrix that lead to reasonable long-run volatility predictions and also a wide range of possible values. The variances of innovations estimated from a VAR(12) on the data using OLS, which is a rough estimate of the long-run mean of the volatilities in the data, are in high density mass areas of the prior. The prior over ν is set to a gamma distribution with mean 40 and variance 10. We truncate this to $\nu \in [6, \infty)$, where the lower bound is a minimal integer that allows a finite first moment of Σ_t. This parameter governs the conditional variance of a volatility shock. As one will see in the log volatility impulse response prior analysis, this prior leads to log volatility movements of a one standard deviation uncertainty shock that covers much the same mass over the log volatility movements of the VAR residuals as that implied by the priors adopted in Clark and Ravazzolo (2015) or Carriero et al. (2017).

Finally, we make an assumption about the initial variance-covariance matrix. The prior distribution of Σ_1 is:

$$\Sigma_1 \sim IW((\nu_0 - k - 1)V_0, \nu_0) \tag{A.26}$$

where $\nu_0 = 20$ and V_0 is such that $vech(V_0) = (I - \Phi^h)^{-1}\mu^h$.

Volatility-in-mean parameter The B^y parameter governs the relationship between the volatilities and the level variables. As $g^y(\Sigma)$ is assumed to be $\log\left(diag\left(\Sigma\right)\right)$, the B^y_{ij} element can be interpreted as an elasticity (percentage change in the variable $y_{i,t}$ to a percentage change in the volatility of the innovation j: $\Sigma_{jj,t}$).

We choose independent normal priors for elements of the B^y parameter that are centered around 0. This choice reflects an ignorance about the sign of the response of macro or financial variables when volatility in the economy increases. We choose prior variances of

10 for all elements of B^y except those governing the impact of volatility shocks on the EBP, which we choose to be 0.05. An interpretation of this prior is that a 1% increase in the volatility of the innovations to any variable leads to either a movement in industrial production, the CPI, and the federal funds rate of between -5.20% and 5.20% at the 90% credible set level. We choose a tighter prior over the EBP spread response to changes in volatility because we are imposing a sign restriction on this response. We choose this prior spread to target a reasonable range of EBP IRFs to our volatility shocks. In terms of elasticities, this prior implies that a 1% increase in the volatility of the innovations leads to a movement in the EBP of between -0.37% and 0.37% at the 90% credible set level.

Rotation matrix Conditional on a reduced-form parameter draw ψ, we draw the rotation matrix Q from the conditional Haar prior. This prior imposes a conditionally uniform distribution over the set of rotation matrices and has been a standard choice in the sign restrictions literature since Uhlig (2005).

C.1.4 Prior implications for the impulse response functions

We look at the prior implications of the joint prior over the reduced form parameters and the rotation matrices, in conjunction with the imposed sign restrictions for the level and volatility impulse response functions. We take 500 draws from the prior distribution and compute impulse response functions for 30 Q rotations per parameter draw, selecting those that satisfy Assumptions $\mathcal{A}_{uf}, \mathcal{A}_{um}$, and $\mathcal{A}_o$.

Figures A-3 and A-4 shows the level IRFs implied by the prior distribution following a financial and macro uncertainty shock, respectively. The bands show the 90% credible sets for the impulse response functions. It is immediately clear from the figures that the IRFs for industrial production, CPI, and the federal funds rate are symmetric and centered around 0%. Moreover, the prior puts ample mass on empirically relevant ranges of the real effects of uncertainty shocks found using uncertainty proxies (e.g. Bloom (2009), Leduc and Liu (2012), Jurado et al. (2015), Caldara et al. (2016)). This result comes from the fact that we are not imposing any sign restrictions on the three impulse response functions, the prior for the B^y parameter matrix is centered around 0, and the Minnesota prior on the Φ^y matrix is centered around independent unit roots. We therefore are confident that we are not biasing the signs of any of the responses of the three macro variables from our sign restrictions.

As expected, we do see a prior effect on the EBP IRF. For the financial uncertainty shock, this prior effect directly follows from the sign restriction. On impact, the $5-95\%$ credible bands range from 0.002% to 0.083%. This range seems relevant. For example, Caldara et al. (2016) finds using financial uncertainty proxies (such as realized stock market volatility) that an uncertainty shock has an impact on the EBP including the upper bound of this range.[4] More macro-based uncertainty proxies, such as measures of forecast dispersion, lead

[4]We are aware that it is technically not appropriate in a Bayesian sense to use posterior results on U.S. data to justify the prior. However, these results use different data to measure uncertainty and alternative identification strategies. Moreover, we are just using these results to give a sense of the reasonableness of the prior. We have tried several different priors on the B^y matrix elements in the EBP equation and find broadly similar posterior results.

Figure A-3 **Prior results:**
Financial uncertainty shock on level variables (Haar)

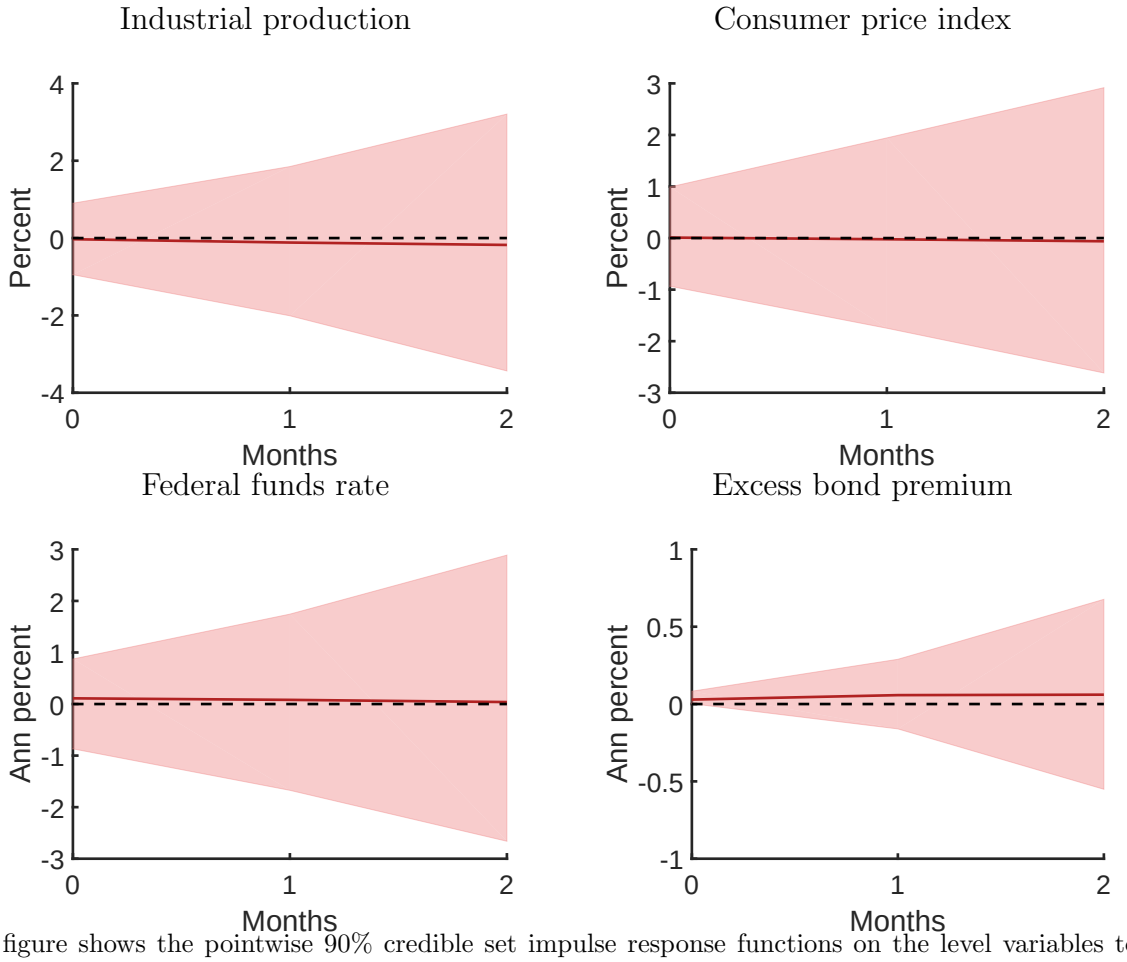

This figure shows the pointwise 90% credible set impulse response functions on the level variables to a 1 standard deviation financial uncertainty shock for the small VAR model. The reduced-form parameters are drawn from their prior distributions. We assume a Haar prior over the rotation matrices. We only keep the impulse response functions that satisfy Assumptions $\mathcal{A}_{uf}, \mathcal{A}_{um}$, and $\mathcal{A}_o$. The dark red line is the impulse response function drawn from a single Q^* that is closest to the pointwise median in a sum of squares sense (median target method of Fry and Pagan (2007)).

to increases in the EBP near the lower bound. From period 1 onwards, we can see that the effects of the sign restriction begin to diminish. The prior distribution includes 0% at the 15% level. By the second period, the prior IRF for EBP is already quite wide around 0%.

The sign restriction also biases the impulse response function of EBP for the macro uncertainty shock. An important point to notice, however, is that we leave the sign of the EBP response to a macro uncertainty shock unrestricted. The $5\% - 95\%$ credible bands range from -0.034% to 0.052%. This happens because of the joint identification restriction with

Figure A-4 **Prior results:**
Macro uncertainty shock on level variables (Haar)

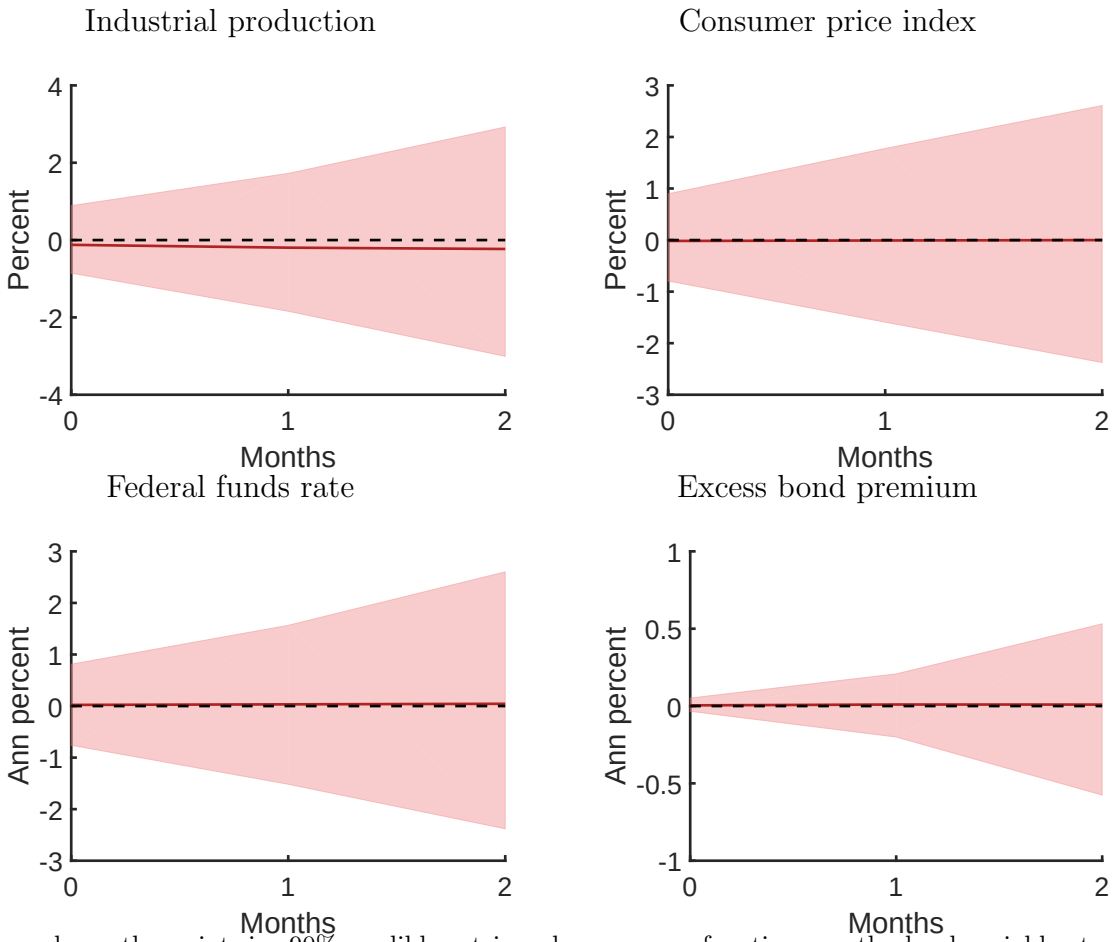

This figure shows the pointwise 90% credible set impulse response functions on the level variables to a 1 standard deviation macro uncertainty shock for the small VAR model. We assume a Haar prior over the rotation matrices. We only keep the impulse response functions that satisfy Assumptions $\mathcal{A}_{uf}, \mathcal{A}_{um}$, and $\mathcal{A}_o$. The dark red line is the impulse response function drawn from a single Q^* that is closest to the pointwise median in a sum of squares sense (median target method of Fry and Pagan (2007)).

the financial uncertainty shock. By assumption, the financial uncertainty shock must lead to a positive increase in the EBP. It also must increase the volatilities of all innovations. These restrictions tend to select B^y parameter matrices that have positive volatility loadings in the EBP equation. This can be confirmed in figure A-5, which compares the unconditional distribution of B^y matrix elements in the EBP equation (light brown) to the distribution of B^y matrix elements in the EBP equation that lead to IRFs that satisfy our sign restrictions. The macro uncertainty shock also increases the volatilities of all innovations. Therefore, this

Figure A-5 **Prior density of B^y matrix elements in the EBP equation**

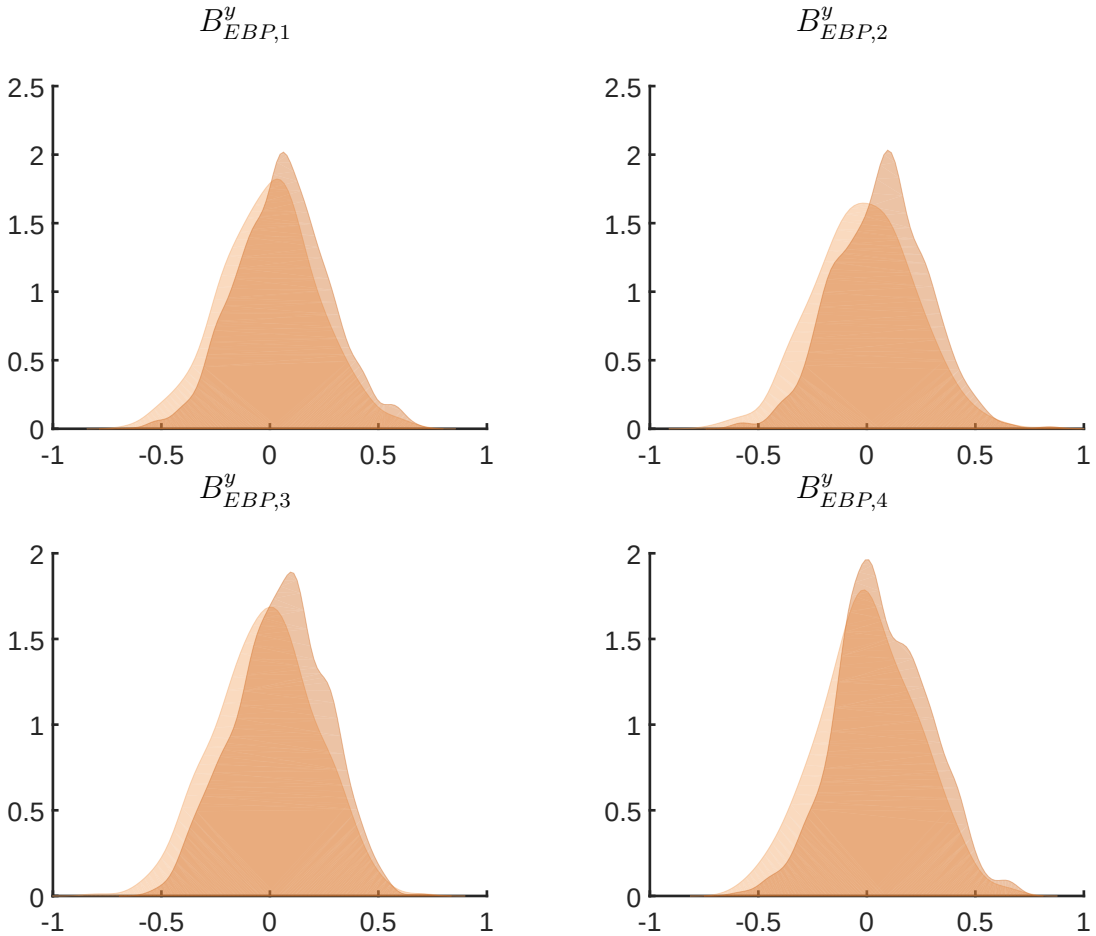

This figure shows the unconditional prior densities of the B^y matrix elements in the EBP equation (light brown) overlaid with the prior densities only considering corresponding to the draws selected that satisfy the sign restrictions laid out in Assumptions $\mathcal{A}_{uf}, \mathcal{A}_{um}$, and $\mathcal{A}_o$ (dark brown).

interaction tends to produce an upward bias on the EBP response for macro uncertainty shocks. A prior that puts a fair amount of weight on a positive impact of macro uncertainty shocks on the EBP does seem reasonable given the known countercyclicality of uncertainty and spreads (Bloom (2014)). The prior, however, does still put weight on no contemporaneous impact and a negative impact. Similarly to the financial uncertainty shocks, moving forward, the prior puts large weight on positive and negative EBP responses to a macro uncertainty shock.

We also analyze the prior implications of the volatility shock sign restrictions on the second moments. Figures A-6 and A-7 show that the responses of log volatility to a financial and

Figure A-6 **Prior results:**
Financial uncertainty shock on log volatility of innovations (Haar)

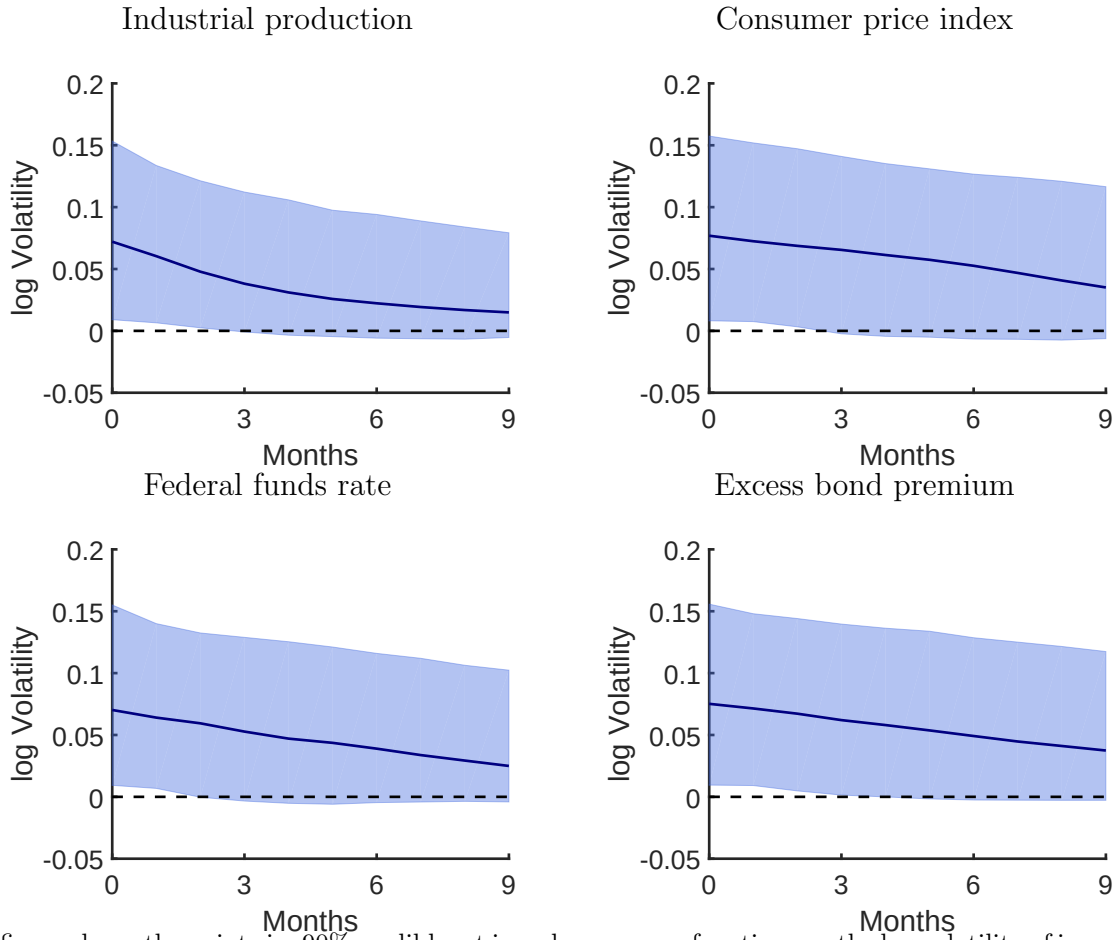

This figure shows the pointwise 90% credible set impulse response functions on the log volatility of innovations to a 1 standard deviation financial uncertainty shock for the small VAR model. We assume a Haar prior over the rotation matrices. We only keep the impulse response functions that satisfy Assumptions $\mathcal{A}_{uf}, \mathcal{A}_{um}$, and $\mathcal{A}_o$. The dark blue line is the impulse response function drawn from a single Q^* that is closest to the pointwise median in a sum of squares sense (median target method of Fry and Pagan (2007)).

macro uncertainty shock, respectively. On impact, we find that the prior for log volatility response ranges from 0.01 to 0.16 at the 90% credible set level for each of the four variables. Given the fairly high prior for the diagonal elements of the A matrix, it is not surprising that the impulse response functions are persistent.

Figure A-7 **Prior results:**
Macro uncertainty shock on log volatility of innovations (Haar)

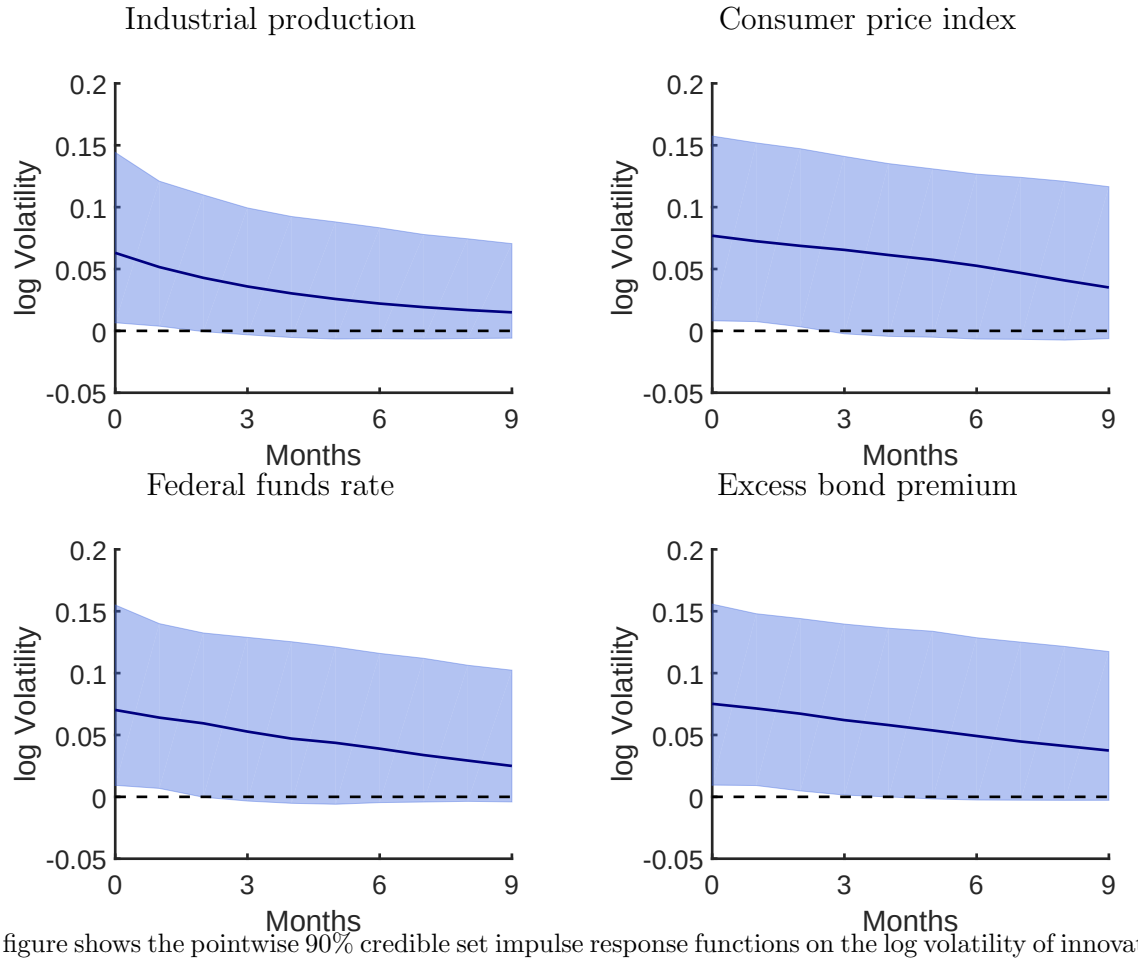

This figure shows the pointwise 90% credible set impulse response functions on the log volatility of innovations to a 1 standard deviation macro uncertainty shock for the small VAR model. We assume a Haar prior over the rotation matrices. We only keep the impulse response functions that satisfy Assumptions $\mathcal{A}_{uf}, \mathcal{A}_{um}$, and $\mathcal{A}_o$. The dark blue line is the impulse response function drawn from a single Q^* that is closest to the pointwise median in a sum of squares sense (median target method of Fry and Pagan (2007)).

Figure A-8 **Wide prior results:**
Financial uncertainty shock on EBP (Haar)

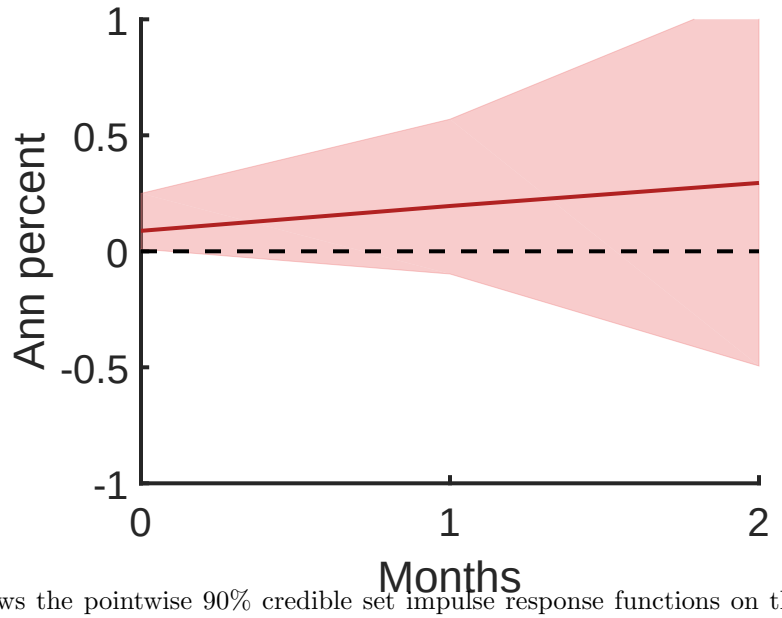

This figure shows the pointwise 90% credible set impulse response functions on the EBP to a 1 standard deviation financial uncertainty shock for the small VAR model. We assume a Haar prior over the rotation matrices and a wider B^y (variance of 0.5) prior on the EBP equation. We only keep the impulse response functions that satisfy Assumptions $\mathcal{A}_{uf}, \mathcal{A}_{um}$, and $\mathcal{A}_o$. The dark red line is the impulse response function drawn from a single Q^* that is closest to the pointwise median in a sum of squares sense (median target method of Fry and Pagan (2007)).

Wide B^y prior on EBP equation The priors on the parameters of the B^y matrix in the EBP equation interact with the sign restrictions to influence not only the sign, but also the magnitudes of the impulse response functions on the EBP from a financial uncertainty shock. We now discuss the effects of a wider B^y prior on the elements in the EBP equation. A wider B^y prior pushes up the distribution of EBP responses to a financial uncertainty shock. We keep our other prior specifications the same, but we increase the variance of the B^y matrix elements in the EBP equation from 0.05 to 0.5.

In figure A-8, we present the prior implications for the EBP IRF to a financial uncertainty shock under the alternative prior. We see that the prior distribution implies a wider range on impact, but also one that is shifted upwards. On impact, the $5\% - 95\%$ credible bands range

from 0.01% to 0.25%. That the credible bands get wider is not surprising given the looser prior on the B^y elements. The prior is shifted up because it is now less likely for a small response to the EBP from a financial uncertainty shock. Given a fixed volatility increase, a higher variance of the B^y prior elements makes it more likely that any one volatility will have a large effect on the EBP, thereby pushing the entire distribution upwards. Large negative values of the B^y parameter matrix elements are also more likely from the unconditional prior, but these draws tend to lead to a violation of the positive sign restriction on the EBP response.

For the alternative sign restriction that we present in a later section in the appendix, the upward bias in the EBP is even more extreme with this wide B^y prior. We have estimated versions of our model with looser priors on B^y and do not find much evidence of large movements in the EBP following either a financial or macro uncertainty shock. Therefore, we take a conservative approach of putting a tighter prior on the B^y elements in the EBP equation.

C.1.5 Estimation of the CAIW-in-VAR model

As described in section A in this appendix, sampling from the posterior distribution of IRFs is done by the following decomposition.

$$p(\psi, Q|Y) = \underbrace{p(Q|\psi)1\{\psi \in \mathbb{P}(\mathcal{R})\}/vol(\mathbb{P}(\mathcal{R}))}_{\text{step 2}} \times \underbrace{p(Y|\psi)p(\psi)/P(Y)}_{\text{step 1}} \tag{A.27}$$

In this section, we describe the initial prior distribution of ψ ($p(\psi)$) and the posterior sampler that generates ψ from the second part (step 1) of this posterior distribution for our empirical exercises.

The Particle Gibbs sampler is used to generate ψ from its posterior distribution (Creal and Tsay, 2015; Creal and Wu, 2017).

Posterior sampler The joint posterior distribution of CAIW-in-VAR model is then

$$p(\mu^y, B^y, \Phi^y, \nu, C, \Phi, \Sigma_{1:T}|Y_{1:T}) \propto p(Y_{1:T}|\mu^y, B^y, \Phi^y, \nu, C, \Phi, \Sigma_{1:T})p(\mu^y, B^y, \Phi^y, \nu, C, \Phi, \Sigma_{1:T}). \tag{A.28}$$

where $Y_{1:T}$ is a vector of observed data.[5]

The algorithm runs on the following cycles, which generate samples from the conditional posterior distribution of sub-block of ψ:

1. $p(\Sigma_{1:T}|\ others)$ for $t = 1, ..., T$: Multivariate stochastic volatilities.
2. $p(\mu^y, B^y, \Phi^y|\ others)$: Parameter in the conditional mean equation.
3. $p(\nu|\ others)$: Parameter in Wishart process.
4. $p(C|\ others)$: Parameter in Wishart process.
5. $p(\Phi|\ others)$: Parameter in Wishart process.

[5]To be more precise, we are also conditioning on the initial lagged observations, $Y_0, Y_{-1}, ..., Y_{-p+1}$ where p is the number of lags. We take this dependency out from the expression for the notational convenience.

Step 1: ($\boldsymbol{\Sigma_{1:T}}$) We draw $\Sigma_{1:T}$ from the full conditional distribution, $p(\Sigma_{1:T}|\mu^y, B^y, \Phi^y, \nu, C, \Phi, data)$, by the particle Gibbs (PG) sampler. The algorithm starts with previous draws of CAIW-in-VAR parameters $((\mu^y)^{old}, (B^y)^{old}, (\Phi^y)^{old}, \nu^{old}, C^{old}, \Phi^{old})$ as well as previous covriance matrix draws $\Sigma_{1:T}^{old}$ from the previous iteration.

We denote $f_{MVN}(y; m, V)$ as a density function of the multivariate normal distribution with mean m and covariance matrix V; $f_{IW}(y; S, \nu)$ be a density function of the inverse Wishart distribution with scale parameter S and degrees of freedom parameter ν. We suppress the superscript "old" in $((\mu^y)^{old}, (B^y)^{old}, (\Phi^y)^{old}, \nu^{old}, C^{old}, \Phi^{old})$ for simplicity.

1. (Initialization) For $m = 2, ..., M$, generate particles,

$$\Sigma_1^{(m)} \sim IW((\nu_0 - n - 1)V_0, \nu_0) \tag{A.29}$$

and $\Sigma_1^{(1)} = \Sigma_1^{old}$. Compute the normalized weights

$$W_1^{(m)} = \frac{f_{MVN}(y_1; \mu^y + \sum_{i=1}^p \Phi_i^y y_{1-i} + B^y log(diag(\Sigma_1^{(m)})), \Sigma_1^{(m)})}{\sum_{m'=1}^M f_{MVN}(y_1; \mu^y + \sum_{i=1}^p \Phi_i^y y_{1-i} + B^y log(diag(f(\Sigma_1^{(m')})), \Sigma_1^{(m')})}, \quad m = 1, 2, ..., M. \tag{A.30}$$

2. (Conditional filtering) For $t = 2, ..., T$,

   (a) For $m = 2, ..., M$, set $\widetilde{\Sigma}_{t-1}^{(m)}$ by resampling particles $\{\Sigma_{t-1}^{(m)}\}_{m=1}^M$ with probabilities $\{W_{t-1}^{(m)}\}_{m=1}^M$. Set $\widetilde{\Sigma}_{t-1}^{(1)} = \Sigma_{t-1}^{(1)}$.

   (b) For $m = 2, ..., M$ generate particles

$$\Sigma_t^{(m)} \sim IW((\nu - n - 1)(C + \Phi \widetilde{\Sigma}_{t-1}^{(m)} \Phi'), \nu), \tag{A.31}$$

   and $\Sigma_t^{(1)} = \Sigma_t^{old}$.

(c) Compute the normalized weights

$$W_t^{(m)} = \frac{f_{MVN}(y_t; \mu^h + \sum_{i=1}^{p} \Phi_i^y y_{t-i} + B^y log(diag(\Sigma_t^{(m)})), \Sigma_t^{(m)})}{\sum_{m'=1}^{M} f_{MVN}(y_t; \mu^y + \sum_{i=1}^{p} \Phi_i^y y_{t-i} + B^y log(diag(\Sigma_t^{(m')})), \Sigma_t^{(m')})}, \quad m = 1, 2, ..., M. \tag{A.32}$$

Throughout the iteration, we store $\left\{\Sigma_{1:T}^{(m)}, W_{1:T}^{(m)}\right\}_{m=1}^{M}$ where the first particle at each point in time is set to the variance-covariance from the previous iteration (i.e., $\Sigma_{1:T}^{old}$).

3. (Initialization of the backward simulation) Draw a particle $\Sigma_T^{new} = \Sigma_T^{(m)}$ with probability $W_T^{(m)}$.

4. (Backward simulation) For $t = T-1, T-2, ..., 1$,

   (a) For $m = 1, 2, ..., M$, compute the normalized conditional weights,

$$W_{t|T}^{(m)} = \frac{W_t^{(m)} f_{IW}(\Sigma_{t+1}^{new} | (\nu - n - 1)(C + \Phi \Sigma_t^{(m)} \Phi'), \nu)}{\sum_{m'=1}^{M} W_t^{(m')} f_{IW}(\Sigma_{t+1}^{new} | (\nu - n - 1)(C + \Phi \Sigma_t^{(m')} \Phi'), \nu)}. \tag{A.33}$$

   (b) Draw a particle $\Sigma_t^{new} = \Sigma_t^{(m)}$ with probability $W_{t|T}^{(m)}$.

The draw $\Sigma_{1:T}^{new}$ is a draw from the full conditional distribution.

Step 2: $(\boldsymbol{\mu^y, B^y, \Phi^y})$ First we transform our model into the following multiple regression form,

$$\widetilde{Y}_t = \widetilde{B} \widetilde{X}_t + \Sigma_t^{1/2} \epsilon_t, \quad \epsilon_t \sim N(0, I)$$

where p is the number of lags in VAR and

$$\begin{aligned} \widetilde{Y}_t &= Y_t' \\ \widetilde{X}_t &= [1, Y_{t-1}', ..., Y_{t-p}', f(\Sigma_t)']' \\ \widetilde{B} &= [\mu^y, \Phi_1^y, ..., \Phi_p^y, B^y]. \end{aligned}$$

Then, we can re-write the equation as

$$\Sigma_t^{-1/2}\widetilde{Y}_t = \left(\widetilde{X}_t' \otimes \Sigma_t^{-1/2}\right) vec\left(\widetilde{B}\right) + \epsilon_t,$$

which is a standard multiple regression with homoscedastic errors. The conditional posterior distribution of (μ^y, B^y, Φ^y) is a multivariate normal distribution under the conjugate prior assumption.

Step 3: $\boldsymbol{\nu}$ The conditional posterior distribution of ν is

$$p(\nu|others) \propto \left(\prod_{t=2}^{T} \frac{|S_{t-1}^{-1}|^{\nu/2}}{2^{\nu n/2}\Gamma_n(\nu/2)} |\Sigma_t|^{-(\nu+n+1)/2} exp\left(-\frac{1}{2} tr(S_{t-1}^{-1}\Sigma_t^{-1})\right)\right) p_G(\nu)\mathbf{1}_{(n+2,M_\nu)}(\nu)$$

where $S_{t-1}^{-1} = (v-n-1)(C+\Phi\Sigma_{t-1}\Phi')$, $\Gamma_k(\cdot)$ is the multivariate gamma function, $p_G(\nu)\mathbf{1}_{(n+2,M_\nu)}(\nu)$ is a term that is proportional to a prior distribution for ν, where $p_G(\nu)$ is a Gamma distribution, and $\mathbf{1}_{(n+2,M_\nu)}(\nu)$ is an indicator function takes value 1 if $\nu \in (n+2, M_\nu)$ and 0 otherwise. To generate ν from this conditional posterior distribution, we employ the Griddy Gibbs algorithm of Ritter and Tanner (1992).

Prior for ν, p_G is a Gamma distribution with mean 40 and variance 10. We truncate this distribution on $[n+2, 70]$. For Griddy Gibbs algorithm, we consider the fixed-width grid on the support of prior distribution with 500 grid points.

Step 4: $\boldsymbol{C}$ The conditional posterior distribution of C is

$$p(C|others) \propto \left(\prod_{t=2}^{T} |S_{t-1}^{-1}|^{\nu/2} |\Sigma_t|^{-(\nu+n+1)/2} exp\left(-\frac{1}{2} tr(S_{t-1}^{-1}\Sigma_t^{-1})\right)\right) \times p_{IW}(C|df, \Psi)$$
$$\times\, p_{IW}\left(\Sigma_1|\nu_0, V_0^{-1}\right), \quad \text{where } V_0^{-1} = (v_0 - n - 1)(I - \phi^h)^{-1}\mu^h,$$

and $S_{t-1}^{-1} = (v-n-1)(C + \Phi\Sigma_{t-1}\Phi')$, and p_{IW} is a density function of the inverse Wishart distribution. In this step, we reparametrize C in the following fashion,

$$C = \begin{pmatrix} d_{11} & 0 & \dots & 0 \\ c_{21} & d_{22} & \dots & 0 \\ \vdots & & \ddots & 0 \\ c_{k1} & c_{k2} & c_{k3} & \dots d_{kk} \end{pmatrix} \begin{pmatrix} d_{11} & 0 & \dots & 0 \\ c_{21} & d_{22} & \dots & 0 \\ \vdots & & \ddots & 0 \\ c_{k1} & c_{k2} & c_{k3} & \dots d_{kk} \end{pmatrix}'.$$

This transformation ensures the positive definiteness of C. To draw C from this conditional posterior distribution, we employ the random-walk Metropolis-Hastings algorithm with a proposal

$$c_{ij}^{*} = c_{ij}^{old} + e_{c(i,j)}, \quad e_{c(i,j)} \sim N(0, \sigma_{c(i,j)}^2)$$
$$\log(d_{ii}^{*}) = \log(d_{ii}^{old}) + e_{d(i,i)}, \quad e_{d(i,i)} \sim N(0, \sigma_{d(i,i)}^2)$$

for $(i,j) = \{i = 1, .., n; j = 1, ..., n, i \geq j\}$. The scale of the proposal distribution $\sigma_{c(i,j)}^2$ and $\sigma_{d(i,j)}^2$ are adaptively chosen so that the resulting acceptance rate is about 30% (Atchadé and Rosenthal, 2005). Note that to compute the acceptance ratio, we need a Jacobian term due to reparametrization,

$$|J| = \underbrace{2^n \prod_{i=1}^{n} d_{ii}^{n+1-i}}_{cholsky\ decomp.} \times \underbrace{\prod_{i=1}^{n} d_{ii}}_{log\ trans.}.$$

Step 5: *A* The conditional posterior distribution of Φ is

$$\begin{aligned} p(\Phi|others) \propto & \left(\prod_{t=2}^{T} |S_{t-1}^{-1}|^{\nu/2} |\Sigma_t|^{-(\nu+n+1)/2} exp\left(-\frac{1}{2} tr(S_{t-1}^{-1}\Sigma_t^{-1}) \right) \right) \\ & \times p_{TN}\left(\Phi_{11}|m_{\Phi(1,1)}, V_{\Phi(1,1)}, 0, \infty\right) \prod_{(i,j)\neq(1,1)} p_N\left(\Phi_{ij}, m_{\Phi(i,j)}, V_{\Phi(i,j)}\right) \\ & \times p_{IW}\left(\Sigma_1|\nu_0, V_0^{-1}\right), \quad \text{where } V_0^{-1} = (v_0 - n - 1)(I - \Phi^h)^{-1}\mu^h. \end{aligned}$$

and $S_{t-1}^{-1} = (v - n - 1)(C + \Phi\Sigma_{t-1}\Phi')$, p_{TN} is a density function of the truncated normal distribution, and p_N is a density function of the normal distribution. Note that the sign of $\Phi_{(1,1)}$ is not identified. Hence, we place the prior distribution over $\Phi_{(1,1)} > 0$.

To draw Φ from this conditional posterior distribution, we employ the element-wise random-walk Metropolis-Hastings algorithm with a proposal,

$$\Phi^*_{(i,j)} = \Phi^{old}_{(i,j)} + w_{i,j}, \quad w_{i,j} \sim N\left(0, \sigma^2_{\Phi_{(i,j)}}\right),$$

where the scale of the proposal distribution $\sigma^2_{\Phi(i,j)}$ is adaptively chosen so that the resulting acceptance rate is about 30% (Atchadé and Rosenthal, 2005) for each (i, j).

Figure A-9 **Financial uncertainty shock on level variables (Haar)**

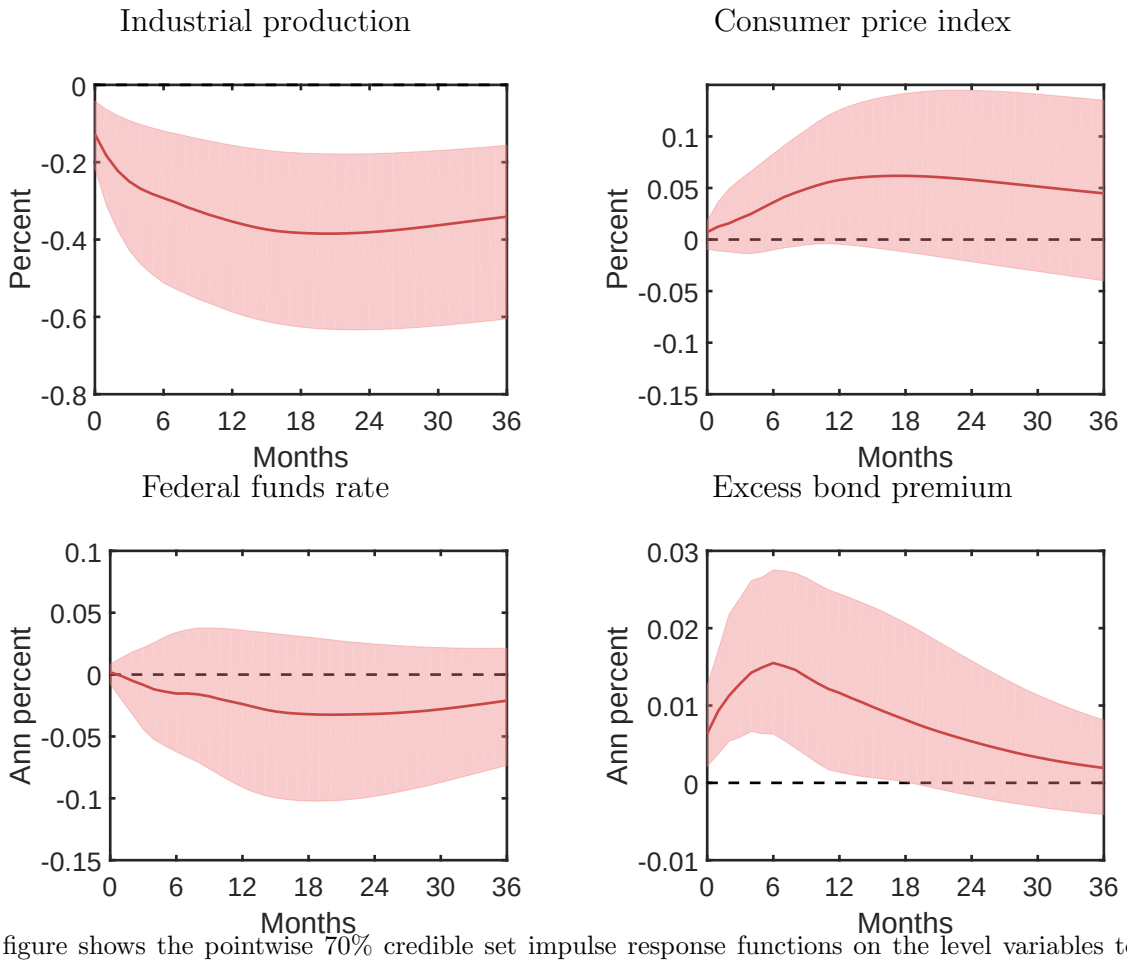

This figure shows the pointwise 70% credible set impulse response functions on the level variables to a 1 standard deviation financial uncertainty shock for the small VAR model. The reduced-form parameters are drawn from their posterior distributions. We assume a Haar prior over the rotation matrices. We only keep the impulse response functions that satisfy Assumptions $\mathcal{A}_{uf}$, $\mathcal{A}_{um}$, and $\mathcal{A}_o$. The dark red line is the impulse response function drawn from a single Q^* that is closest to the pointwise median in a sum of squares sense (median target method of Fry and Pagan (2007)).

C.1.6 Posterior results for level variables

In this section, we plot the level responses to all variables following financial (figure A-9) and macro (figure A-10) uncertainty shocks. Relative to the main text, the only additional IRF that is included here is for the CPI. As one can see, there is little response to the prices following either uncertainty shock, and the differences in the responses between the two uncertainty shocks are negligible.

Figure A-10 **Macro uncertainty shock on level variables (Haar)**

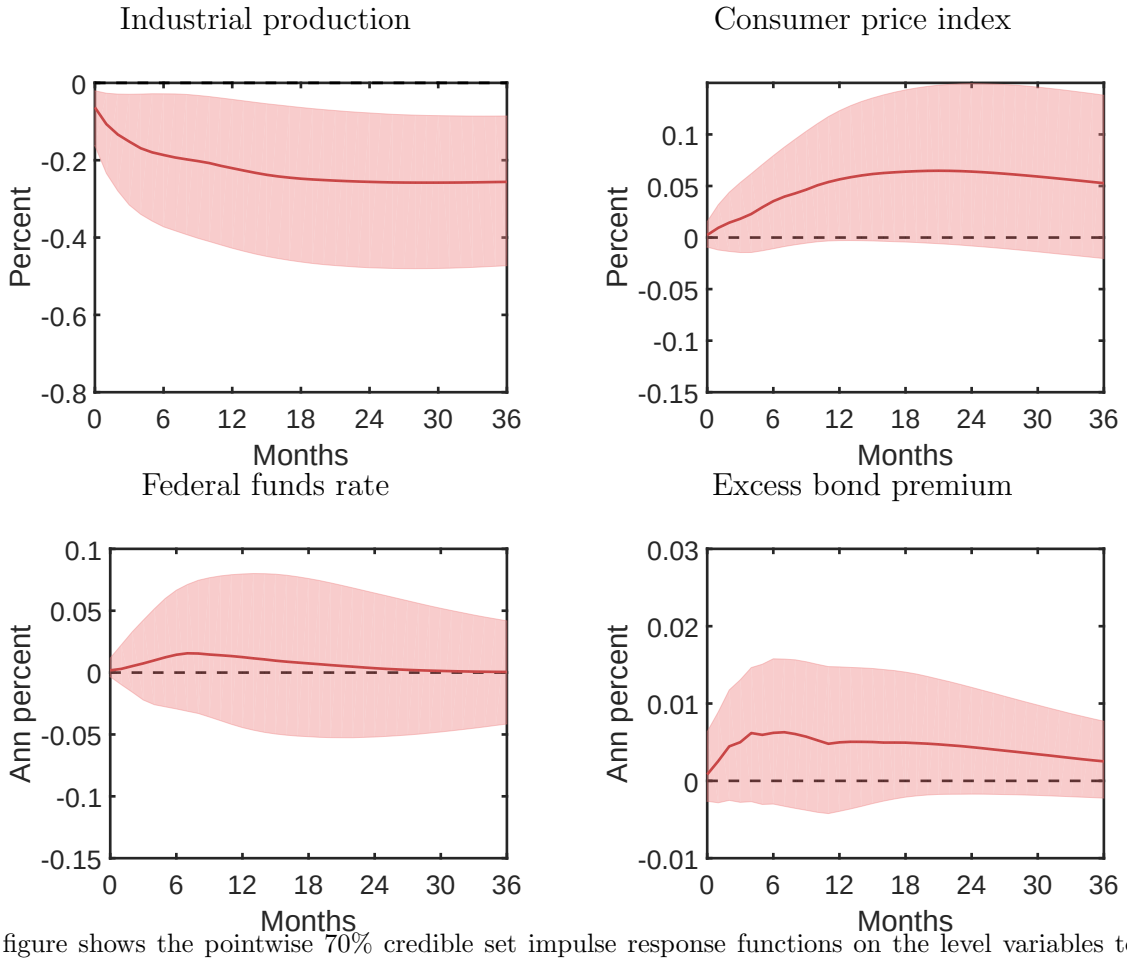

This figure shows the pointwise 70% credible set impulse response functions on the level variables to a 1 standard deviation macro uncertainty shock for the small VAR model. The reduced-form parameters are drawn from their posterior distributions. We assume a Haar prior over the rotation matrices. We only keep the impulse response functions that satisfy Assumptions $\mathcal{A}_{uf}$, $\mathcal{A}_{um}$, and $\mathcal{A}_o$. The dark red line is the impulse response function drawn from a single Q^* that is closest to the pointwise median in a sum of squares sense (median target method of Fry and Pagan (2007)).

C.1.7 Posterior results for log volatility

We discuss here the effects of the financial and macro uncertainty shocks on the log volatility of the innovations. We find in figures A-11 and A-12 that financial uncertainty shocks lead to larger increases in industrial production and EBP volatilities relative to macro uncertainty shocks. Although the credible sets are wide, the posterior median financial uncertainty impulse response increases the log volatility of the innovation to industrial production by 0.09 and the log volatility of the innovation to the EBP by 0.11. On the other hand, the median

Figure A-11 **Posterior results:**
Financial uncertainty shock on log volatility of innovations (Haar)

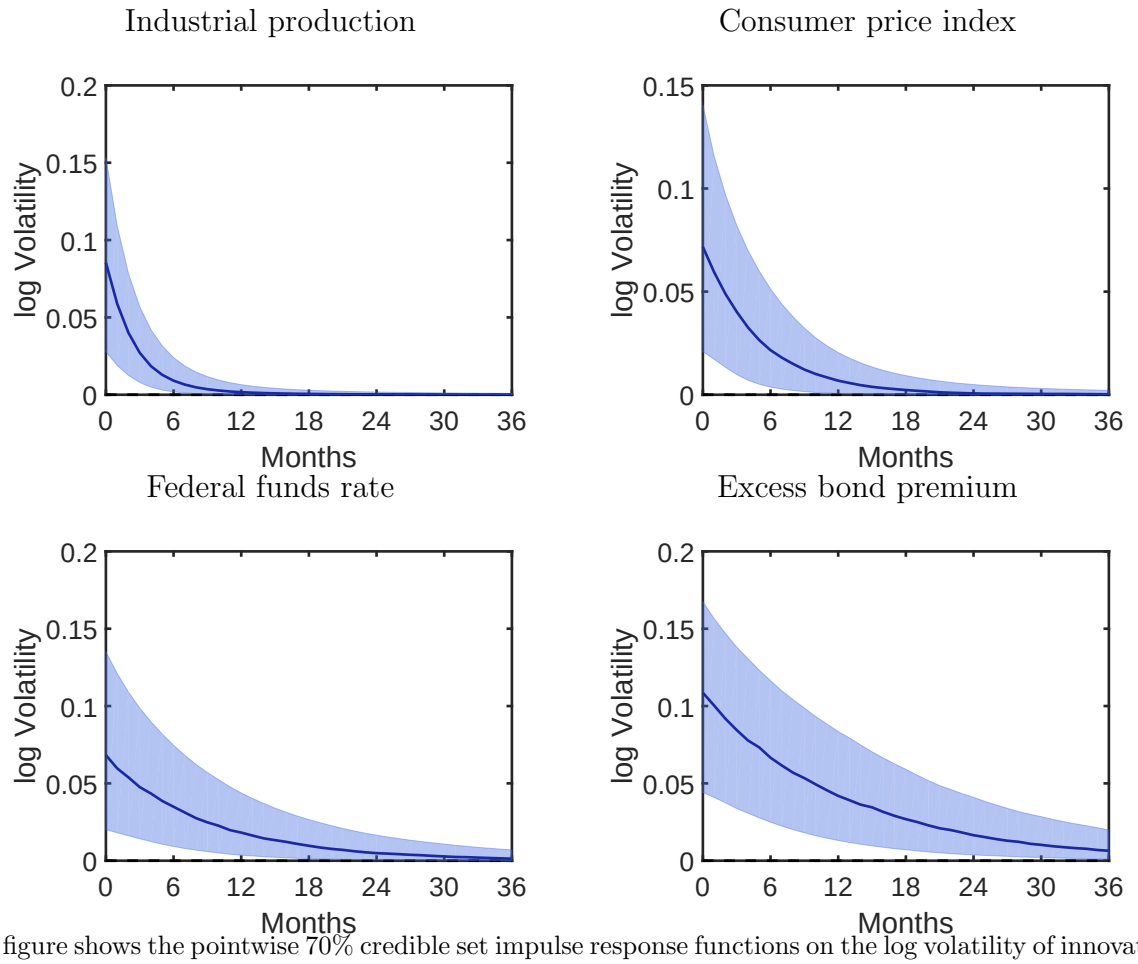

This figure shows the pointwise 70% credible set impulse response functions on the log volatility of innovations to a 1 standard deviation financial uncertainty shock for the small VAR model. The reduced-form parameters are drawn from their posterior distributions. We assume a Haar prior over the rotation matrices. We only keep the impulse response functions that satisfy Assumptions $\mathcal{A}_{uf}$, $\mathcal{A}_{um}$, and $\mathcal{A}_o$. The dark blue line is the impulse response function drawn from a single Q^* that is closest to the pointwise median in a sum of squares sense (median target method of Fry and Pagan (2007)).

response for macro uncertainty shocks only reach to 0.06 for industrial production innovation log volatility and 0.06 for EBP innovation log volatility on impact. The persistence of excess bond premium volatility is also higher for financial uncertainty shocks. The responses for CPI and federal funds rate volatilities are similar across the two volatility shocks.

Figure A-12 **Posterior results:**
Macro uncertainty shock on log volatility of innovations (Haar)

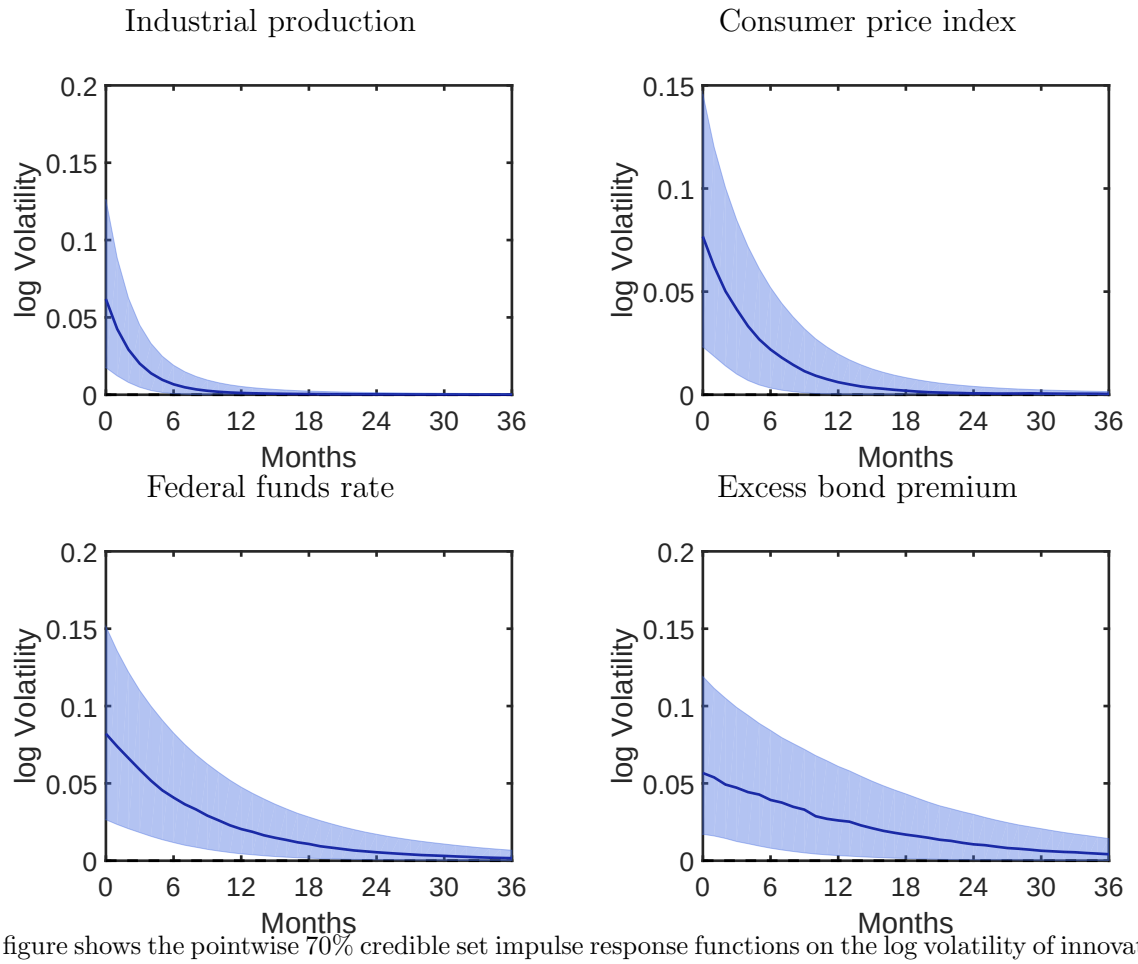

This figure shows the pointwise 70% credible set impulse response functions on the log volatility of innovations to a 1 standard deviation macro uncertainty shock for the small VAR model. The reduced-form parameters are drawn from their posterior distributions. We assume a Haar prior over the rotation matrices. We only keep the impulse response functions that satisfy Assumptions $\mathcal{A}_{uf}$, $\mathcal{A}_{um}$, and $\mathcal{A}_o$. The dark blue line is the impulse response function drawn from a single Q^* that is closest to the pointwise median in a sum of squares sense (median target method of Fry and Pagan (2007)).

C.1.8 Posterior results for forecast error variances

Figures A-13 and A-14 show the effects of financial and macro uncertainty shocks on the forecast error variances of variables (FEV). The FEV of all four variables increase in a persistent manner in response to both financial and macro uncertainty shocks. Even at a horizon of 3 years, there is evidence across the board that the forecastability of the variables has declined. Overall, we find that the financial uncertainty shock generates a larger increase

Figure A-13 **Posterior results:**
Financial uncertainty shock on forecast error variances of variables (Haar)

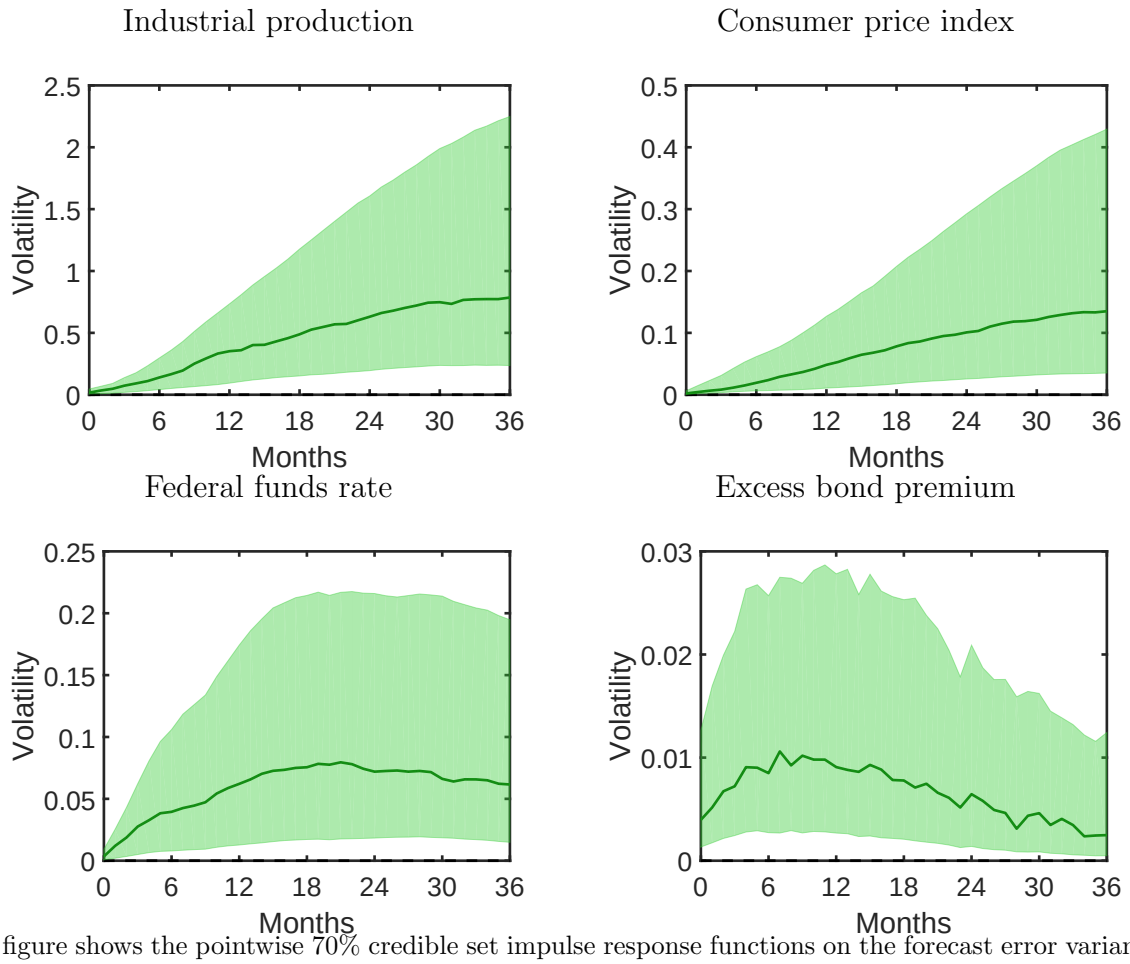

This figure shows the pointwise 70% credible set impulse response functions on the forecast error variance of the variables to a 1 standard deviation financial uncertainty shock in the small VAR model. The reduced-form parameters are drawn from their posterior distributions. We assume a Haar prior over the rotation matrices. We only keep the impulse response functions that satisfy Assumptions $\mathcal{A}_{uf}$, $\mathcal{A}_{um}$, and $\mathcal{A}_o$. The dark green line is the impulse response function drawn from a single Q^* that is closest to the pointwise median in a sum of squares sense (median target method of Fry and Pagan (2007)).

in the FEV for industrial production, the consumer price index, and the excess bond premium. Of particular interest are the FEV responses of industrial production and the excess bond premium. At the posterior median impulse response function, industrial production uncertainty is around 1/3 higher after 3 years following the financial uncertainty shock when compared to the macro uncertainty shock. As one may expect, the largest relative differences in the FEV occur for the excess bond premium, where the upper bounds of the 70% credible sets are up to 50% higher after 1 year following a financial uncertainty shock.

Figure A-14 **Posterior results:**
Macro uncertainty shock on forecast error variances of variables (Haar)

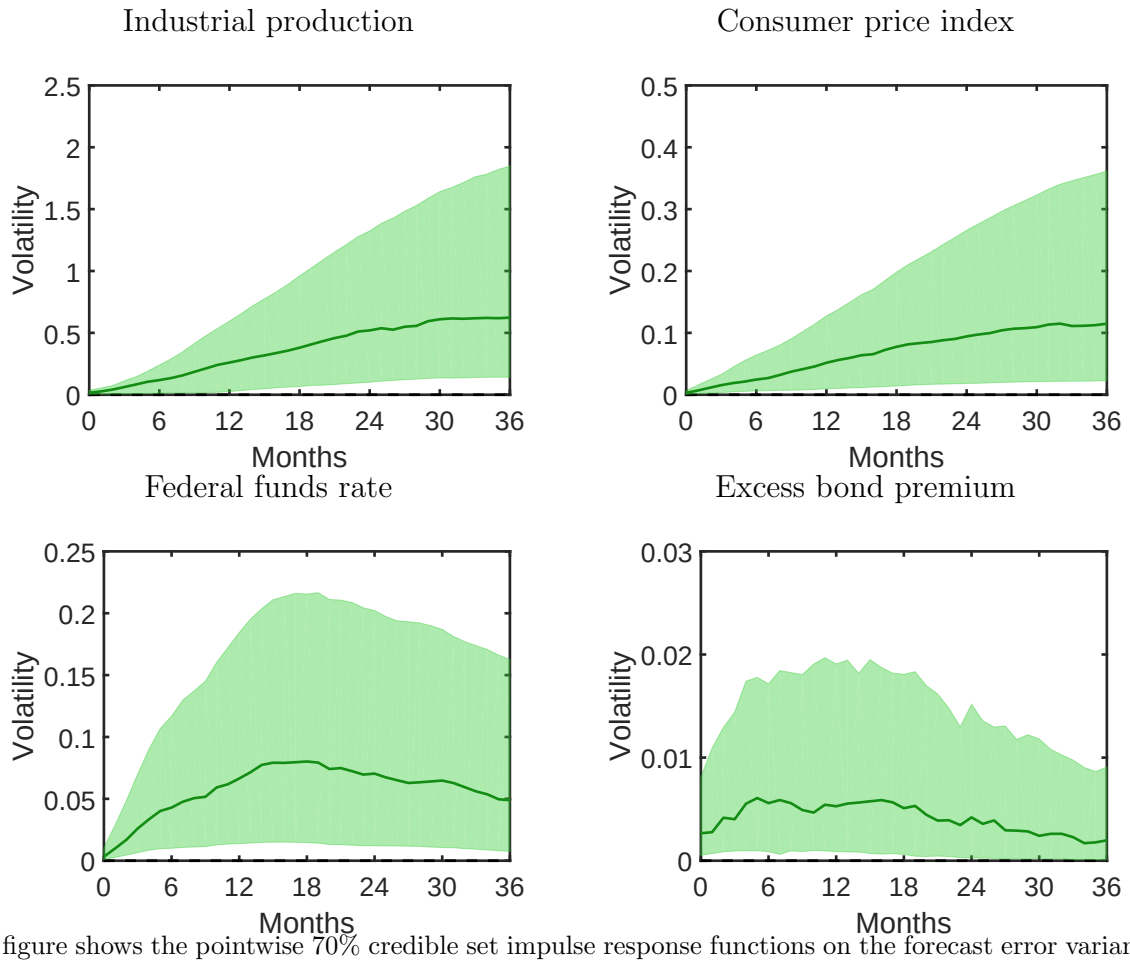

This figure shows the pointwise 70% credible set impulse response functions on the forecast error variance of the variables to a 1 standard deviation macro uncertainty shock in the small VAR model. The reduced-form parameters are drawn from their posterior distributions. We assume a Haar prior over the rotation matrices. We only keep the impulse response functions that satisfy Assumptions $\mathcal{A}_{uf}$, $\mathcal{A}_{um}$, and $\mathcal{A}_o$. The dark green line is the impulse response function drawn from a single Q^* that is closest to the pointwise median in a sum of squares sense (median target method of Fry and Pagan (2007)).

C.1.9 Comparison of posterior median and median target method

We present a comparison between the posterior pointwise median and the median target method of Fry and Pagan (2007) as measures of central tendency of the credible set. The discussion of our implementation of the median target method can be found in the "Point estimator" subsection of section A.1 (Fully Bayesian approach with a flat prior).

Figure A-15 shows a comparison between the posterior pointwise median response (dark solid red line) and the response using the median target method for a financial uncertainty.[6] To give a sense of the scale of uncertainty around the IRFs, we also show the 70% credible sets assuming a conditional Haar prior, which give us the tightest credible sets among the methods we consider. We find that differences between the posterior pointwise median response and the median target method response is negligible.

[6]The results from the macro uncertainty shock (not shown) convey the same picture.

Figure A-15 **Posterior results:**
Financial uncertainty shock on level variables (Haar)

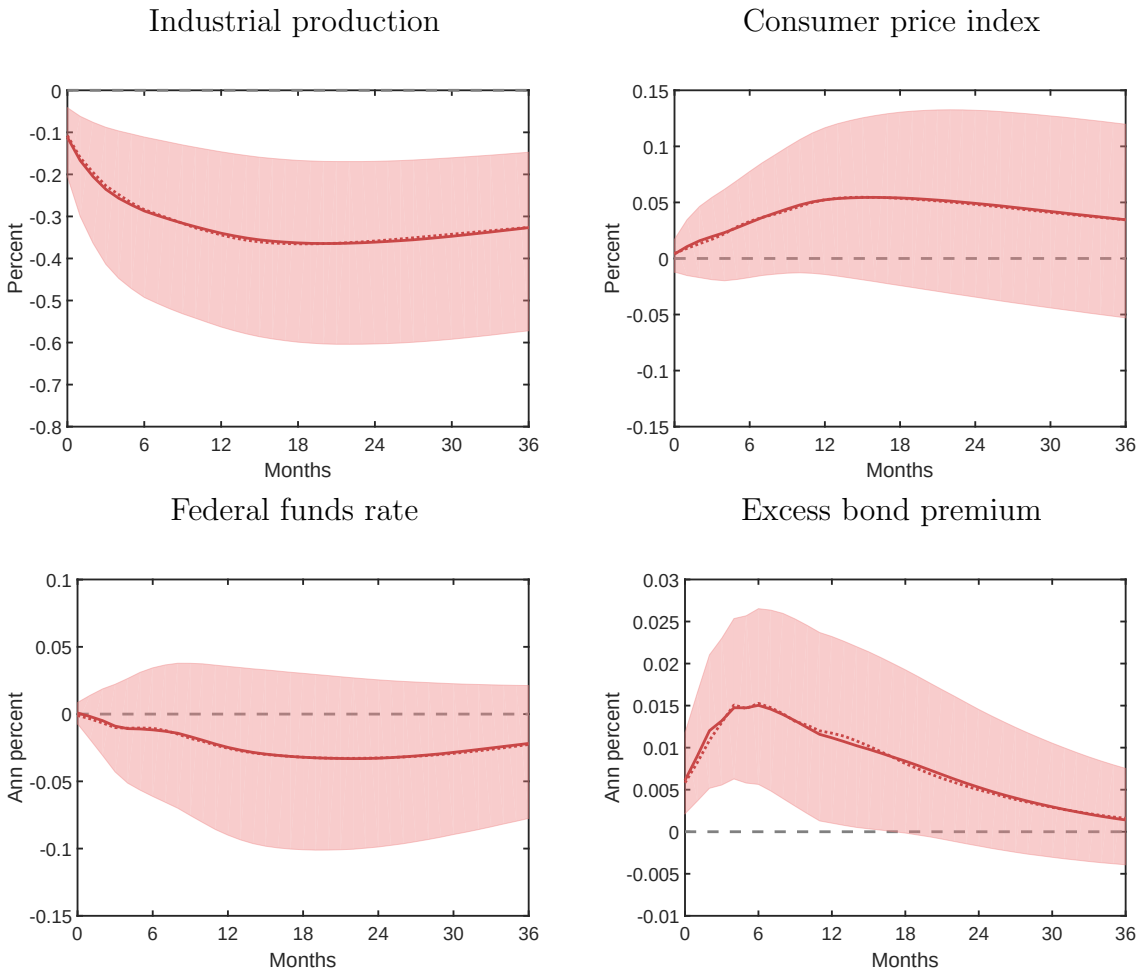

This figure shows the pointwise 70% credible set impulse response functions on the level variables to a 1 standard deviation macro uncertainty shock for the small VAR model. We assume a Haar prior over the rotation matrices. We only keep the impulse response functions that satisfy Assumptions $\mathcal{A}_{uf}, \mathcal{A}_{um}$, and $\mathcal{A}_o$. The dark red line is the pointwise median response. The dark red dotted line is the impulse response function drawn from a single Q^* that is closest to the pointwise median in a sum of squares sense (median target method of Fry and Pagan (2007)).

C.1.10 The identified set at the posterior mean

To give a further sense of the impact of the Haar prior on our results, we present a comparison of the identified set and the 70% credible bands implied by the Haar prior at the posterior mean (Moon et al. (2017)).[7]

[7] We take 20,000 Q proposals from a Haar distribution. We construct the identified set as the maximum and minimum of the accepted proposals.

Figure A-16 **Financial uncertainty shock on level variables (Haar prior vs identified set at the posterior mean)**

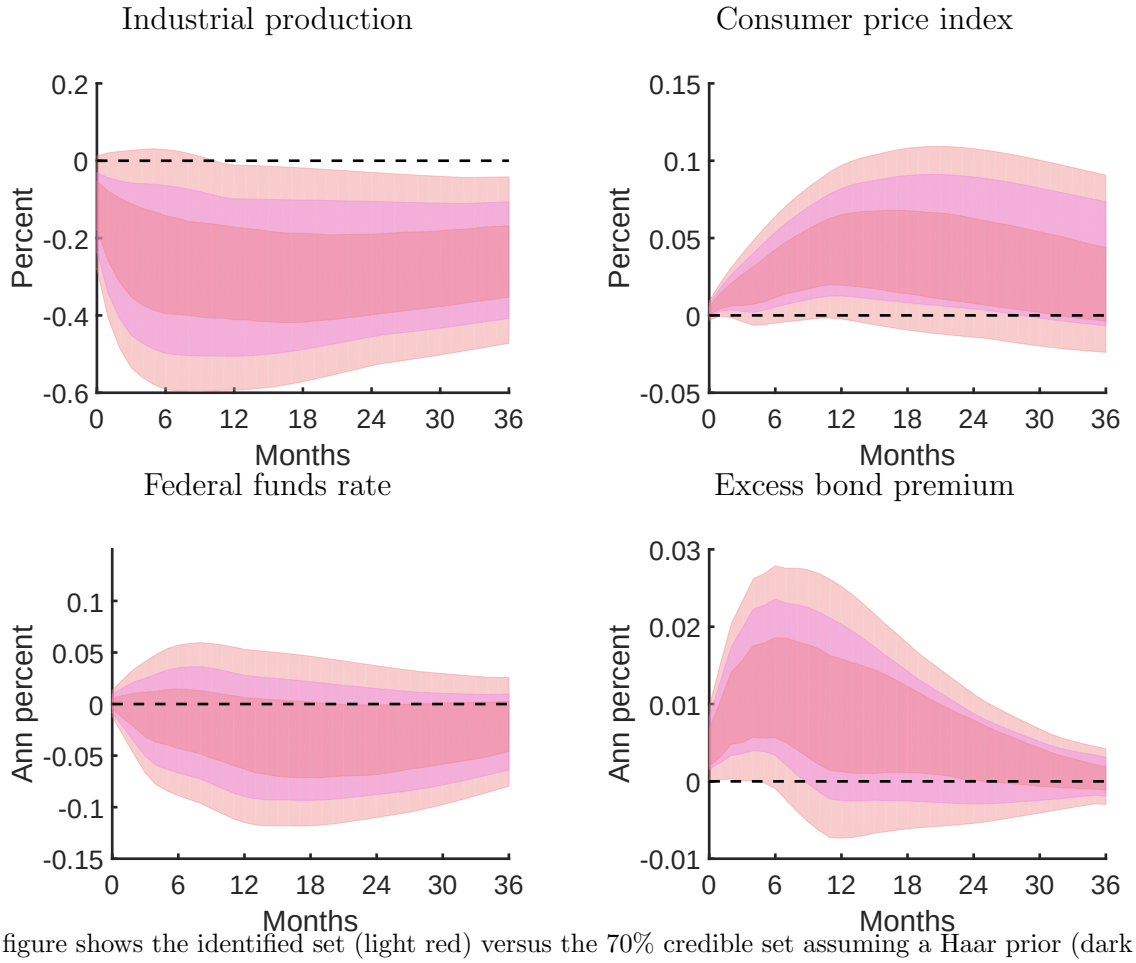

This figure shows the identified set (light red) versus the 70% credible set assuming a Haar prior (dark red) impulse response functions on the level variables to a 1 standard deviation financial uncertainty shock for the small VAR model. The pink shaded area represents a hypothetical "middle 70%" of the identified set at every horizon. To construct the pink shaded area, for each horizon, we find the midpoint of the identified set and then add/subtract 35% of the total length of the identified set to each side of the midpoint. The reduced-form parameters are fixed at their posterior means. We only keep the impulse response functions that satisfy Assumptions $\mathcal{A}_{uf}, \mathcal{A}_{um}$, and $\mathcal{A}_o$.

Figure A-16 shows the identified sets at the posterior mean for a financial uncertainty shock (light red interval). No movement in industrial production is consistent with the financial uncertainty shock for the first year after the shock. The identified set begins to shrink in the medium and long run, however, with the set lying between -0.03% and -0.53% after two years. There is marginal evidence of an increase in the CPI for around 1 year financial uncertainty shock, although the effect in the long run appears transient.

Figure A-17 **Macro uncertainty shock on level variables (Haar prior vs identified set at the posterior mean)**

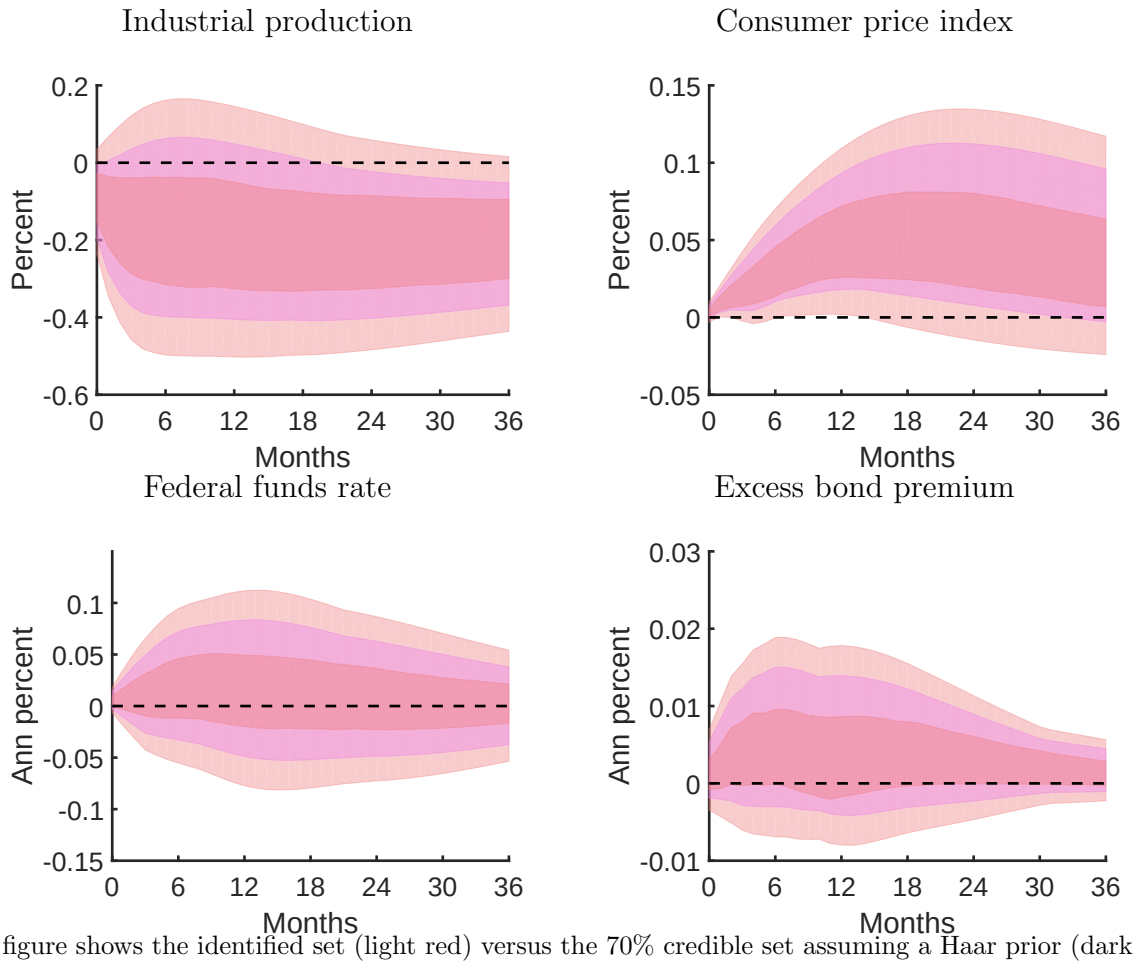

This figure shows the identified set (light red) versus the 70% credible set assuming a Haar prior (dark red) impulse response functions on the level variables to a 1 standard deviation financial uncertainty shock for the small VAR model. The pink shaded area represents a hypothetical "middle 70%" of the identified set at every horizon. To construct the pink shaded area, for each horizon, we find the midpoint of the identified set and then add/subtract 35% of the total length of the identified set to each side of the midpoint. The reduced-form parameters are fixed at their posterior means. We only keep the impulse response functions that satisfy Assumptions $\mathcal{A}_{uf}, \mathcal{A}_{um}$, and $\mathcal{A}_o$.

The identified set of the federal funds rate response also includes 0%, although a decline of around -0.12% is also consistent with the data. Finally, the identified set of the EBP response shows the looseness of the sign restriction. The EBP increases on impact, with values ranging from near 0% to 0.011% all possible. After 5 months, however, the identified set includes 0%.

Figure A-17 shows the results from a macro uncertainty shock. The identified sets are

similarly wide. Comparing these identified sets to those from a financial uncertainty shock, we see evidence that the macro uncertainty shock's identified set of the IRF is consistent with no response in industrial production for the entire horizon considered. After one year, the magnitudes of the difference between the identified sets are substantial as well: the identified set is between -0.59% and -0.01% for the financial uncertainty shock versus -0.50% and 0.15% for the macro uncertainty shock. Moreover, the macro uncertainty shock's identified set for the federal funds rate is more symmetric as well, with relatively equal amounts of mass placed on increases and decreases. The identified set on the excess bond premium is likewise wide around 0%.

The darker red shaded areas show the 70% credible sets at the posterior mean assuming a Haar prior. By comparing the darker red areas with the lighter red ones, we get a sense of how much information the Haar prior is introducing. In our case, we see that the Haar prior credible sets of the IRFs are tighter than the identified sets, as would be expected when introducing a prior distribution for Q. It is the case, however, that the IRFs assuming a Haar prior generally maintain the same shape as the identified sets and generally shrink the upper and lower bounds of the set by approximately equal amounts.

Another useful comparison to show these facts is by comparing the dark red area to the pink shaded area. This pink shaded area is a hypothetical pointwise "middle 70%" of the identified set. A way to interpret this interval is if one were to assume a uniform prior over the length of the identified set at each horizon of the IRF, this set would be the 70% credible set over this prior. One important point to emphasize is that this set in fact does not correspond to any prior distribution over the rotation matrix, in accordance with the results of Baumeister and Hamilton (2015). It is simply a way to compare the Haar prior assumption with an impossible "uniform prior at every horizon" IRF. One sees that indeed the Haar prior induces a tighter credible set relative to this uniform benchmark. However, one can more clearly see that the Haar prior preserves the general shape of the IRFs and it also in general places most of its mass near the center of the identified set.

Before we close the discussion on the comparison, it is important to point out that the basic qualitative conclusions about the relative effects of financial and macro uncertainty shocks continue to hold whether one looks at the identified set at the posterior mean or the Haar prior conditional on the posterior mean of ψ. The identified sets for the financial uncertainty shock are shifted lower for industrial production and the federal funds rate relative to those for the macro uncertainty shock.

Figure A-18 **Posterior results:**
Financial uncertainty shock on level variables (Prior robust)

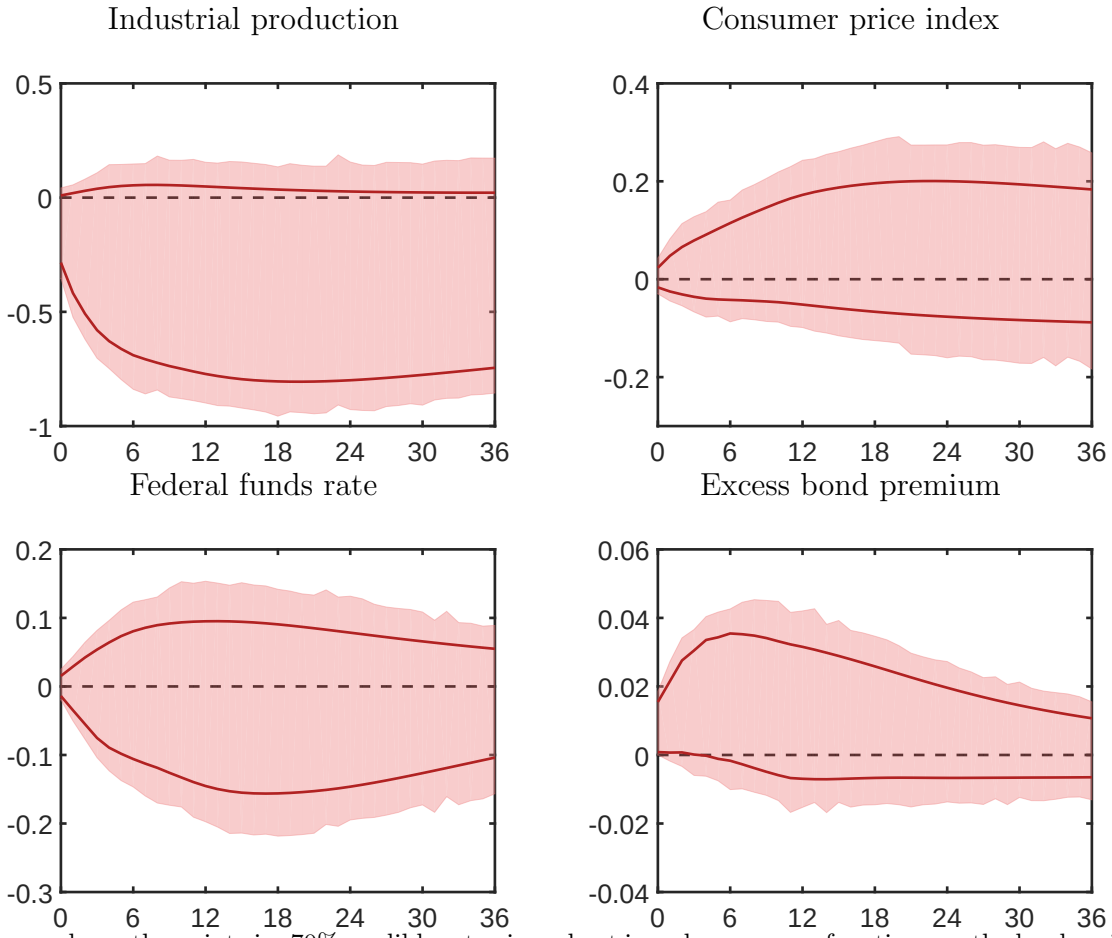

This figure shows the pointwise 70% credible set prior robust impulse response functions on the level variables to a 1 standard deviation financial uncertainty shock for the small VAR model. The reduced-form parameters are drawn from their posterior distributions. We only keep the impulse response functions that satisfy Assumptions $\mathcal{A}_{uf}, \mathcal{A}_{um}$, and $\mathcal{A}_o$. The dark red line is the posterior mean bounds.

C.1.11 Prior robust results

In this subsection, we keep the same set of sign restrictions (Assumptions $\mathcal{A}_{uf}$, $\mathcal{A}_{um}$, and $\mathcal{A}_o$), but instead of assuming a Haar prior over the rotation matrices, we assume a prior robust setup as in Giacomini and Kitagawa (2015).

Insisting on robustness to all possible priors over the rotation matrices widens the credible

Figure A-19 **Posterior results:**
Macro uncertainty shock on level variables (Prior robust)

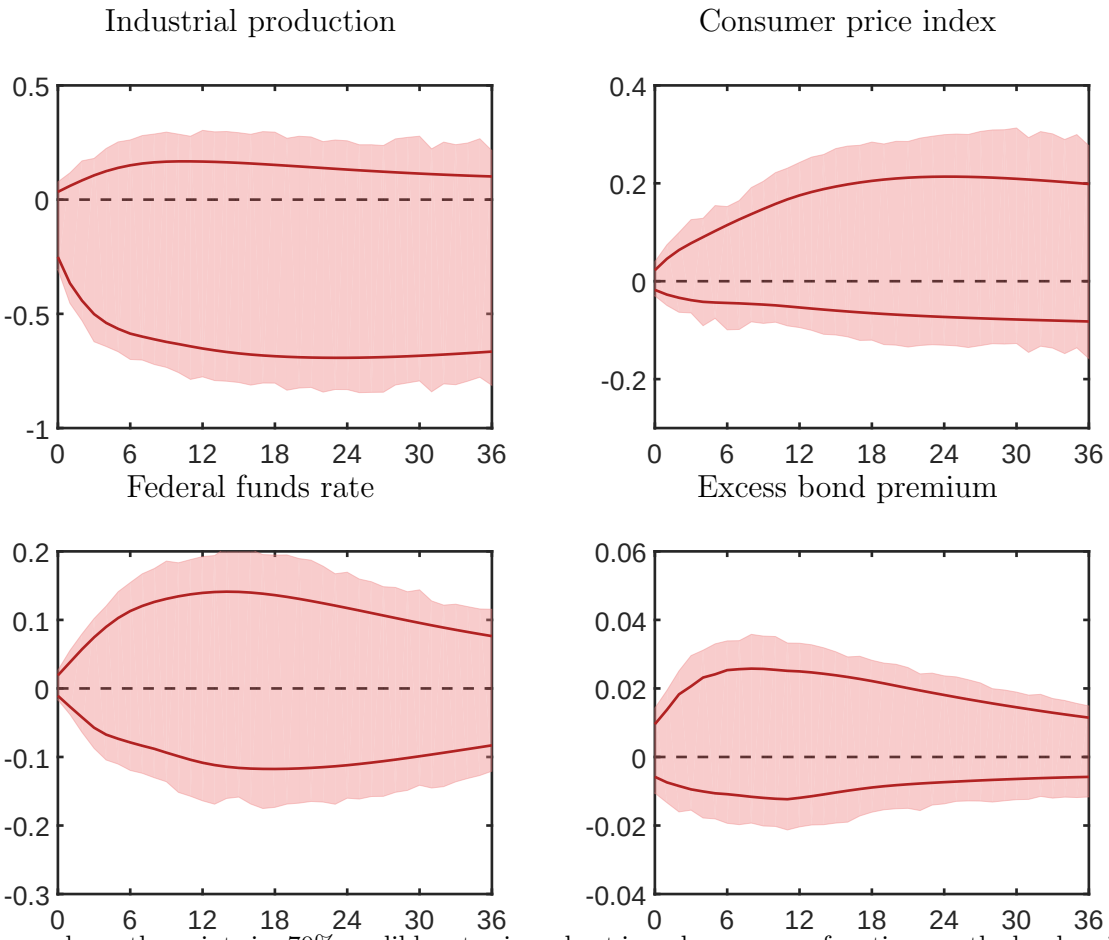

This figure shows the pointwise 70% credible set prior robust impulse response functions on the level variables to a 1 standard deviation macro uncertainty shock for the small VAR model. The reduced-form parameters are drawn from their posterior distributions. We only keep the impulse response functions that satisfy Assumptions $\mathcal{A}_{uf}, \mathcal{A}_{um}$, and $\mathcal{A}_o$. The dark red line is the posterior mean bounds.

sets of the IRFs for both financial and macro uncertainty shocks. Looking at figures A-18 and A-19, we see that all impulse response functions now cover 0% for both uncertainty shocks. This result underscores the importance of measuring financial and macro volatility well when applying prior robust sign restrictions, which is the motivating reason for us to consider a large-scale volatility model as in Carriero et al. (2017). A less accurate measure of volatility may make inference of its real effects more uncertain, which additionally widens the credible sets.

Nevertheless, when comparing the credible sets between the two uncertainty shocks, the

important qualitative conclusions from our results in the main text continue to hold. The credible sets of industrial production and the federal funds rate responses are shifted downwards following a financial uncertainty shock when compared to a macro uncertainty shock. Therefore, we can still say that there is more evidence that a financial uncertainty shock leads to a decline in the economy relative to a macro uncertainty shock.

C.1.12 Alternative scaling of IRF

In the main draft of the paper, we present impulse response functions to 1 standard deviation financial and macro uncertainty shocks. By considering 1 standard deviation structural shocks, we compare structural shocks with equal size. An alternative empirical exercise we perform is to investigate the effects of financial and macro uncertainty shocks that lead to equal increases in average volatility (i.e., equal impact). We do this by adjusting the size of the structural shocks such that they lead to, on average, 10% increases in the volatilities (variance) on impact of observables. More specifically, we set the size of the i-th uncertainty shock to s_i such that the following relationship holds:

$$10\% = \frac{1}{n}\sum_{j=1}^{n}\left(\frac{E[h_{j,t}|v_{i,t}^{*}=s_i;R_t,\psi]-E[h_{j,t}|v_{i,t}^{*}=0;R_t,\psi]}{E[h_{j,t}|v_{i,t}^{*}=0;R_t,\psi]}\times 100\right), \tag{A.34}$$

where $R_t = chol(\Omega(h_{t-1};\omega))Q$ and $Q \in \mathbb{Q}(\psi,\mathcal{R})$. This normalization scheme implies that the average (across observables) percentage point impact of financial and macro uncertainty shocks are the same in the initial period.

As we will see below, this alternative exercise enables us to further decompose the difference in effects of financial and macro uncertainty shocks. We note that structural financial uncertainty shocks lead to larger increases in average volatility relative to the same-sized structural macro uncertainty shock.[8] We view this as an outcome of the estimation in con-

[8]Figure A-20 shows the distributions of the scaling factors s_i for the financial and macro uncertainty shocks assuming a conditional Haar prior. That the distribution of the scaling factor for the macro uncertainty shocks is to the right of the one for the financial uncertainty shocks means that larger structural macro

Figure A-20 **Posterior results:**
Histogram of scaling factors (Blue: s_i for financial uncertainty shocks, Red: s_i for macro uncertainty shocks) (Haar)

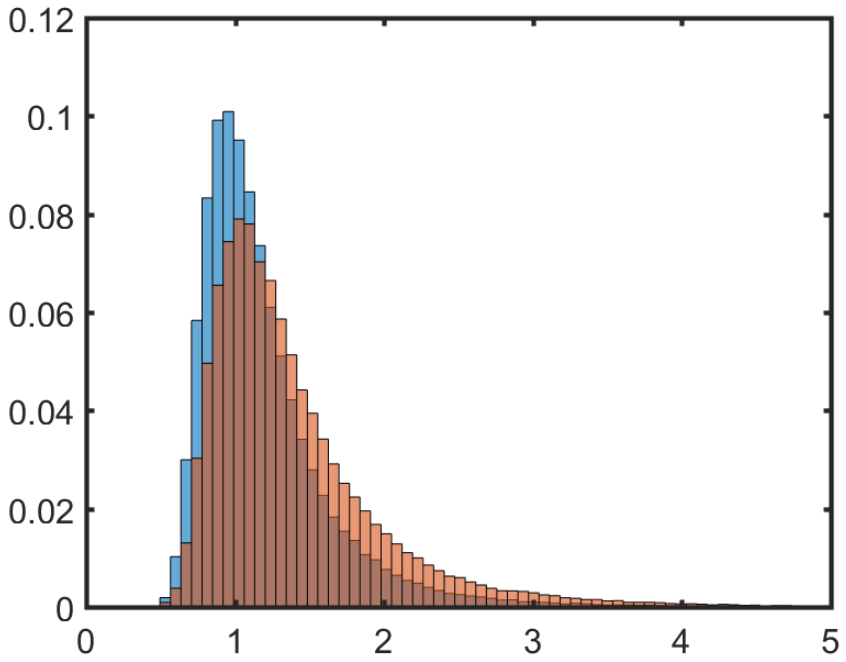

This figure shows the posterior distributions of the scaling factors s_i needed for financial (blue) and macro (red) uncertainty shocks to produce 10% average increases in volatility.

junction with our identifying assumptions for the two structural uncertainty shocks. In this exercise, however, we ask: given the same increase in average volatility, how large are the real effects of financial and macro uncertainty shocks? We continue to find more evidence that financial uncertainty shocks lead to declines in industrial production relative to macro uncertainty shocks. These results suggest that the more negative real effects from financial uncertainty shocks not only come from the fact that they produce larger increases in average volatility, but also because the composition of the volatility increases implied by the sign restrictions are more impactful to the real economy.

It is important to remember, however, that even though this exercise is quite useful to understand our main empirical results, it is difficult to map these results into a statement

uncertainty shocks are needed to hit the 10% average volatility increase. The same qualitative picture holds for the prior robust results.

about the current and future impact of financial and macro uncertainty shocks on the U.S. economy, as these 10% average increases in volatility are generated by potentially different-sized structural uncertainty shocks (as figure A-20 also shows). Specifically, in simulations from the model economy, the plausibility or likelihood of seeing such increases in volatility may differ across the structural shocks.

In this section, we consider the small-scale VAR (example 1 in the main text), and present IRFs based on the fully Bayesian approach with the conditional Haar prior as well as the robust Bayesian approach.

Results. Figure A-21 shows the 70% credible set effects of financial and macro uncertainty shocks that lead to 10% average increases in volatility, assuming a conditional Haar prior. Our main results remain true in that the effects of financial uncertainty shocks on IP are larger than those of macro uncertainty shocks even after the average volatility normalization.

Figure A-22, which shows the 70% prior robust credible set effects of such uncertainty shocks, tells us that this result is not driven by the Haar prior. By imposing our sign restrictions, the 70% prior robust credible set for IP to the financial uncertainty shocks truncates the positive region more aggressively, which leads to the differences we see in the IRFs in figure A-21. However, the lower bounds of the prior robust credible sets become more similar, which is different from what we find in the IRFs that specify equal-sized structural uncertainty shocks (figures A-17 and A-18).

In percentage point terms, financial uncertainty shocks tend to increase EBP volatility relatively more than they increase the volatilities of the other variables. The same is not true for macro uncertainty shocks that have the same average volatility impact. This larger relative increase in spread volatility leads to more evidence of a decline in industrial production following financial uncertainty shocks.

In sum, our main finding that financial uncertainty shocks have larger negative effects on IP is driven by two factors. First, controlling for the volatility size of the uncertainty

Figure A-21 **Posterior results:**
Effects of uncertainty shocks that lead to a 10% average increase in volatility (Haar)

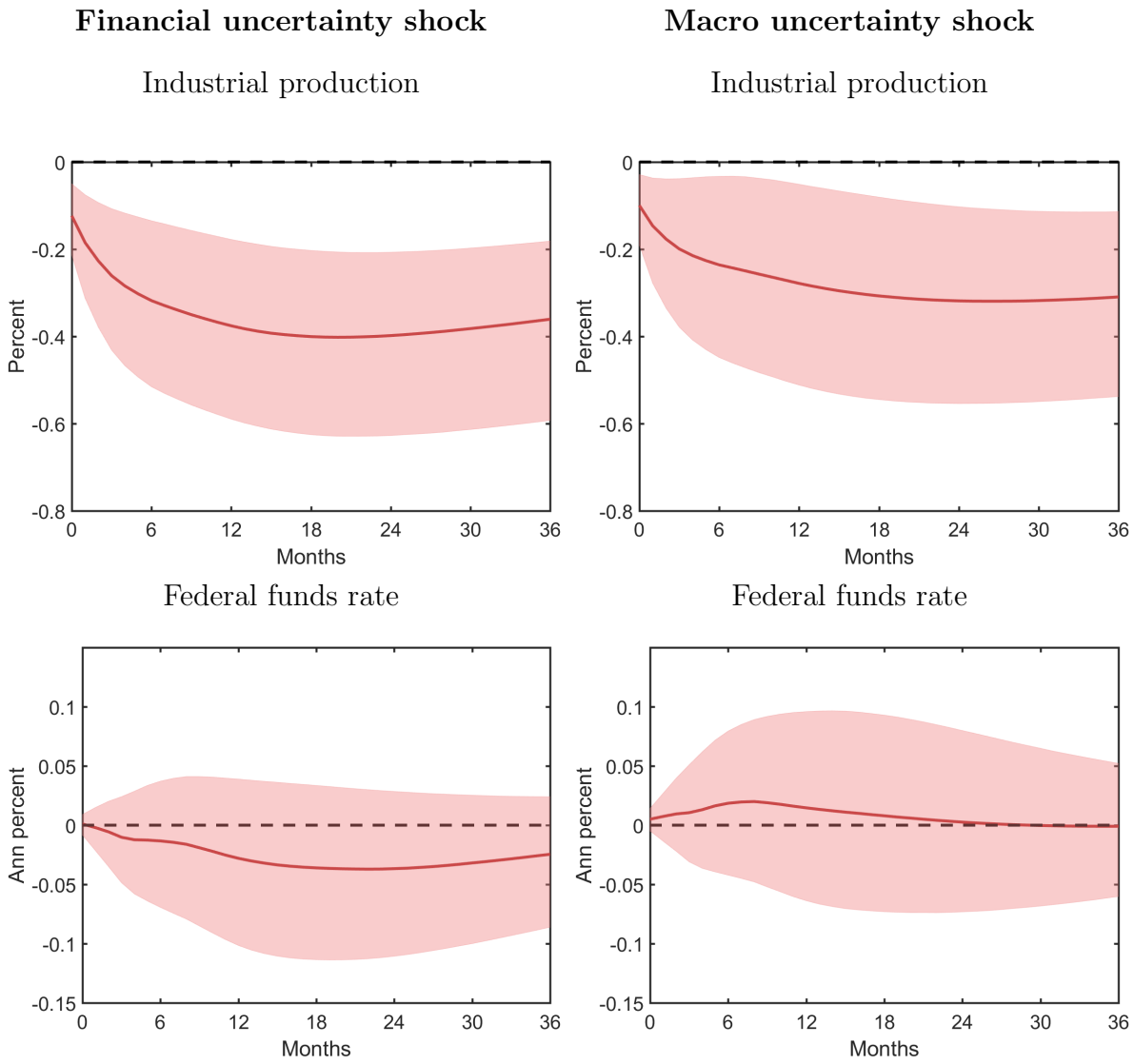

This figure shows the pointwise median and 70% credible set impulse response functions on industrial production to a a financial and macro uncertainty shock that each lead to a 10% increase in industrial production volatility (variance) for the small VAR model. We assume a Haar prior over the rotation matrices. The reduced-form parameters are drawn from their posterior distributions.

shocks, the composition of the increase in volatility from financial uncertainty shocks rule out positive responses of IP. Second, a one standard deviation financial uncertainty shock leads to a larger overall volatility response and lowers the lower bound of the IP responses.

Figure A-22 **Posterior results:**
Effects of uncertainty shocks that lead to a 10% average increase in volatility (Prior robust)

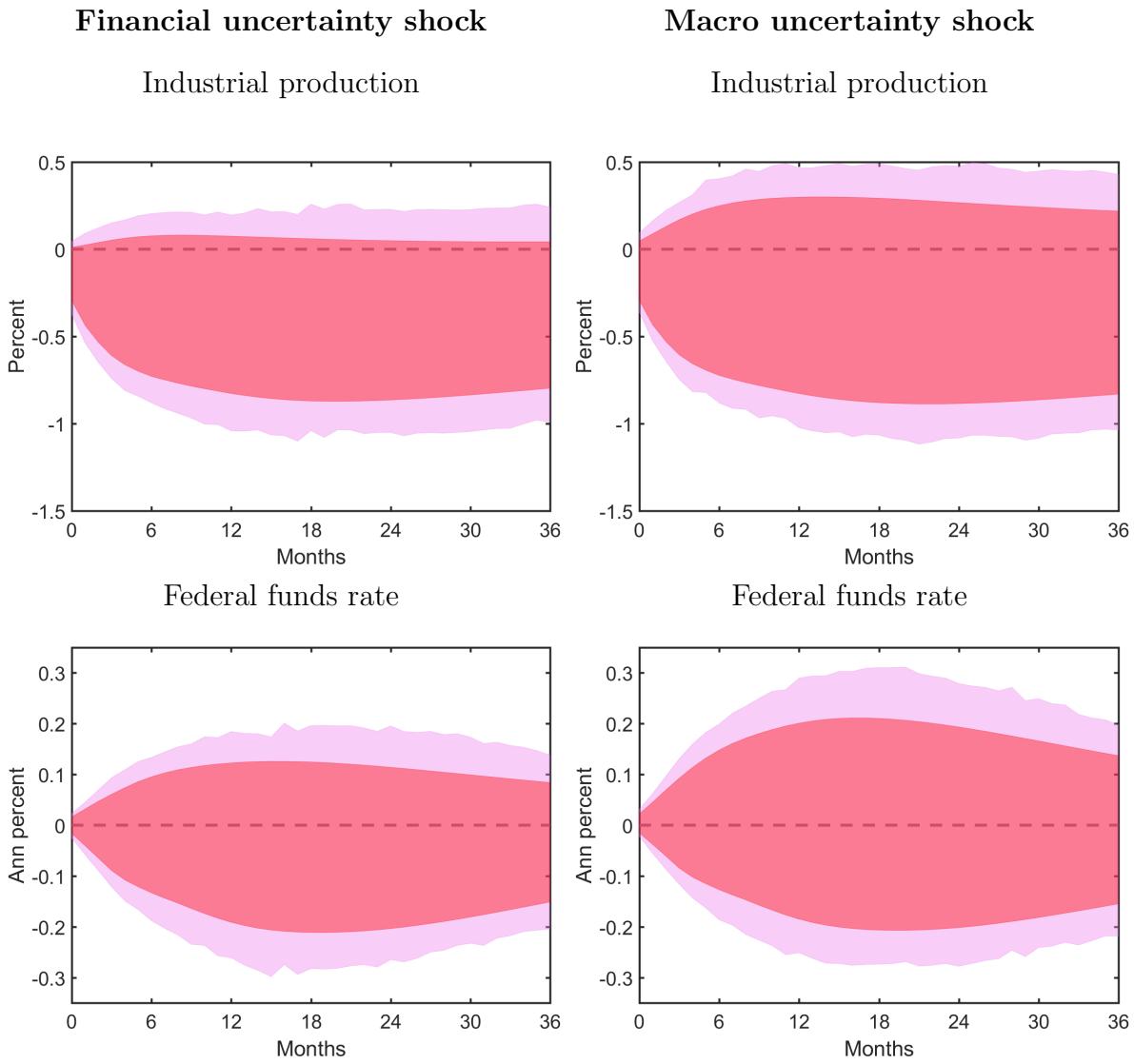

This figure shows the pointwise 70% credible set prior robust impulse response functions (light pink) on industrial production to a a financial and macro uncertainty shock that each lead to a 10% average increase in volatility (variance) for the small VAR model. We present the pointwise posterior mean bounds (dark pink). The reduced-form parameters are drawn from their posterior distributions.

C.1.13 Results from a traditional sign restriction on the EBP response

An alternative sign restriction that we consider is one on the signs of the EBP response to the two uncertainty shocks. Specifically, we consider the following sign restriction:

Assumption $\mathcal{A}^3_{uf}$ (Financial uncertainty shock). The uncertainty shock satisfies $\mathcal{A}^3_{uf,1}$ and $\mathcal{A}^3_{uf,2}$:

$$\mathcal{A}^3_{uf,1} : IRF[\Sigma_{ii,t+h}|v^*_t = e_1; R_t] > 0 \text{ for } h = 0 \text{ and } i = 1, 2, 3, 4.$$

$$\mathcal{A}^3_{uf,2} : IRF[EBP_{t+h}|v^*_t = e_1; R_t] > 0 \text{ for } h = 0,\ 1,\ 2.$$

Assumption $\mathcal{A}^3_{um}$ (Macro uncertainty shock). The uncertainty shock satisfies $\mathcal{A}^3_{um,1}$ and $\mathcal{A}^3_{um,2}$:

$$\mathcal{A}^3_{um,1} : IRF[\Sigma_{ii,t+h}|v^*_t = e_2; R_t] > 0 \text{ for } h = 0 \text{ and } i = 1, 2, 3, 4.$$

$$\mathcal{A}^3_{um,2} : IRF[EBP_{t+h}|v^*_t = e_2; R_t] < 0 \text{ for } h = 0,\ 1,\ 2.$$

Assumption $\mathcal{A}^3_o$ (Other second moment shocks).

$$\mathcal{A}^3_0 : \text{For each } j \neq 1, 2, \text{ at least one of the conditions specified in}$$

$$\mathcal{A}^3_{uf,1}, \mathcal{A}^3_{uf,2} \text{and at least one in } \mathcal{A}^3_{um,1}, \mathcal{A}^3_{um,2} \text{ does not hold.}$$

This assumption says that a financial uncertainty shock must increase the EBP for 2 months in addition to increasing aggregate volatility on impact. On the other hand, a macro uncertainty shock decreases the EBP for 2 months in addition to increasing aggregate volatility on impact. Similar to Example 1 in the main text, we impose an additional assumption $\mathcal{A}^3_o$ to ensure that there within each Q we consider, there is a unique financial and macro uncertainty shock.

The motivation for this sign restriction is similar to that for the sign restriction in the main text. Namely, through the lens of a structural model with financial frictions, insofar as a financial uncertainty shock reduces the incentive to invest and a macro uncertainty shock increases the incentive to invest, spreads should increase from a financial uncertainty shock and decrease from a macro uncertainty shock.

Prior implications for the impulse response functions Figures A-23 and A-24 show the prior-implied level impulse response functions following a financial and macro uncertainty shock, respectively. There are several important similarities between these IRFs and those from the sign restrictions in the main text. First, it is still the case that our sign restrictions do not bias the sign of the responses on IP, the CPI, or the federal funds rate. There is still a bias in the excess bond premium from the sign restriction. Indeed, as the sign restrictions on the EBP are assumed to hold for 2 months after the financial or macro uncertainty shocks, the lower 5% (upper 95%) bounds of the credible sets after the financial and macro uncertainty shocks reach 0.01 (-0.01%) by month 2, thereby ruling out smaller responses of the EBP to the two uncertainty shocks. By the third and fourth months, however, the credible sets begin to include both positive and negative responses in the EBP, although the effects of the sign restrictions still remain.

Figures A-25 and A-26 show the log volatility responses to the two uncertainty shocks. Like before, the prior puts mass on a wide range of responses to both uncertainty shocks.

There is an important difference from before, however, in the prior behavior of the IRFs with the alternative sign restrictions. Specifically, a financial uncertainty shock now no longer leads to larger increases in volatility relative to a macro uncertainty shock. This is because a financial uncertainty shock no longer must lead to a larger increase in the EBP than a macro uncertainty shock does. It is this relative sign restriction that tends to generate larger volatility moves following a financial uncertainty shock. This has implications for the width of the level IRFs as well. We note that the alternative sign restriction does not lead to a looser IRF restriction for the financial uncertainty shock when compared to the macro uncertainty shock. Indeed, financial and macro uncertainty shocks both have a $5\% - 95\%$ range of around 1.6%.

Posterior results Figures A-27 and A-28 show the posterior results from the two uncertainty shocks. Many of the same qualitative conclusions continue to hold. For instance, a

Figure A-23 **Prior results:**
Financial uncertainty shock on level variables (Haar)

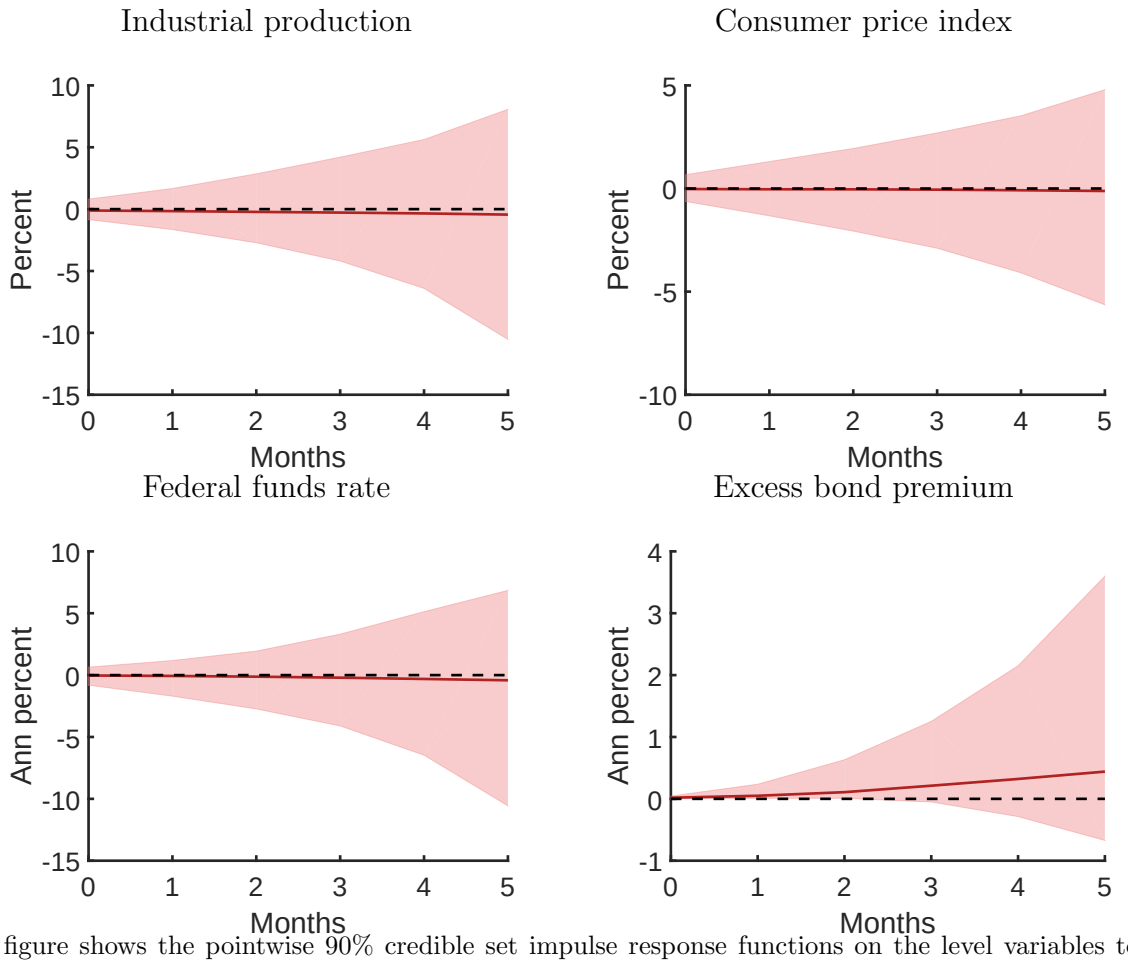

This figure shows the pointwise 90% credible set impulse response functions on the level variables to a 1 standard deviation financial uncertainty shock for the small VAR model. The reduced-form parameters are drawn from their prior distributions. We assume a Haar prior over the rotation matrices. We only keep the impulse response functions that satisfy Assumptions $\mathcal{A}^3_{uf}, \mathcal{A}^3_{um}, \mathcal{A}^3_{o}$. The dark red line is the impulse response function drawn from a single Q^* that is closest to the pointwise median in a sum of squares sense (median target method of Fry and Pagan (2007)).

financial uncertainty shock leads to a deeper and more immediate decline in industrial production when compared to a macro uncertainty shock. In fact, for the first two years after the macro uncertainty shock, the 70% credible set contains 0%. Additionally, the second panels of the two figures show that both uncertainty shocks continue to have little impact on the CPI.

Although the federal funds rate movements are not significant following either the financial or macro uncertainty shock, we do find that there is more evidence of a decline in the federal

Figure A-24 **Prior results:**
Macro uncertainty shock on level variables (Haar)

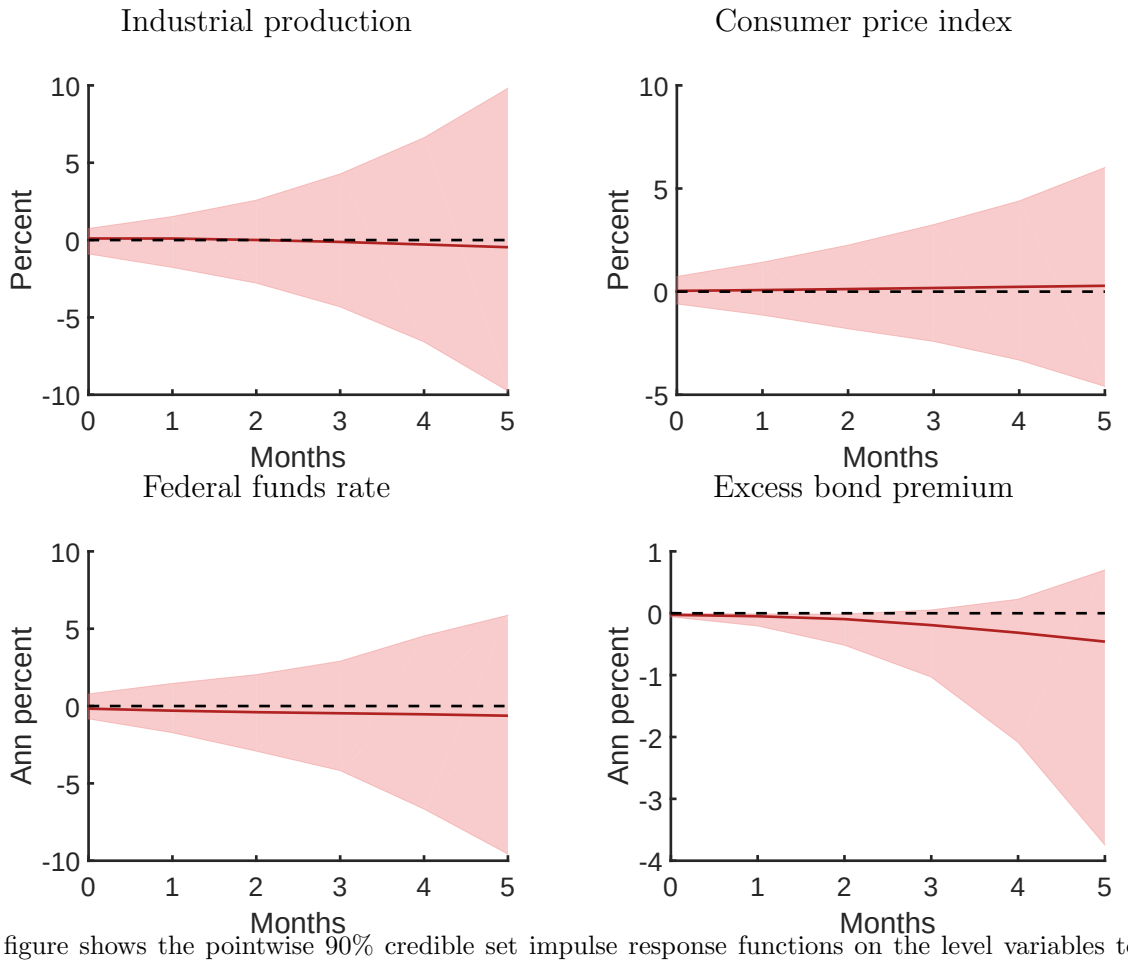

This figure shows the pointwise 90% credible set impulse response functions on the level variables to a 1 standard deviation financial uncertainty shock for the small VAR model. The reduced-form parameters are drawn from their prior distributions. We assume a Haar prior over the rotation matrices. We only keep the impulse response functions that satisfy Assumptions $\mathcal{A}^3_{uf}, \mathcal{A}^3_{um}, \mathcal{A}^3_o$. The dark red line is the impulse response function drawn from a single Q^* that is closest to the pointwise median in a sum of squares sense (median target method of Fry and Pagan (2007)).

funds rate following a financial uncertainty shock. The posterior median decline is around -0.03% after 2 years. In contrast, the posterior median shows an increase in the federal funds rate of over 0.05% following a macro uncertainty shock.

One final interesting note is the response of the EBP to the two uncertainty shocks. While the sign restrictions separating the financial and macro uncertainty shocks are symmetric, we do find a different posterior response across the two uncertainty shocks. A financial uncertainty shock leads to a persistent increase in the excess bond premium. The 70%

Figure A-25 **Prior results:**
Financial uncertainty shock on log volatility of innovations (Haar)

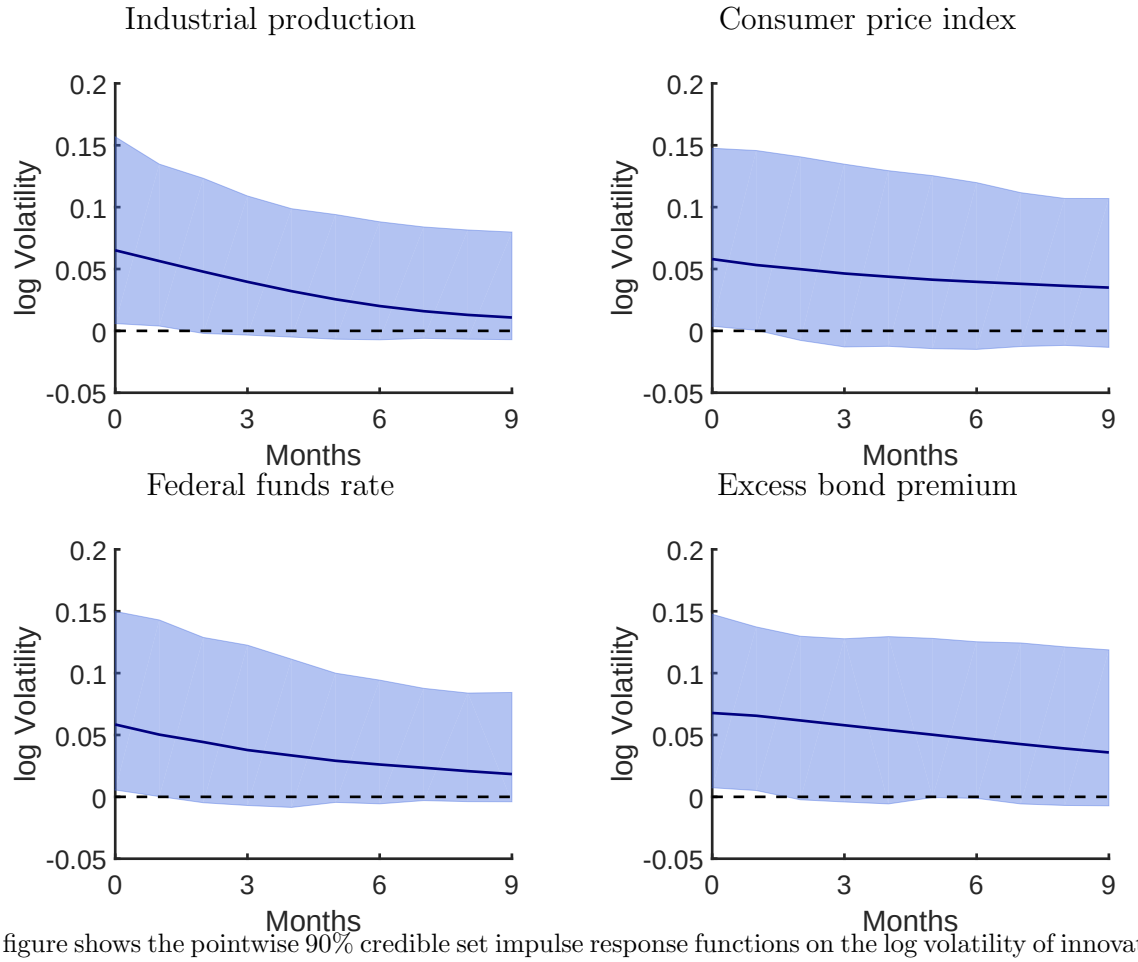

This figure shows the pointwise 90% credible set impulse response functions on the log volatility of innovations to a 1 standard deviation financial uncertainty shock for the small VAR model. The reduced-form parameters are drawn from their prior distributions. We assume a Haar prior over the rotation matrices. We only keep the impulse response functions that satisfy Assumptions $\mathcal{A}^3_{uf}, \mathcal{A}^3_{um}, \mathcal{A}^3_o$. The dark blue line is the impulse response function drawn from a single Q^* that is closest to the pointwise median in a sum of squares sense (median target method of Fry and Pagan (2007)).

credible sets do not include 0% nearly one year. On the other hand, a macro uncertainty shock leads to a much more transitory decline in the EBP. After 3 months, the impulse response function includes 0% at the 70% level.

Finally, we also look at the volatility responses to the two uncertainty shocks, shown in figures A-29 and A-30. Relative to a macro uncertainty shock, a financial uncertainty shock produces a larger and more persistent response in EBP volatility. The volatility movements for innovations in the other three series are generally similar, although there is evidence of

Figure A-26 **Prior results:**
Macro uncertainty shock on log volatility of innovations (Haar)

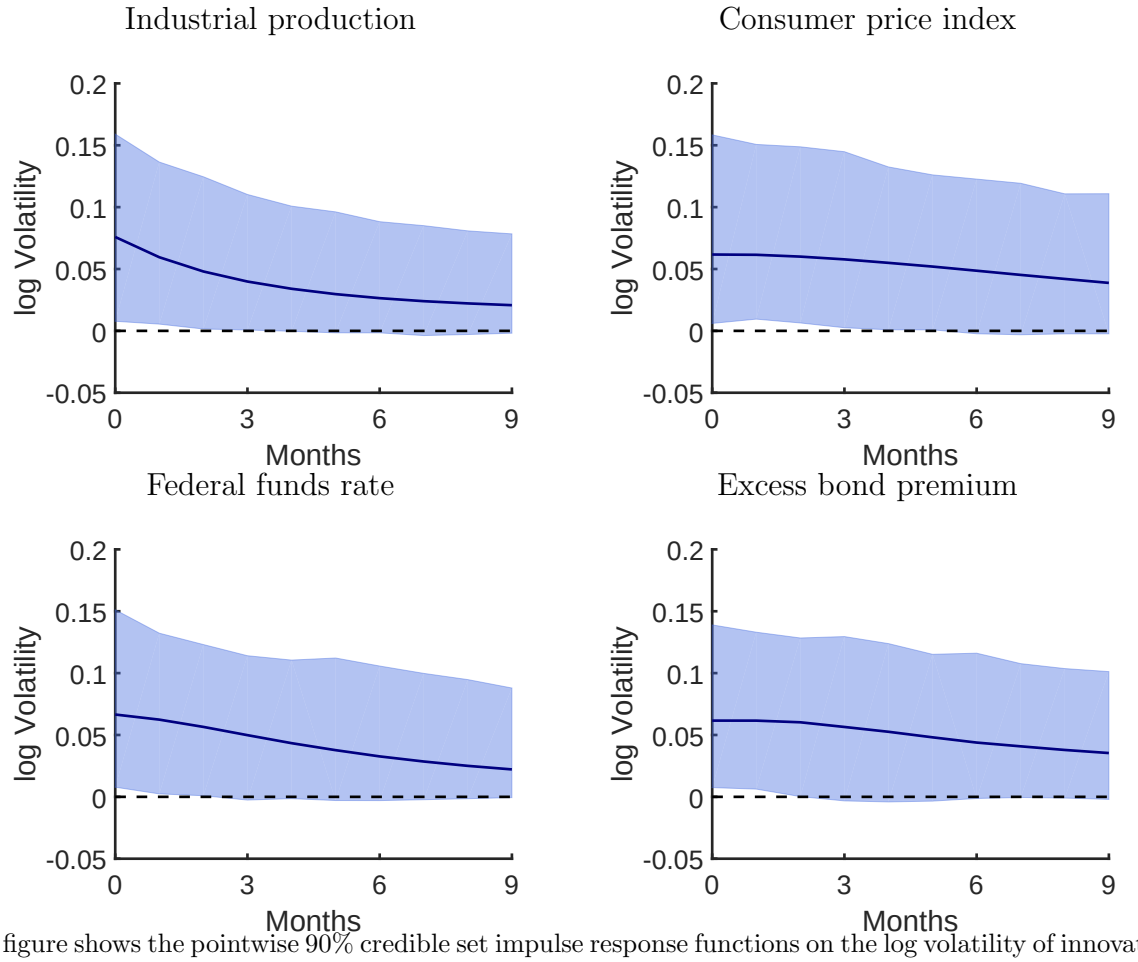

This figure shows the pointwise 90% credible set impulse response functions on the log volatility of innovations to a 1 standard deviation macro uncertainty shock for the small VAR model. The reduced-form parameters are drawn from their prior distributions. We assume a Haar prior over the rotation matrices. We only keep the impulse response functions that satisfy Assumptions $\mathcal{A}^3_{uf}, \mathcal{A}^3_{um}, \mathcal{A}^3_o$. The dark blue line is the impulse response function drawn from a single Q^* that is closest to the pointwise median in a sum of squares sense (median target method of Fry and Pagan (2007)).

a larger movement in federal funds rate volatility following a macro uncertainty shock.

Figure A-27 **Posterior results:**
Financial uncertainty shock on level variables (Haar)

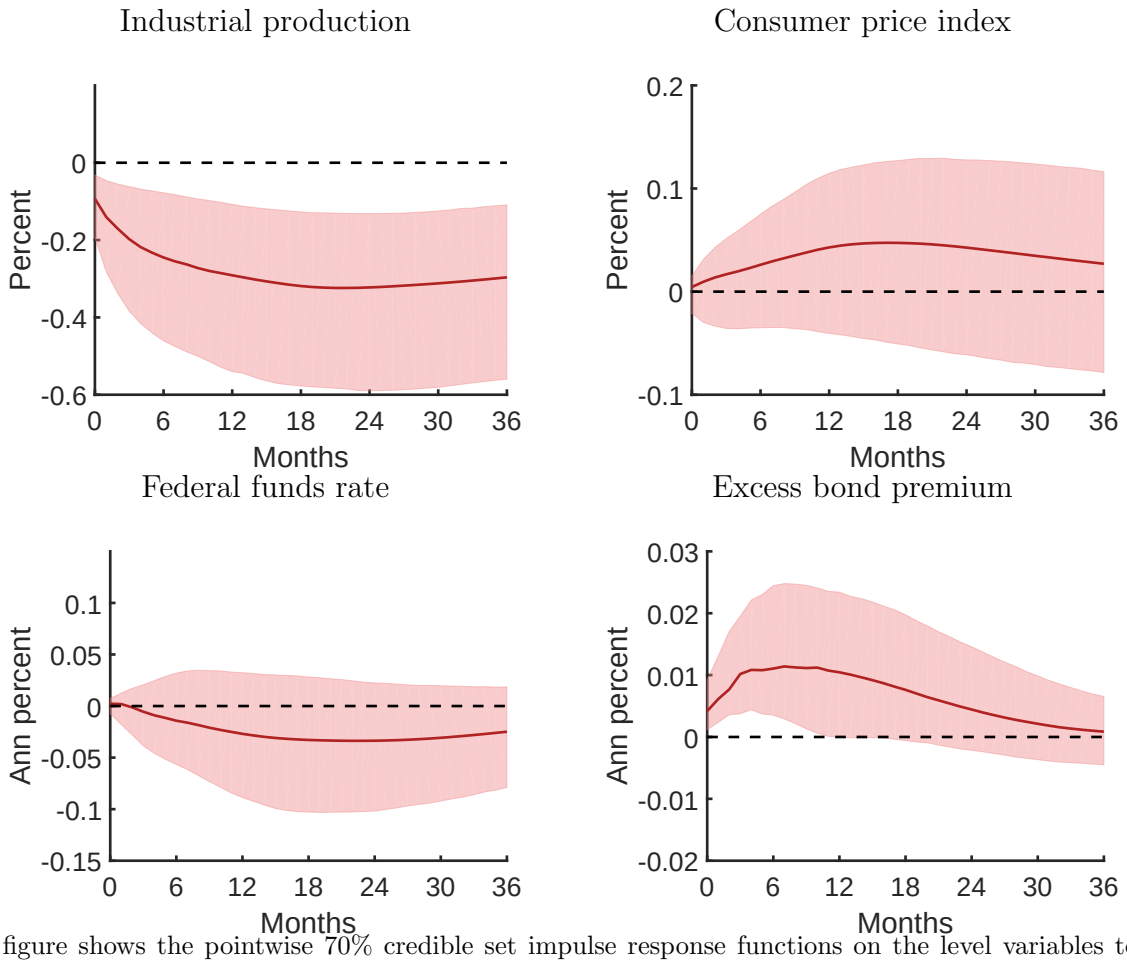

This figure shows the pointwise 70% credible set impulse response functions on the level variables to a 1 standard deviation financial uncertainty shock for the small VAR model. The reduced-form parameters are drawn from their posterior distributions. We assume a Haar prior over the rotation matrices. We only keep the impulse response functions that satisfy Assumptions $\mathcal{A}^3_{uf}, \mathcal{A}^3_{um}, \mathcal{A}^3_{o}$. The dark red line is the impulse response function drawn from a single Q^* that is closest to the pointwise median in a sum of squares sense (median target method of Fry and Pagan (2007)).

Figure A-28 **Posterior results:**
Macro uncertainty shock on level variables (Haar)

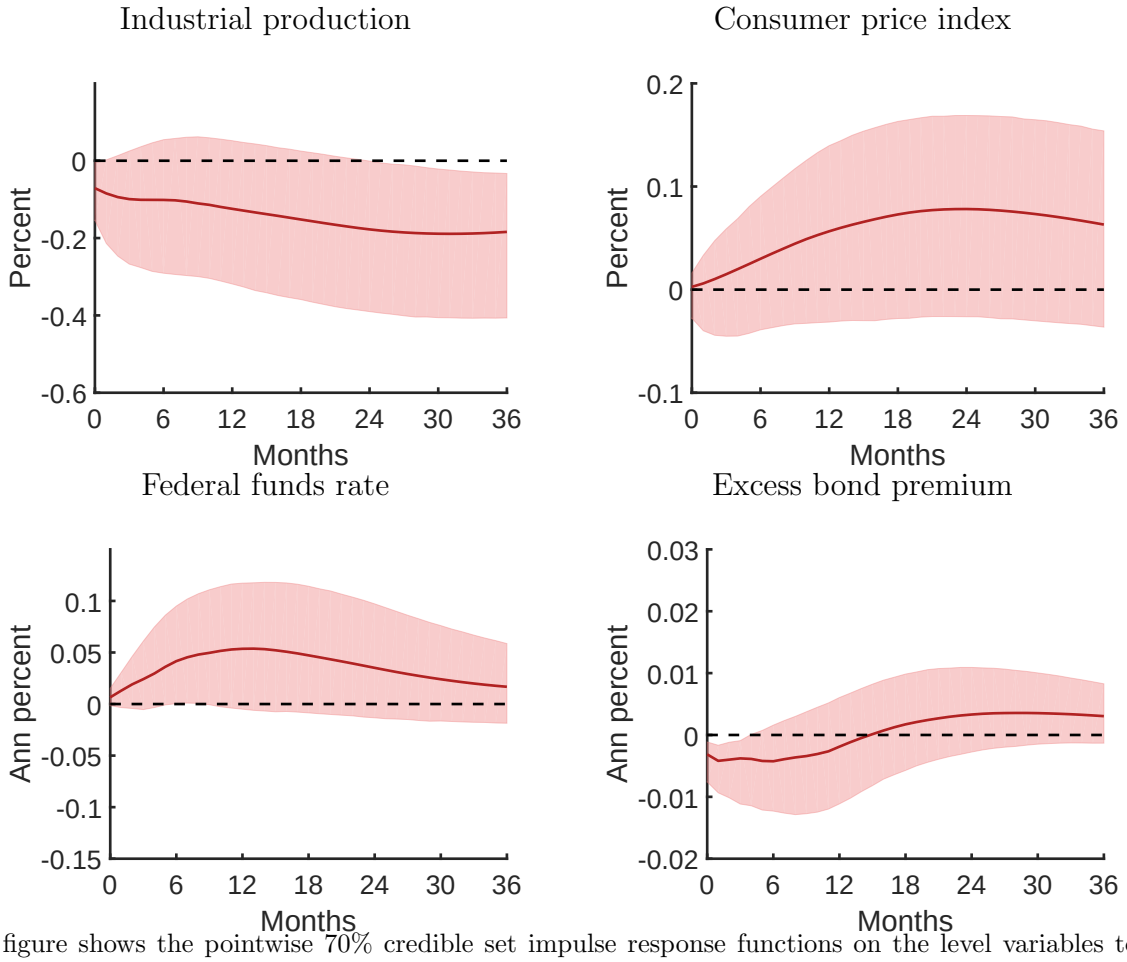

This figure shows the pointwise 70% credible set impulse response functions on the level variables to a 1 standard deviation macro uncertainty shock for the small VAR model. The reduced-form parameters are drawn from their posterior distributions. We assume a Haar prior over the rotation matrices. We only keep the impulse response functions that satisfy Assumptions $\mathcal{A}^3_{uf}, \mathcal{A}^3_{um}, \mathcal{A}^3_{o}$. The dark red line is the impulse response function drawn from a single Q^* that is closest to the pointwise median in a sum of squares sense (median target method of Fry and Pagan (2007)).

Figure A-29 **Posterior results:**
Financial uncertainty shock on log volatility of innovations (Haar)

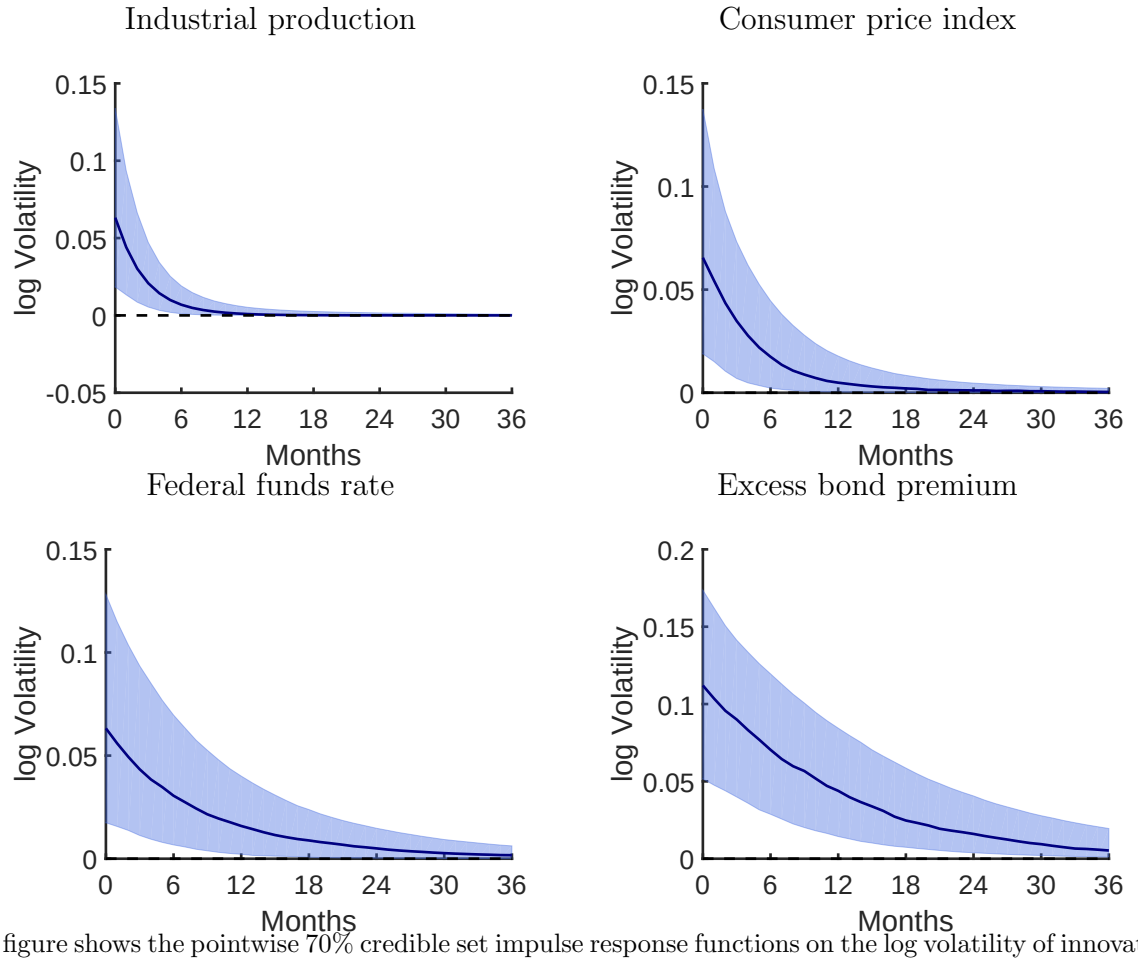

This figure shows the pointwise 70% credible set impulse response functions on the log volatility of innovations to a 1 standard deviation financial uncertainty shock for the small VAR model. The reduced-form parameters are drawn from their posterior distributions. We assume a Haar prior over the rotation matrices. We only keep the impulse response functions that satisfy Assumptions $\mathcal{A}^3_{uf}, \mathcal{A}^3_{um}, \mathcal{A}^3_o$. The dark blue line is the impulse response function drawn from a single Q^* that is closest to the pointwise median in a sum of squares sense (median target method of Fry and Pagan (2007)).

Figure A-30 **Posterior results:**
Macro uncertainty shock on log volatility of innovations (Haar)

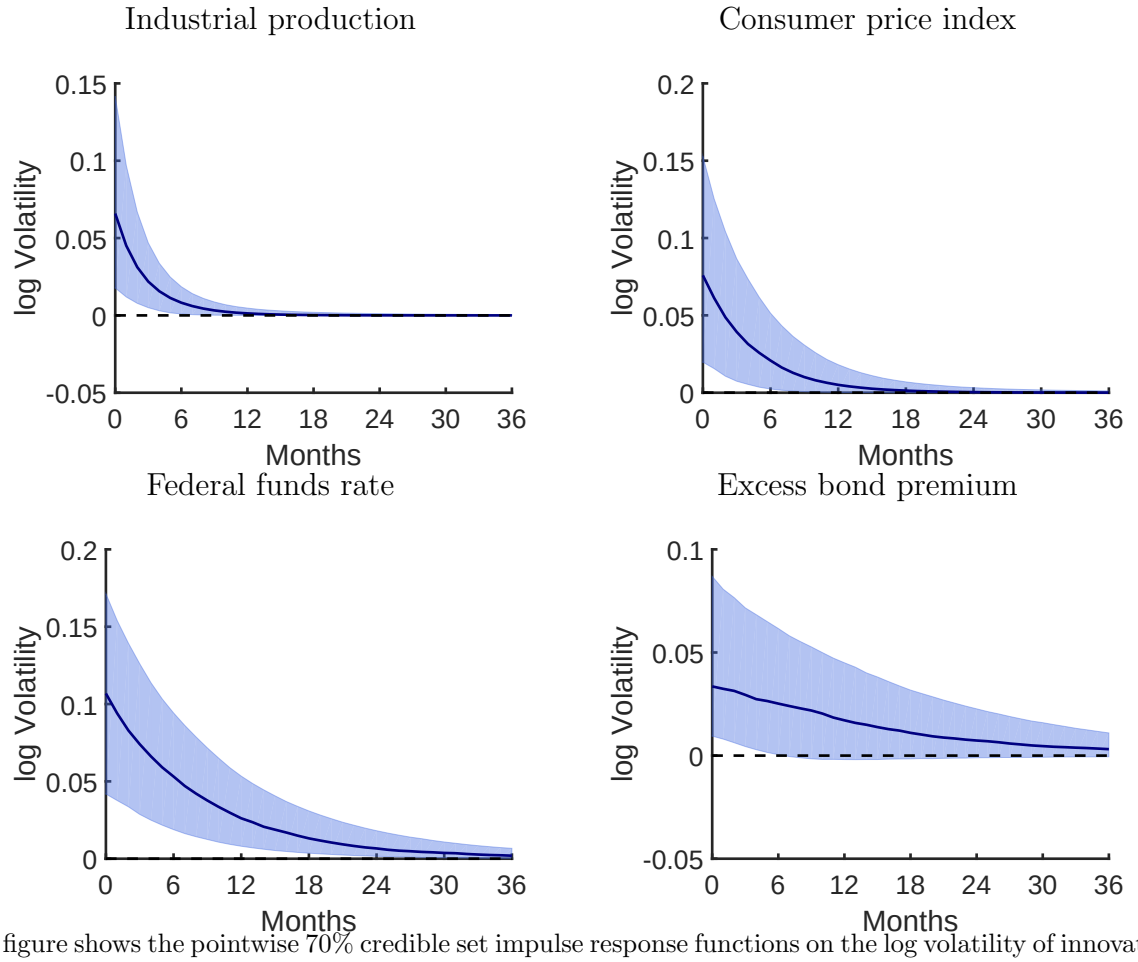

This figure shows the pointwise 70% credible set impulse response functions on the log volatility of innovations to a 1 standard deviation macro uncertainty shock for the small VAR model. The reduced-form parameters are drawn from their posterior distributions. We assume a Haar prior over the rotation matrices. We only keep the impulse response functions that satisfy Assumptions $\mathcal{A}^3_{uf}, \mathcal{A}^3_{um}, \mathcal{A}^3_o$. The dark blue line is the impulse response function drawn from a single Q^* that is closest to the pointwise median in a sum of squares sense (median target method of Fry and Pagan (2007)).

C.1.14 Stochastic volatility estimates

Estimated stochastic volatility (standard deviations) series are presented in figure A-31. The posterior moments of $\Sigma_{1:T}$ (median, 15% and 85% quantiles) are based on the marginal posterior distribution of $\Sigma_{1:T}$ obtained by marginalizing the following joint posterior distribution,

$$p(\psi, Q|Y) \propto p(Y|\psi)\{\psi \in \mathbb{P}(\mathcal{R})\}p(\psi)p(Q|\psi). \tag{A.35}$$

Posterior draws from this joint posterior distribution are given by the algorithm described in the section A.1.

Figure A-31 **Estimated stochastic volatilities (log volatility) of innovations**

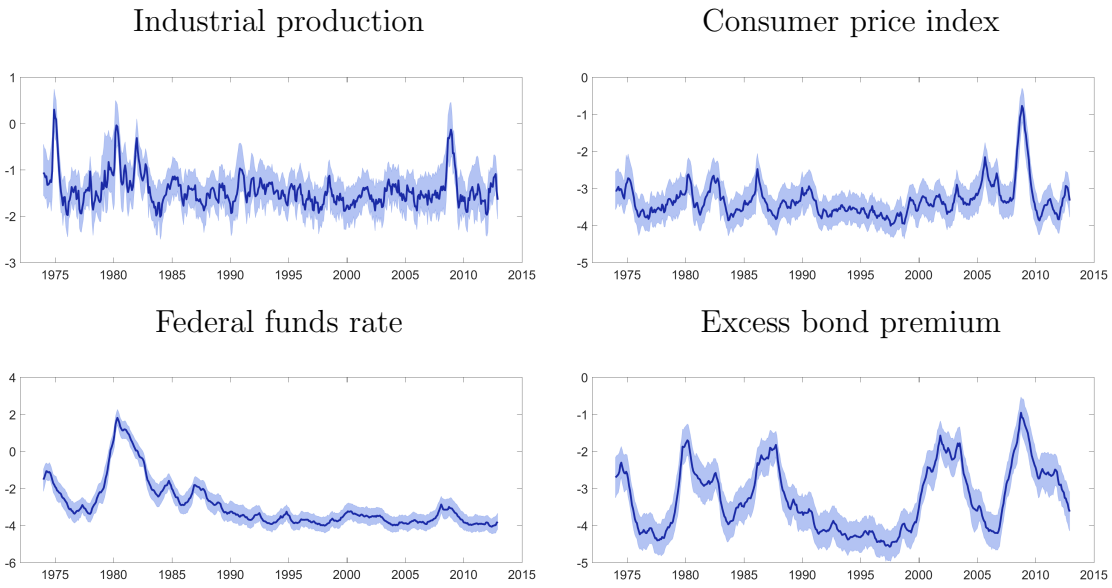

This figure shows the stochastic volatility estimates (log volatility) of the innovations. The shaded areas show the pointwise 70% credible sets. The dark blue line is the posterior median.

C.1.15 Convergence of the posterior sampler

To check whether our posterior sampling algorithm has converged or not, we compute and report Gelman-Rubin diagnostic statistics (Gelman and Rubin, 1992; Brooks and Gelman, 1997) for the our first application (CAIW-in-VAR model, section C.1.5).

Procedure.

1. We run the posterior sampler for ψ described in section C.1.5 with initial value close to the center of the prior distribution described in section C.1.3. We obtain 10,000,000 posterior draws of ψ. Then, we compute posterior mean and posterior variance of ψ using these posterior draws.
2. We set a starting value of the posterior sampler by drawing from the multivariate normal distribution with the mean from the step 1 and the variance four times larger than the posterior variance from the step 1. We did three sets of experiments
   (a) Run 20 different MCMC chains (of length 200,000 draws) from the posterior sampler.
   (b) Run 10 different MCMC chains (of length 500,000 draws) from the posterior sampler.
   (c) Run 10 different MCMC chains (of length 100,000 draws) from the posterior sampler.
3. Compute Gelman-Rubin diagnostic statistics (Gelman and Rubin, 1992; Brooks and Gelman, 1997).

Essentially, we run the posterior sampler on the same data set used in our empirical exercise in section 5.1. The Gelman-Rubin statistic is based on the comparison of within-chain variance and cross-chain variance of draws from the posterior sampler.

Results. Table A-1, Table A-2, and Table A-3 report the Gelman-Rubin diagnostic statistic. We compute Gelman-Rubin statistic for each elements in parameters $\psi_r = (B^y, \Phi^y, \mu^y, \Phi, C, \nu)$. Because there are many elements in each parameter, we report median, 90% quantile and maximum statistics (largest and second largest) among elements in each $B^y, \Phi^y, \mu^y, \Phi, C, \nu$.

For each chain, we generate 200,000 posterior draws saving parameter for every 20 draws in the first experiment. We generate 500,000 posterior draws saving parameter for every 50 draws in the second experiment. We generate 100,000 posterior draws for every 20 draws in the third experiment. To compute R_c, we discard the first 10% of draws from the kept posterior draws.

In theory, $\sqrt{R_c}$ should be close to 1 as the posterior sampler converges to its invariant distribution and numbers less than 1.1 are oftentimes regarded as an indicator for the convergence of the posterior sampler.

As can be seen from the tables A-1, A-2, and A-3, the $\sqrt{R_c}$ statistics are less than 1.1 for most of the cases, indicating that the posterior sampler converged. For experiment 3, there are only two parameters (out of 245 parameters) that have slightly larger $\sqrt{R_c}$ than 1.1. For other cases, all $\sqrt{R_c}$ statistics are less than 1.1. We produce the Figures in the main text based on the draws from the first experiment while we produce the Figures in the appendix based on the draws from the third experiment. In practice, the results are quantitatively similar regardless of whether we use draws from experiment 1 or experiment 3.

Table A-1 Gelman-Rubin's $\sqrt{R_c}$, Experiment 1

	Median	90% quantile	Largest	Second largest	Total number of elements
Φ	1.00	1.01	1.02	1.01	16
C	1.00	1.01	1.01	1.01	16
ν	1.00	1.00	1.00	1.00	1
μ^y	1.00	1.00	1.00	1.00	4
B^y	1.00	1.01	1.03	1.01	16
Φ^y	1.00	1.00	1.02	1.02	192

Table A-2 Gelman-Rubin's $\sqrt{R_c}$, Experiment 2

	Median	90% quantile	Largest	Second largest	Total number of elements
Φ	1.00	1.01	1.01	1.01	16
C	1.00	1.01	1.01	1.01	16
ν	1.00	1.00	1.00	1.00	1
μ^y	1.00	1.00	1.00	1.00	4
B^y	1.00	1.02	1.03	1.02	16
Φ^y	1.00	1.00	1.01	1.01	192

Table A-3 Gelman-Rubin's $\sqrt{R_c}$, Experiment 3

	Median	90% quantile	Largest	Second largest	Total number of elements
Φ	1.01	1.02	1.05	1.02	16
C	1.00	1.03	1.06	1.03	16
ν	1.00	1.00	1.00	1.00	1
μ^y	1.01	1.02	1.02	1.01	4
B^y	1.01	1.05	1.19	1.05	16
Φ^y	1.00	1.00	1.10	1.09	192

C.2 Example 2: Carriero et al. (2017) model

We begin by presenting the complete model of Carriero et al. (2017), which is as follows:

$$
\begin{aligned}
Y_t &= \Phi(L)Y_{t-1} + \Pi_m(L)\log m_t + \Pi_f(L)\log f_t + v_t \\
v_t &= A^{-1}\Lambda_t^{0.5}\epsilon_t, \epsilon_t \sim N(0, I) \\
\log \lambda_{j,t} &= \begin{cases} \beta_{m,j}\log m_t + \log h_{j,t}, \ j = 1, ..., n_m \\ \beta_{f,j}\log f_t + \log h_{j,t}, \ j = n_m + 1, ..., n \end{cases} \\
\log h_{j,t} &= \gamma_{j,0} + \gamma_{j,1}\log h_{j,t-1} + e_{j,t}, e_{j,t} \sim N(0, \phi_j)
\end{aligned}
$$

where $\log m_t$ is the macro volatility factor, $\log f_t$ is the financial volatility factor, $\log h_{j,t}$ capture idiosyncratic series-specific volatility shocks, and A^{-1} is a lower triangular matrix. The parameters $\Phi(L), \Pi_m(L)$, and $\Pi_f(L)$ are lag polynomials. We follow the specification in Carriero et al. (2017) and allow for 6 lags in the VAR $\Phi(L)$ and 2 lags for the uncertainty factors in the conditional mean $\Pi_m(L)$ and $\Pi_f(L)$.

The financial and macro volatility factors are the key objects of interest for our purposes. By assumption, the macro volatility factor loads onto the volatilities of 18 macro variables, as defined by Carriero et al. (2017). This means that β_m is nonzero only for the first n_m data series. The financial volatility factor loads onto the volatilities of 12 financial variables. Therefore, β_f is nonzero only for the last $n - n_m$ series.[9] The two factors are modeled as a VAR(2). Importantly, the δ matrix allows for past values of level variables to impact volatilities, which helps control for endogenous movements in volatility not from volatility shocks.

[9]The data series contained in each category is in a later section of the appendix appendix. One can also find them in the Carriero et al. (2017) paper.

$$\begin{bmatrix} \log m_t \\ \log f_t \end{bmatrix} = D(L) \begin{bmatrix} \log m_{t-1} \\ \log f_{t-1} \end{bmatrix} + \begin{bmatrix} \delta_m' \\ \delta_f' \end{bmatrix} y_{t-1} + \begin{bmatrix} u_{m,t} \\ u_{f,t} \end{bmatrix}, \begin{bmatrix} u_{m,t} \\ u_{f,t} \end{bmatrix} \sim N(0, \Phi_u)$$

C.2.1 Prior specification

Carriero et al. (2017) use Bayesian methods to estimate the model. The model is completed by specifying prior distributions on the parameters. As the draws from the posterior distribution are directly made available in the data appendix of the published version of the paper, we do not reestimate the model. For the purposes of the analysis of the prior implications for the impulse response functions, however, we must construct the prior.

We follow closely Appendix A.1 in the working paper version of Carriero et al. (2017). Note that in analyzing the prior implications of the impulse response functions to the volatility shocks, we only need to consider the priors for the conditional mean parameters $\Phi(L), \Pi_m(L), \Pi_f(L)$ and the volatility parameters $D(L), \delta, \Phi_u$. Therefore, in our discussion of the prior, we focus on these parameters.

The priors for all parameters in the conditional mean equation $(\Phi(L), \Pi_m(L), \Pi_f(L))$ are specified in a Minnesota-type fashion centered around 0 with diagonal variance covariance matrix. For lag l of the $\log m_t$ and $\log f_t$ terms in equation i, we use prior variances of $\frac{\theta_3^2 \sigma_i^2}{l^2}$. For lag l of variable j in equation i, we use prior variances of $\frac{\theta_1^2}{l^2}$ if $i = j$ and $\frac{\theta_1^2 \theta_2^2}{l^2} \frac{\sigma_i^2}{\sigma_j^2}$ otherwise. We set $\theta_1 = 0.2, \theta_2 = 0.5, \theta_3 = 1000$. To determine the σ_i terms, we use estimates of the standard deviations from equation-by-equation $AR(6)$ models.[10]

For the parameters in the volatility equation, we choose normal distributions with diagonal variance covariance matrix for $D(L)$ and δ. $D(1)$ has a mean at a diagonal matrix with diagonal elements 0.8. $D(L)$ for $L > 1$ and δ parameters have mean 0. The variances of all elements in $D(L)$ are 0.04. The variances of all elements in δ are 0.16. For Φ_u we choose

[10] Following Carriero et al. (2017), we first standardize each series to have 0 mean and unit variance.

Table A-4 **Prior results:**
Impact effects of financial and macro uncertainty shocks (prior robust)

	Fin unc		Macro unc	
	15%	85%	15%	85%
IP (%)	−91.9	96.7	−95.1	94.7
PCE (%)	−24.0	23.1	−26.3	23.9
Federal funds rate (annualized %)	−70.0	70.1	−68.3	71.4
Spread, Baa-10y Treasury (annualized %)	−18.4	30.2	−30.1	18.6
Macro volatility	−0.10	0.11	0.11	0.00
Financial volatility	0.00	0.11	−0.11	0.11

This table shows the 70% prior robust credible sets on impact to a 1 standard deviation financial uncertainty and macro uncertainty shock in the Carriero et al. (2017) model. The reduced-form paramters are drawn from the prior distributions of the model. We only keep the impulse response functions that satisfy Assumptions $\mathcal{A}^2_{uf}$ and $\mathcal{A}^2_{um}$.

an inverse Wishart distribution with mean 0.01 times the identity matrix and degrees of freedom 10.

Prior implications for the impulse response functions The priors of Carriero et al. (2017) lead to wide prior distributions for both financial and macro uncertainty shocks identified by prior robust sign restrictions. Table A-4 shows the 70% credible sets for the impact effects of both uncertainty shocks. One can see that the especially loose priors on $\Pi_m(L)$ and $\Pi_f(L)$ lead to an extremely large range of possible responses of the level variables to both uncertainty shocks. The ranges appear comparable across the shocks and there does not seem to be any notable bias in the signs as well on the variables in which the sign restrictions are not directly imposed. In fact, even the credible set for the spreads has sufficient coverage of both positive and negative values. For the volatilities, the restrictions on the financial uncertainty shock does not seem to lead to any bias on the macro volatility factor, and vice versa. From these results, we are comfortable that our prior robust restrictions are extremely loose.

Macroeconomic variables	Financial variables
All employees, total nonfarm ($\Delta \log$)	S&P500 ($\Delta \log$)
Industrial production index ($\Delta \log$)	Spread, Baa-10y Treasury
Capacity utilization: manufacturing (Δ)	Excess return
Help wanted to unemployed ratio (Δ)	SMB FF factor
Unemployment rate (Δ)	HML FF factor
Real personal income ($\Delta \log$)	Momentum factor
Weekly hours: goods-producing	R15-R11
Housing starts (log)	Industry 1 return
Housing permits (log)	Industry 2 return
Real consumer spending ($\Delta \log$)	Industry 3 return
Real manuf. and trade sales ($\Delta \log$)	Industry 4 return
ISM: new orders index	Industry 5 return
Orders for durable goods ($\Delta \log$)	
Avg. hourly earnings, goods-producing ($\Delta^2 \log$)	
PPI, finished goods ($\Delta^2 \log$)	
PPI, commodities ($\Delta^2 \log$)	
PCE price index ($\Delta^2 \log$)	
Federal funds rate (Δ)	

Table A-5 This table shows the data on which the model of Carriero et al. (2017) is estimated (1959M1-2014M12).

C.2.2 Data

Carriero et al. (2017) has a complete discussion of the data used to estimate the model. We briefly discuss several key aspects of the data, but for further details, we refer the reader to that paper. Table A-5 lists all of the data on which the model is estimated, as well as the division between macro and financial variables. The data is monthly and its range is $1959M9 - 2014M7$.

C.2.3 Posterior results for level variables

Figures A-32 and A-33 show the 70% prior robust credible sets for the responses of industrial production, the federal funds rate, the PCE price index, and the BAA - 10 year Treasury spreads to a financial and macro uncertainty shock. The only difference relative to the main text is that we have included the response of the PCE price index to both uncertainty

Figure A-32 **Financial uncertainty shock on level variables (prior robust)**

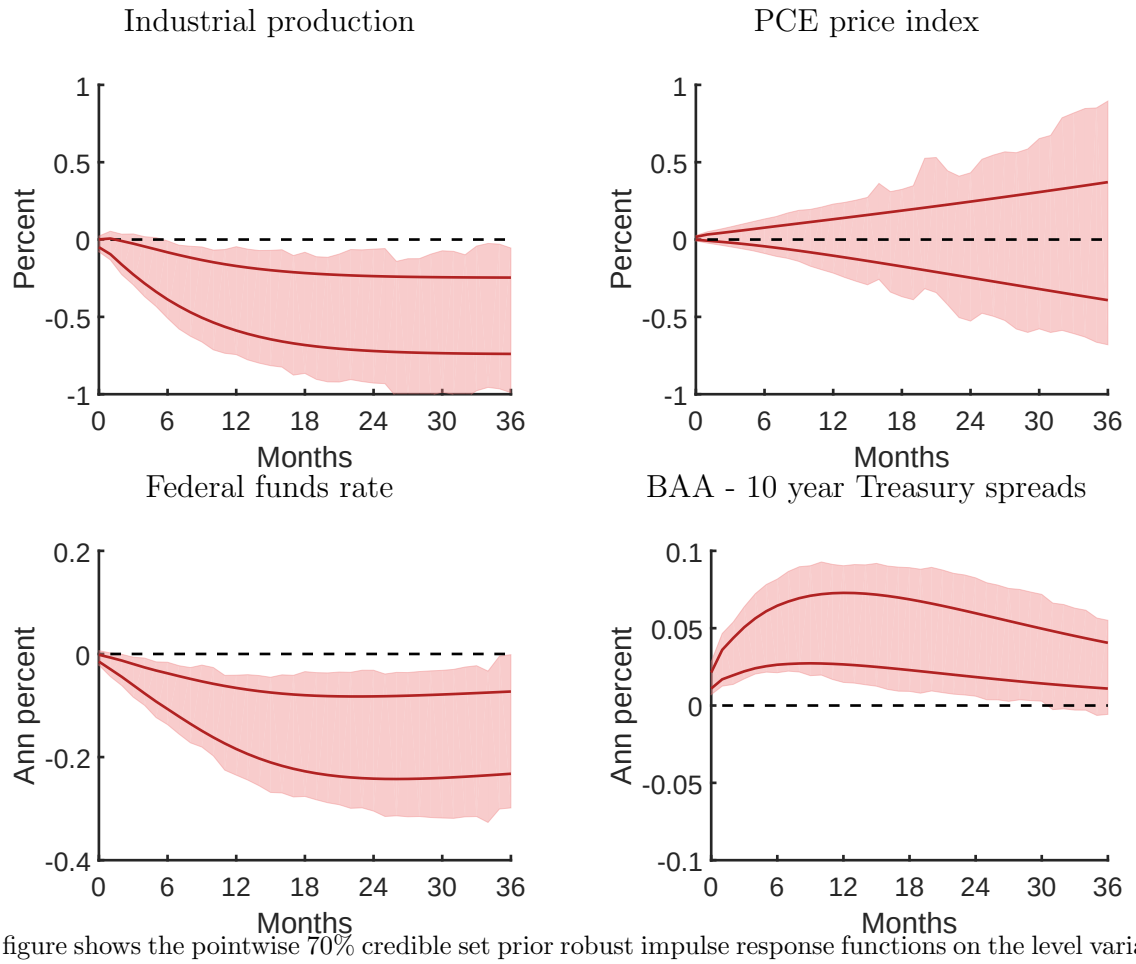

This figure shows the pointwise 70% credible set prior robust impulse response functions on the level variables to a 1 standard deviation financial uncertainty shock for the Carriero et al. (2017) model. The dark red lines are the posterior mean bounds. We only keep the impulse response functions that satisfy Assumptions $\mathcal{A}^2_{uf}$ and $\mathcal{A}^2_{um}$. The reduced-form parameters are drawn from their posterior distributions.

shocks. As one can see, the prior robust credible sets of the PCE price index responses to both uncertainty shocks are wide.

C.2.4 Posterior results for volatility factors

In this section, we turn to the movements in volatilities following the financial and macro uncertainty shocks. Figure A-34 shows the volatility effects of a financial uncertainty shock. Although the set is wide, at the 70% level, the prior robust set puts most of its mass on a persistent increase in financial volatility. Interestingly, there is some evidence that a

Figure A-33 **Macro uncertainty shock on level variables (prior robust)**

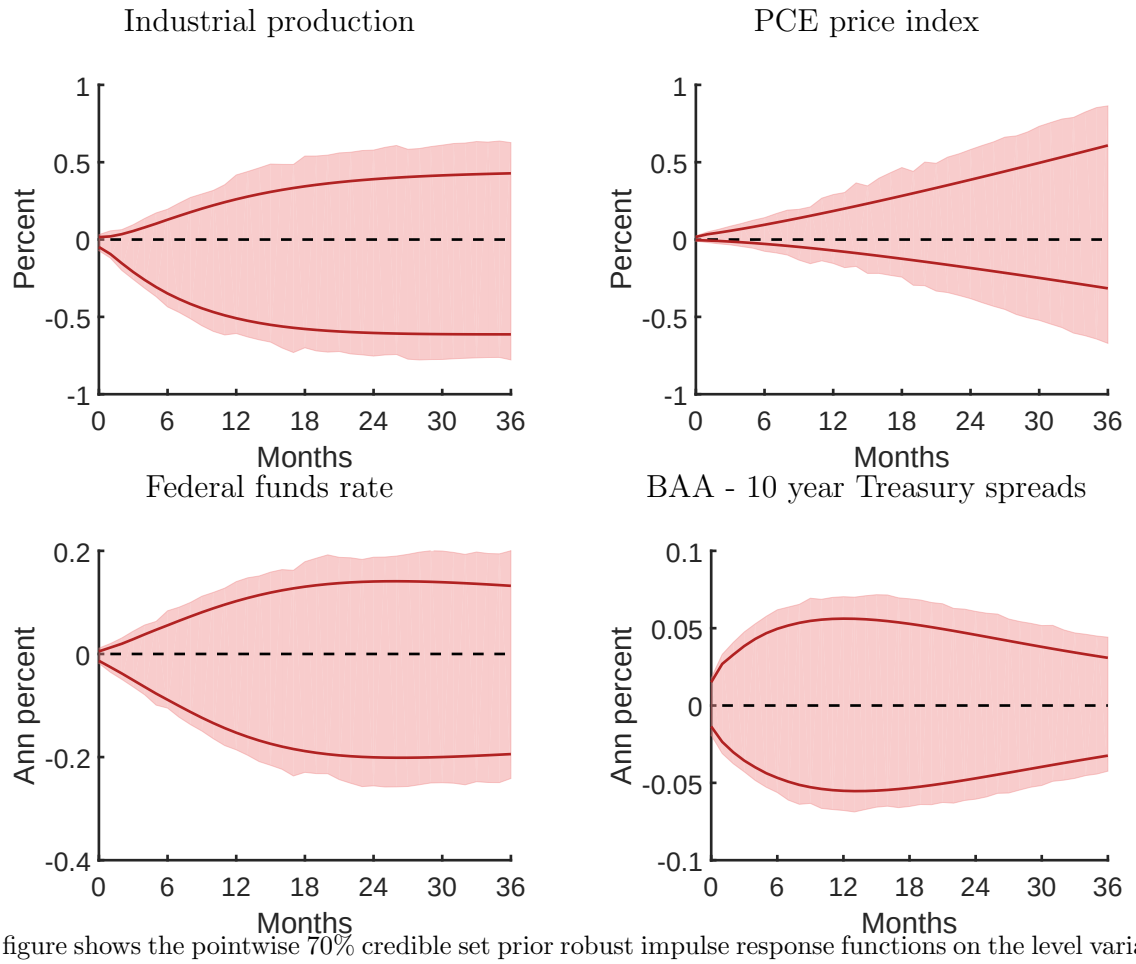

This figure shows the pointwise 70% credible set prior robust impulse response functions on the level variables to a 1 standard deviation macro uncertainty shock for the Carriero et al. (2017) model. The dark red lines are the posterior mean bounds. We only keep the impulse response functions that satisfy Assumptions $\mathcal{A}^2_{uf}$ and $\mathcal{A}^2_{um}$. The reduced-form parameters are drawn from their posterior distributions.

financial uncertainty shock shifts the prior robust set over macro volatility upwards. On the other hand, there is little evidence that a macro uncertainty shock restricts the financial volatility robust set in either direction. In fact, comparing the 70% sets on the responses of macro volatility to financial and macro uncertainty shocks, we see that on impact, a higher response of macro volatility to a financial uncertainty shock versus a macro uncertainty shock is consistent with the data and identification scheme. Moreover, moving forward, the financial uncertainty shock credible sets puts more weight on an increase in macro volatility than the macro uncertainty shock does.

Figure A-34 **Financial uncertainty shock on volatility factors (prior robust)**

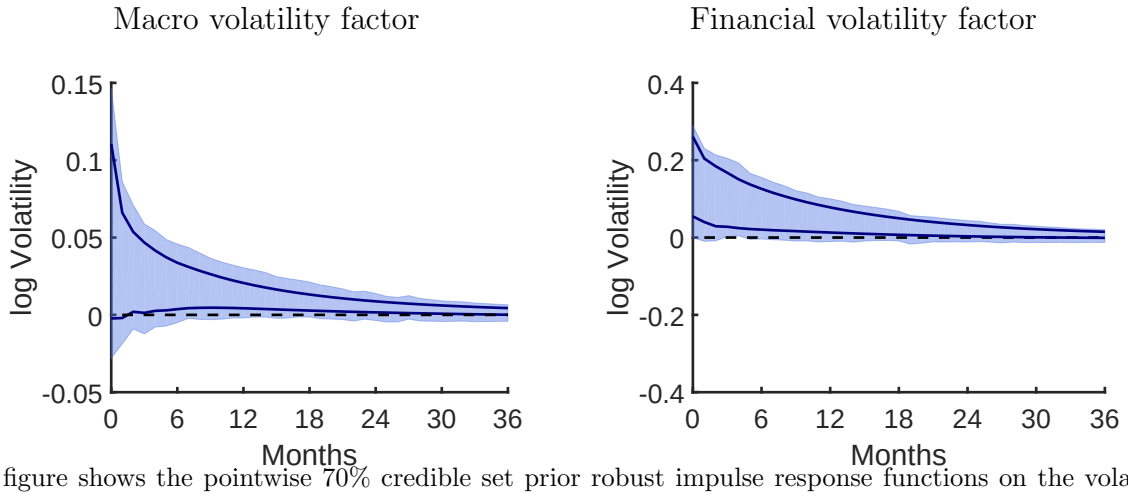

This figure shows the pointwise 70% credible set prior robust impulse response functions on the volatility factors to a 1 standard deviation financial uncertainty shock for the Carriero et al. (2017) model. The dark blue lines are the posterior mean bounds. We only keep the impulse response functions that satisfy Assumptions $\mathcal{A}^2_{uf}$ and $\mathcal{A}^2_{um}$. The reduced-form parameters are drawn from their posterior distributions.

Figure A-35 **Macro uncertainty shock on volatility factors (prior robust)**

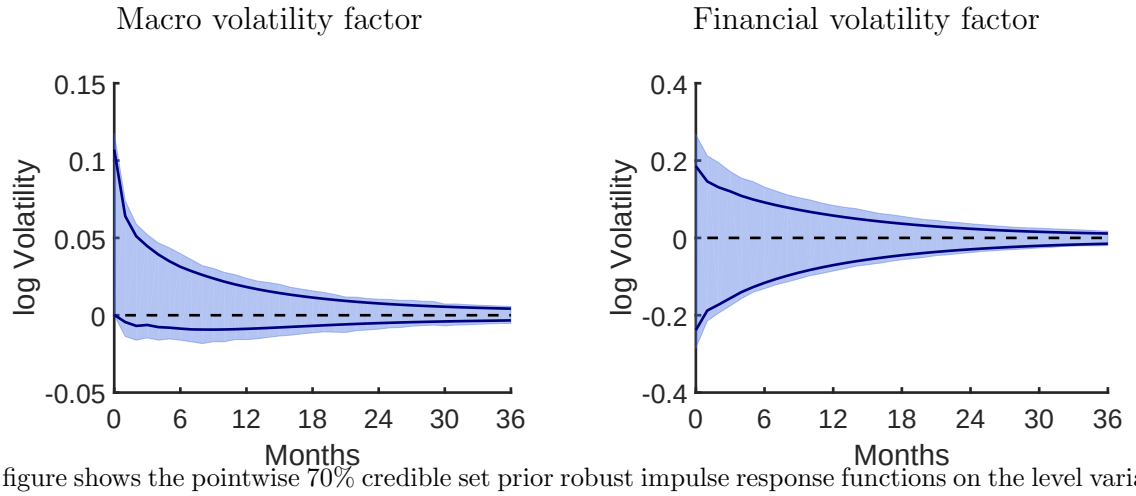

This figure shows the pointwise 70% credible set prior robust impulse response functions on the level variables to a 1 standard deviation macro uncertainty shock for the Carriero et al. (2017) model. The dark blue lines are the posterior mean bounds. We only keep the impulse response functions taht satisfy Assumptions $\mathcal{A}^2_{uf}$ and $\mathcal{A}^2_{um}$. The reduced-form parameters are drawn from their posterior distributions.

C.2.5 Identified sets at the posterior mean parameters

This subsection analyzes the amount of shrinkage of the identified sets over impulse response functions at the posterior mean reduced-form parameters following macro and financial uncertainty shocks. Figures A-36 and A-37 show that for the level impulse response functions,

both sets of sign restrictions impose a fair amount of shrinkage of the identified sets relative to the unrestricted set of impulse response functions. This shows that the sign restrictions we impose do have identifying power in practice.

Comparing the two identified sets, we see that the financial uncertainty shock has identified sets over industrial production and the federal funds rate that are more negative than those of the macro uncertainty shock. For both variables, the financial uncertainty shock identified sets contain the lower bound of possible impulse response functions. On the other hand, for the macro uncertainty shock, the identified sets are wide and cover 0% for both variables. There is evidence, however, that large increases in both variables following a macro uncertainty shock are ruled out. For the BAA - 10 year Treasury spreads, the identified set of the financial uncertainty shock impulse response function is tight at the upper bound of possible impulse response functions, whereas the identified set of the macro uncertainty shock is more symmetric around 0%. Across the 4 variables, it appears that the identified sets for the financial uncertainty shock is tighter than those for the macro uncertainty shock.

Figures A-38 and A-39 show the corresponding identified sets for the volatility factors. For the financial uncertainty shock identified set, we see that the identified sets for both the macro and financial volatility factors do not contain 0 for the entire horizon. On the other hand, for the macro uncertainty shock identified set, we see that the financial volatility factor is essentially unrestricted.

C.2.6 Extension of volatility sign restriction to 2 months

It is of interest to extend the volatility sign restrictions for both uncertainty shocks to 2 months (a modification of $\mathcal{A}^2_{uf,1}$ and $\mathcal{A}^2_{um,1}$ to $h = 0, 1, 2$), while maintaining the restrictions on the relative signs of the BAA spread impact response ($\mathcal{A}^2_{ufm,2}$). This tighter sign restriction leads to more significant responses in industrial production and the federal funds rate to a financial uncertainty shock (Figure A-40).

Figure A-36 **Financial uncertainty shock on level variables (identified set at the posterior mean)**

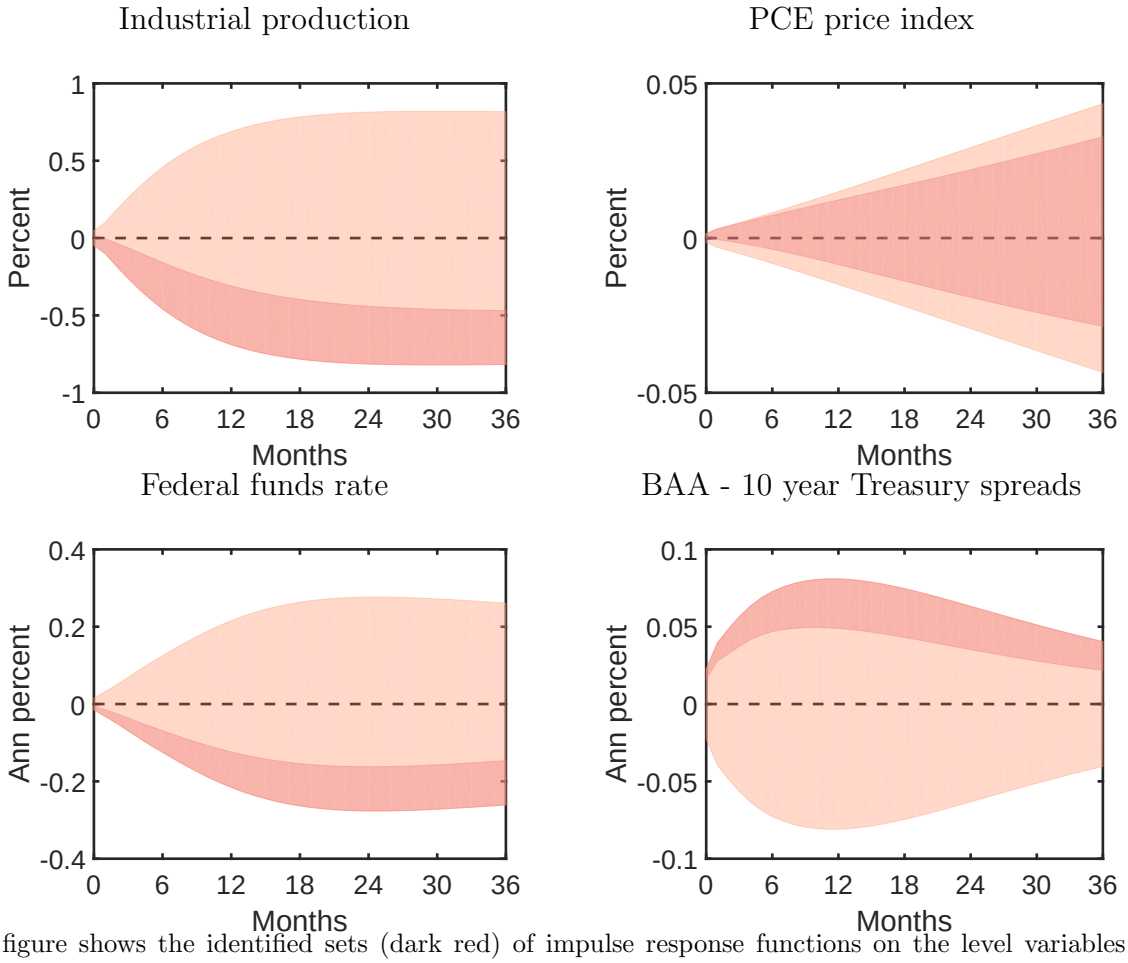

This figure shows the identified sets (dark red) of impulse response functions on the level variables to a 1 standard deviation financial uncertainty shock for the Carriero et al. (2017) model. The reduced-form parameters are fixed at their posterior means. For comparison purposes, the light red is the unrestricted set of impulse response functions.

Figure A-41 shows the responses of the two volatility factors to a financial uncertainty shock. The tighter sign restriction on financial volatility moves the lower bound of the 70% credible set to not include 0 for around a year and half. The responses of macro volatility to a financial volatility shock are similar.

The responses to a macro uncertainty shock (not shown) continue to be similar.

Figure A-37 **Financial uncertainty shock on level variables (identified set at the posterior mean)**

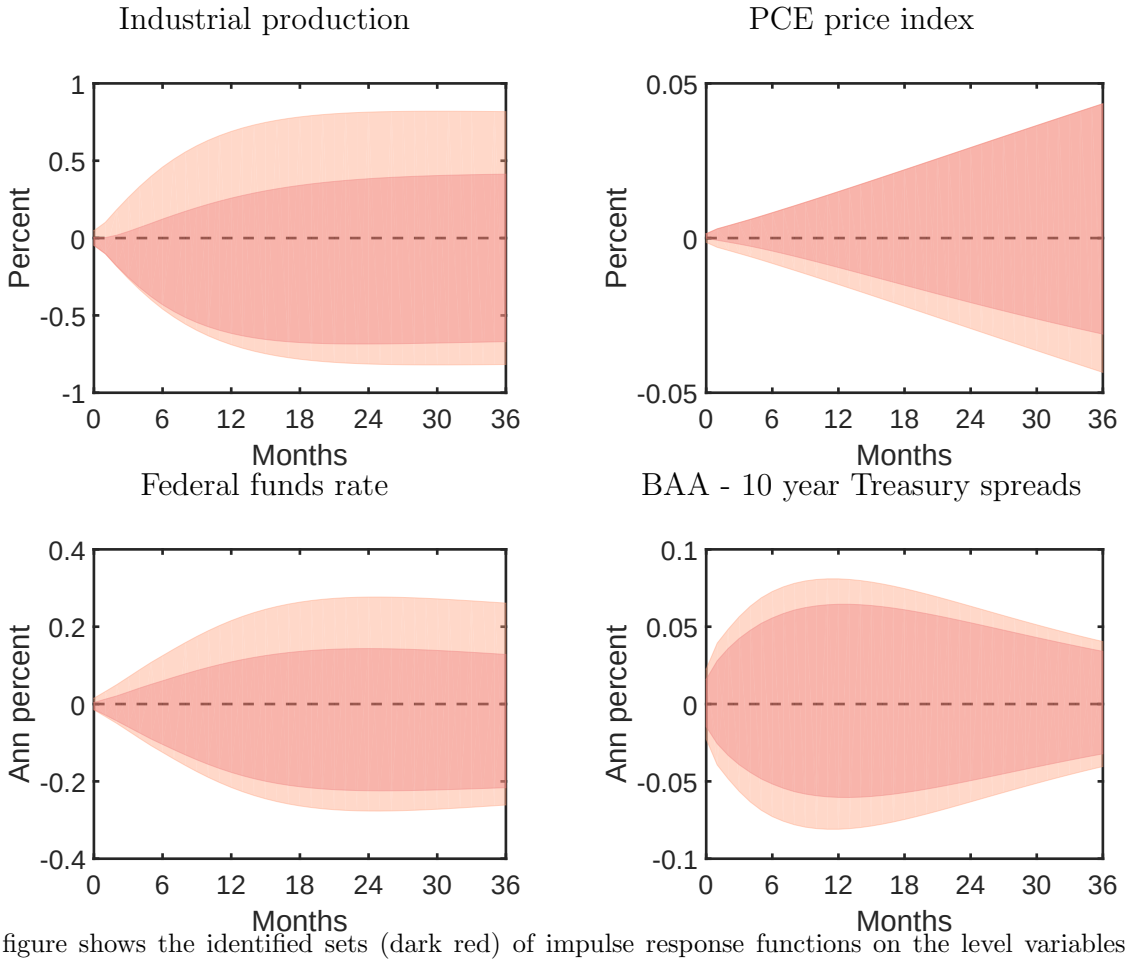

This figure shows the identified sets (dark red) of impulse response functions on the level variables to a 1 standard deviation macro uncertainty shock for the Carriero et al. (2017) model. The reduced-form parameters are fixed at their posterior means. For comparison purposes, the light red is the unrestricted set of impulse response functions.

C.2.7 Results from Haar prior

We present some additional results from assuming a Haar prior for the rotation matrices. For these results, we go back to our original sign restrictions assumptions (Assumptions $\mathcal{A}^2_{uf}$ and $\mathcal{A}^2_{um}$), but instead of identifying the shocks in a prior robust fashion, we apply the Haar prior. The inclusion of a prior on the set of rotation matrices allows us to say more about the responses to financial and macro uncertainty shocks.

Figure A-38 **Financial uncertainty shock on volatility factors (identified set at posterior mean)**

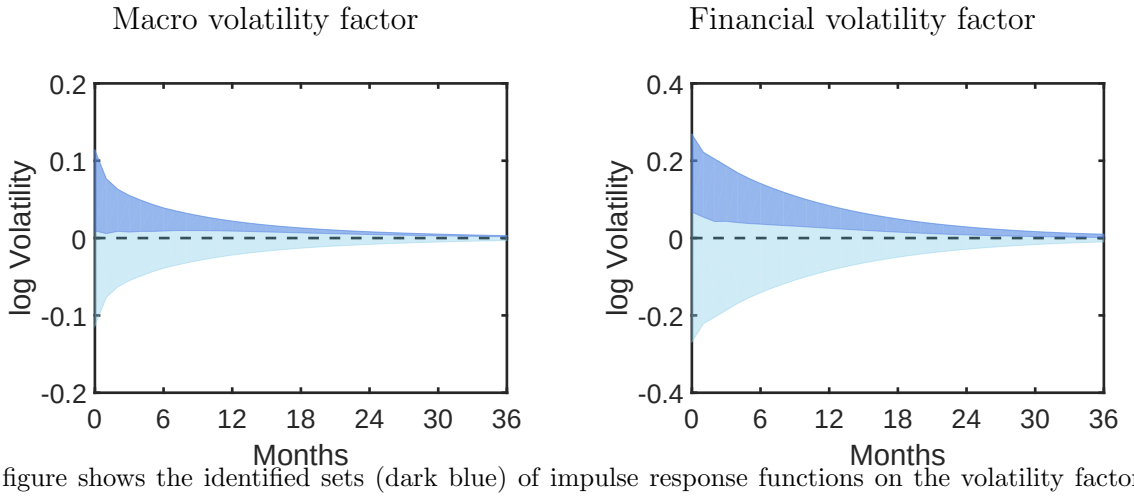

This figure shows the identified sets (dark blue) of impulse response functions on the volatility factors to a 1 standard deviation financial uncertainty shock for the Carriero et al. (2017) model. The reduced-form parameters are fixed at their posterior means. For comparison purposes, the light blue is the unrestricted set of impulse response functions.

Figure A-39 **Macro uncertainty shock on volatility factors (identified set at posterior mean)**

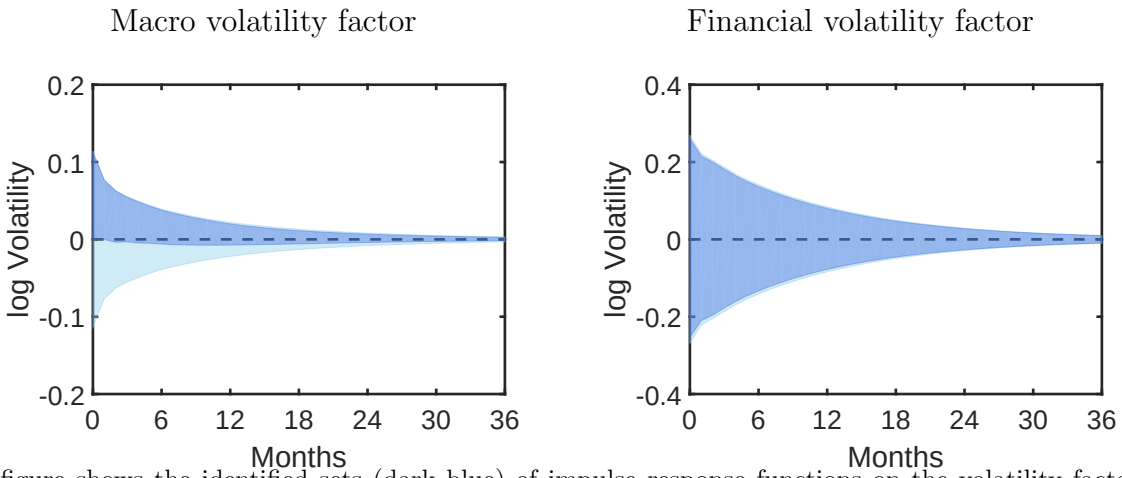

This figure shows the identified sets (dark blue) of impulse response functions on the volatility factors to a 1 standard deviation macro uncertainty shock for the Carriero et al. (2017) model. The reduced-form parameters are fixed at their posterior means. For comparison purposes, the light blue is the unrestricted set of impulse response functions.

Prior implications for the impulse response functions We begin by looking at the prior implications for the impulse response functions implied by the Haar prior. Table A-6 shows that although the Haar prior restrictions do tighten up the responses of the variables

Figure A-40 **Posterior results:**
Financial uncertainty shock on level variables (prior robust)

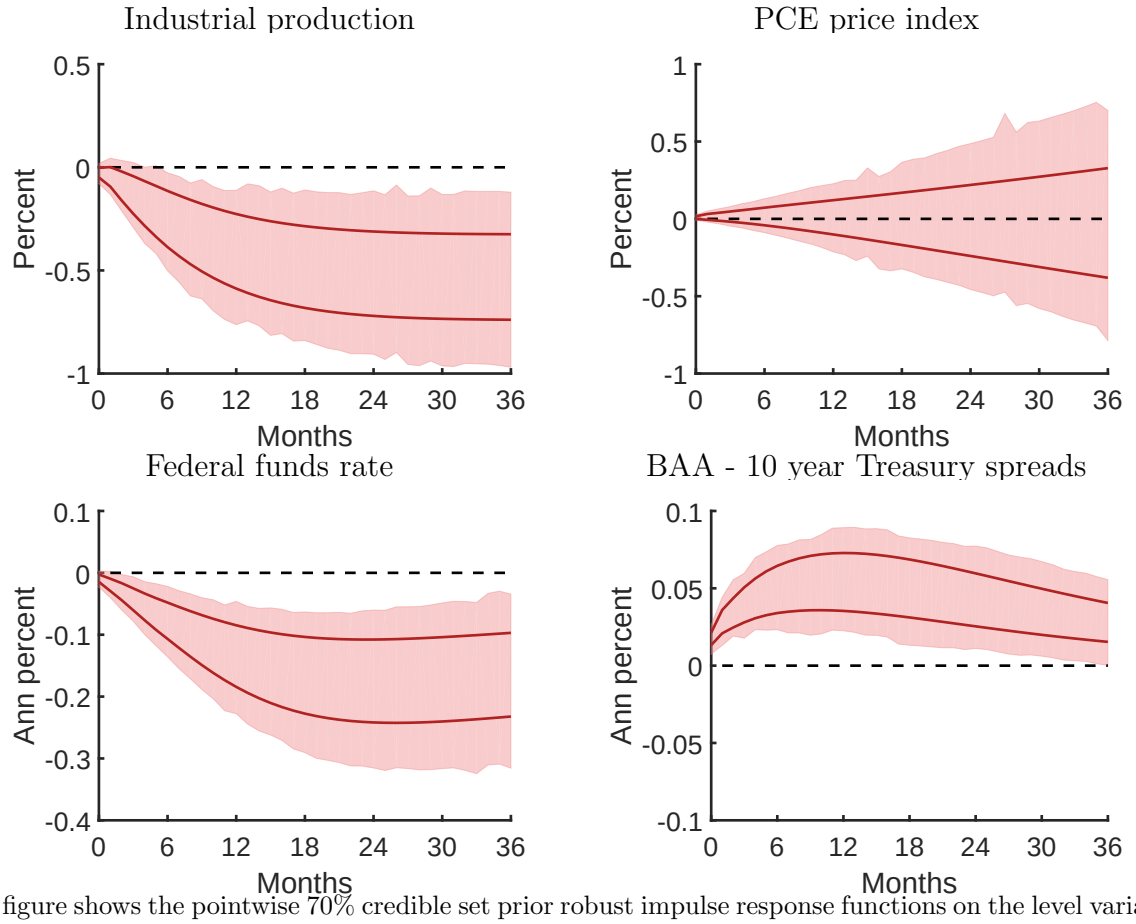

This figure shows the pointwise 70% credible set prior robust impulse response functions on the level variables to a 1 standard deviation financial uncertainty shock for the Carriero et al. (2017) model assuming that the volatility sign restrictions hold for 2 months (modification of Assumptions $\mathcal{A}^2_{uf,1}$ and $\mathcal{A}^2_{um,1}$). The dark red lines are the posterior mean bounds. The reduced-form parameters are drawn from their posterior distributions.

to the two uncertainty shocks, the credible sets remain wide.

Posterior results Figures A-42 and A-43 show the 70% posterior credible sets of the level variable responses to a financial uncertainty and macro uncertainty shock.

One sees that many of the conclusions found in the main text continue to hold. In response to a financial uncertainty shock, industrial production immediately declines. The response appears permanent, settling at a posterior median value of around -0.6%. On the other hand, a macro uncertainty shock produces little evidence of a movement in industrial

Figure A-41 **Posterior results:**
Financial uncertainty shock on volatility factors (prior robust)

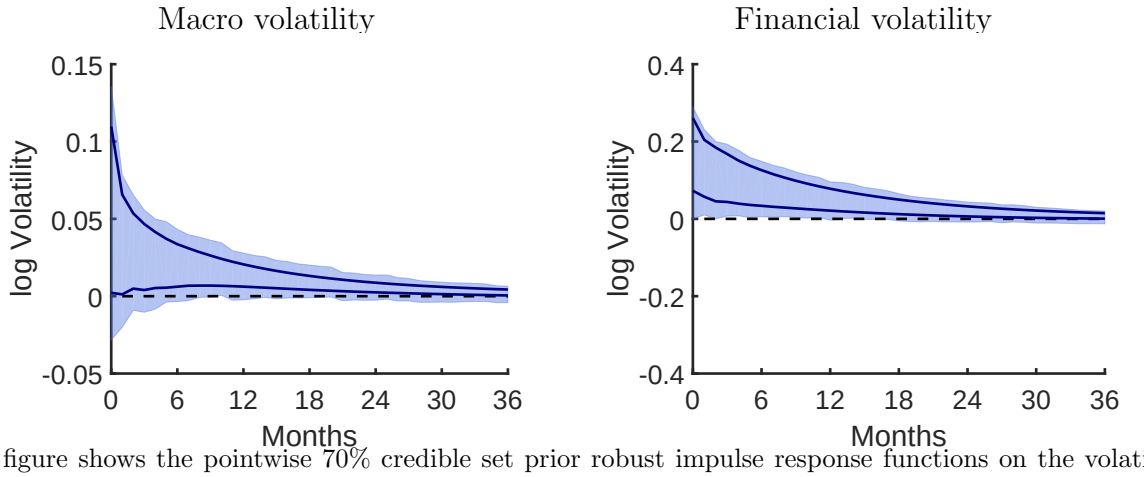

This figure shows the pointwise 70% credible set prior robust impulse response functions on the volatility factors to a 1 standard deviation financial uncertainty shock for the Carriero et al. (2017) model assuming that the volatility sign restrictions hold for 2 months (modification of Assumptions $\mathcal{A}^2_{uf,1}$ and $\mathcal{A}^2_{um,1}$). The dark blue lines are the posterior mean bounds. The reduced-form parameters are drawn from their posterior distributions.

production, although the posterior median decline is negative. There is little evidence of a movement in the PCE following a financial uncertainty shock, whereas there is some mild evidence of an increase in the price level on impact from a macro uncertainty shock. These credible sets, however, are quite wide. On balance, there is some evidence of a macro uncertainty shock being more inflationary than a financial uncertainty shock. A financial uncertainty shock produces a pronounced decline in the federal funds rate that reaches around -0.2% nearly 2 years after the shock. On the other hand, a macro uncertainty shock produces little movement. By assumption, a financial uncertainty shock must lead to a larger initial increase in spreads relative to a macro uncertainty shock. We see that this assumption leads to a financial uncertainty shock having a hump-shaped and long-lasting response in BAA-10 year Treasury spreads, with a peak at the posterior median of around 0.06%. A macro uncertainty shock produces little response.

Figure A-44 shows the volatility factor responses to financial and macro uncertainty shocks. We find that a financial uncertainty shock leads to persistent increases in both financial and macro volatility. The heightened volatility lasts for around 2 years after the

Table A-6 **Prior results:**
Impact effects of financial and macro uncertainty shocks (Haar)

	Fin unc		Macro unc	
	15%	85%	15%	85%
IP (%)	−66.4	65.9	−66.4	65.9
PCE (%)	−15.8	16.2	−15.8	16.2
Federal funds rate (%)	−47.5	47.0	−47.5	47.0
Spread, Baa-10y Treasury (%)	−4.7	23.7	−23.5	4.7
Macro volatility	−0.08	0.08	0.02	0.10
Financial volatility	0.02	0.10	−0.08	0.08

This table shows the 70% credible sets on impact to a 1 standard deviation financial uncertainty and macro uncertainty shock in the Carriero et al. (2017) model. The reduced-form paramters are drawn from the prior distributions of the model. We assume a Haar prior over the rotation matrices. We only keep the impulse response functions that satisfy Assumptions $\mathcal{A}^2_{uf}$ and $\mathcal{A}^2_{um}$.

uncertainty shock. The macro volatility shock, on the other hand, only increases the macro volatility factor. Moreover, the macro volatility factor increase is not persistent, lasting for around half a year.

Results from an alternative sign restriction on the S&P500 To separate out financial and macro uncertainty shocks, we impose an alternative sign restriction on the S&P500 instead of on the BAA spreads. We therefore replace assumption $\mathcal{A}^2_{ufm}$ with assumption $\mathcal{A}^2_{u'fm}$:

$$\mathcal{A}^2_{u'fm} : IRF[SP500_{t+h}|v^*_t = e_1; R_t] < IRF[SP500_{t+h}|v^*_t = e_2; R_t]$$
$$\text{for } h = 0.$$

This assumption says that a financial uncertainty shock must decrease S&P500 stock returns by more than a macro uncertainty shock on impact. The motivation for this restriction also comes from the structural model. Insofar as a financial uncertainty shock produces a decline in investment that decreases the price of capital by more than a macro uncertainty shock does, one should expect that a financial uncertainty shock leads to a larger decline in returns to capital, which would lead to a larger decline in stock prices. We maintain an

Figure A-42 **Posterior results:**
Financial uncertainty shock on level variables (Haar)

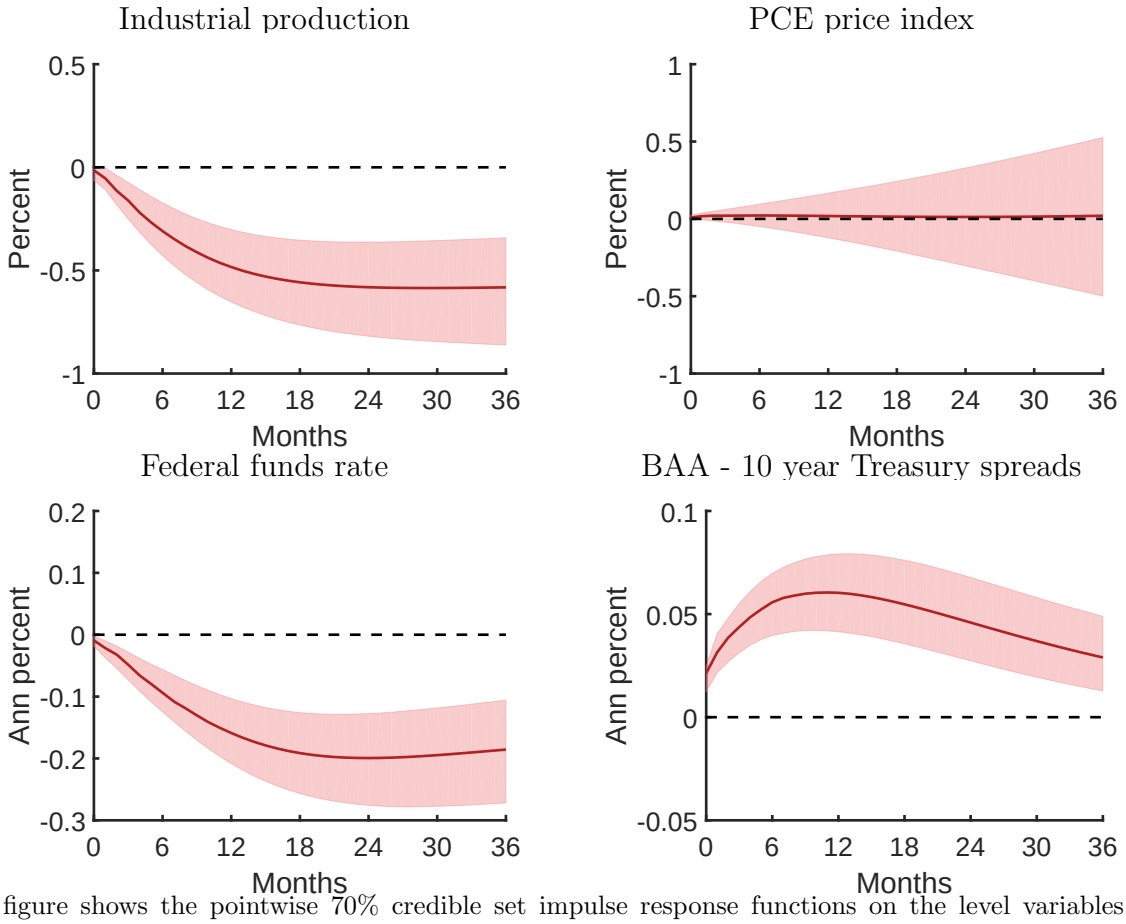

This figure shows the pointwise 70% credible set impulse response functions on the level variables to a 1 standard deviation financial uncertainty shock for the Carriero et al. (2017) model. The reduced-form parameters are drawn from their posterior distributions. We assume a Haar prior over the rotation matrices. We only keep the impulse response functions that satisfy Assumptions $\mathcal{A}^2_{uf}$ and $\mathcal{A}^2_{um}$. The dark red line is the impulse response function drawn from a single Q^* that is closest to the pointwise median in a sum of squares sense (median target method of Fry and Pagan (2007)).

assumption of the Haar prior over the rotation matrices.

Figure A-46 shows the posterior results.[11] They are largely qualitatively consistent with those produced by the main set of sign restrictions considered in the paper, although the separation between the two types of uncertainty shocks is a bit weaker. This may be expected given the high short-term volatility of stock price movements. There is some mild

[11] The prior implications for the impulse response functions are similar to those from the Haar prior with the BAA spread identification, except with the bias in the signs on the S&P500 response instead of the spread response.

Figure A-43 **Posterior results:**
Macro uncertainty shock on level variables (Haar)

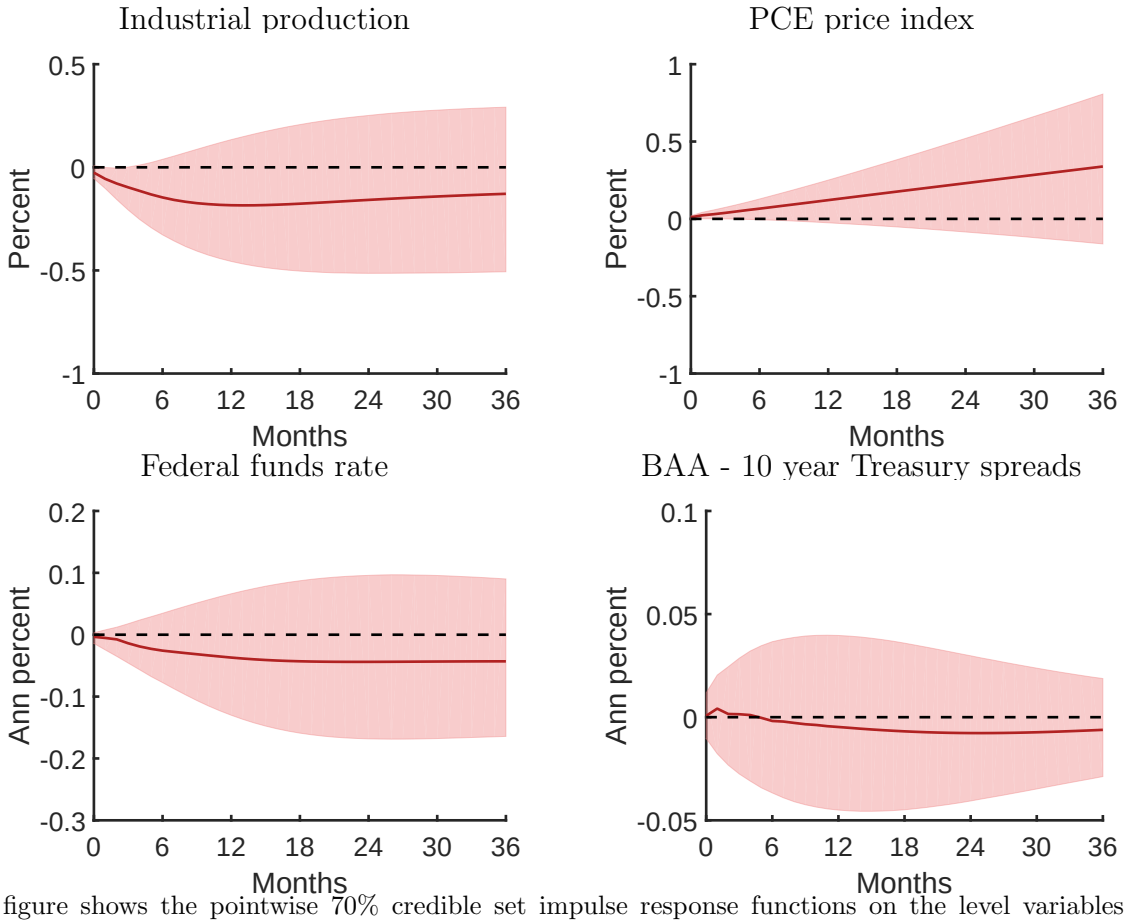

This figure shows the pointwise 70% credible set impulse response functions on the level variables to a 1 standard deviation macro uncertainty shock for the Carriero et al. (2017) model. The reduced-form parameters are drawn from their posterior distributions. We assume a Haar prior over the rotation matrices. We only keep the impulse response functions that satisfy Assumptions $\mathcal{A}^2_{uf}$ and $\mathcal{A}^2_{um}$. The dark red line is the impulse response function drawn from a single Q^* that is closest to the pointwise median in a sum of squares sense (median target method of Fry and Pagan (2007)).

evidence of a decline in industrial production following a financial uncertainty shock, especially in the longer run. The 70% credible sets of the response from industrial production following a macro uncertainty shock covers 0% after some marginal evidence of a decline in the immediate months. Like with the spread identification, there is more evidence of an increase in the price level from a macro uncertainty shock and more evidence of a decline in the federal funds rate from a financial uncertainty shock. BAA-10 year Treasury spreads increase strongly in response to a financial uncertainty shock, but barely move at all following

Figure A-44 **Posterior results:**
Financial uncertainty shock on volatility factors (Haar)

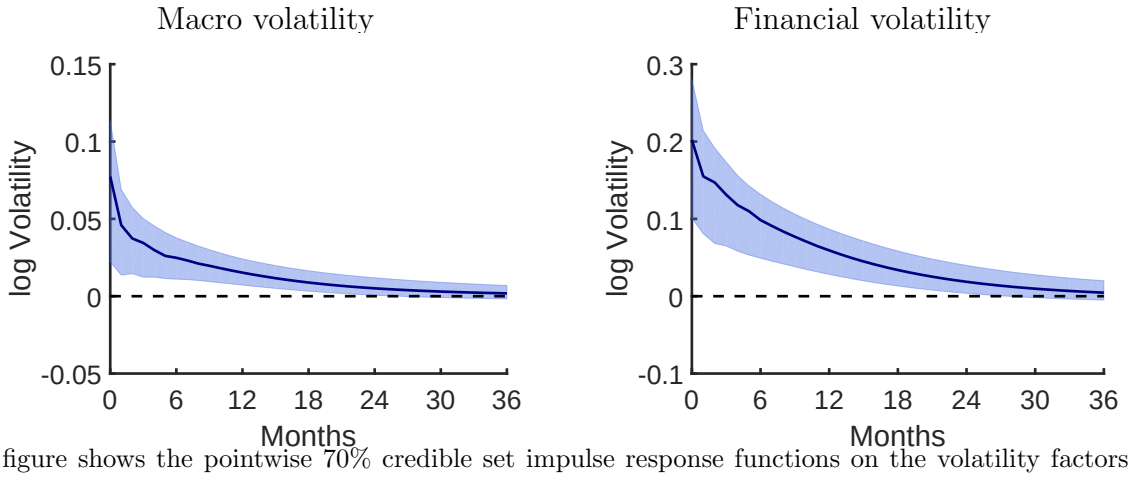

This figure shows the pointwise 70% credible set impulse response functions on the volatility factors to a 1 standard deviation financial uncertainty shock for the Carriero et al. (2017) model. The reduced-form parameters are drawn from their posterior distributions. We assume a Haar prior over the rotation matrices. We only keep the impulse response functions that satisfy Assumptions $\mathcal{A}^2_{uf}$ and $\mathcal{A}^2_{um}$. The dark blue line is the impulse response function drawn from a single Q^* that is closest to the pointwise median in a sum of squares sense (median target method of Fry and Pagan (2007)).

Figure A-45 **Posterior results:**
Macro uncertainty shock on volatility factors (Haar)

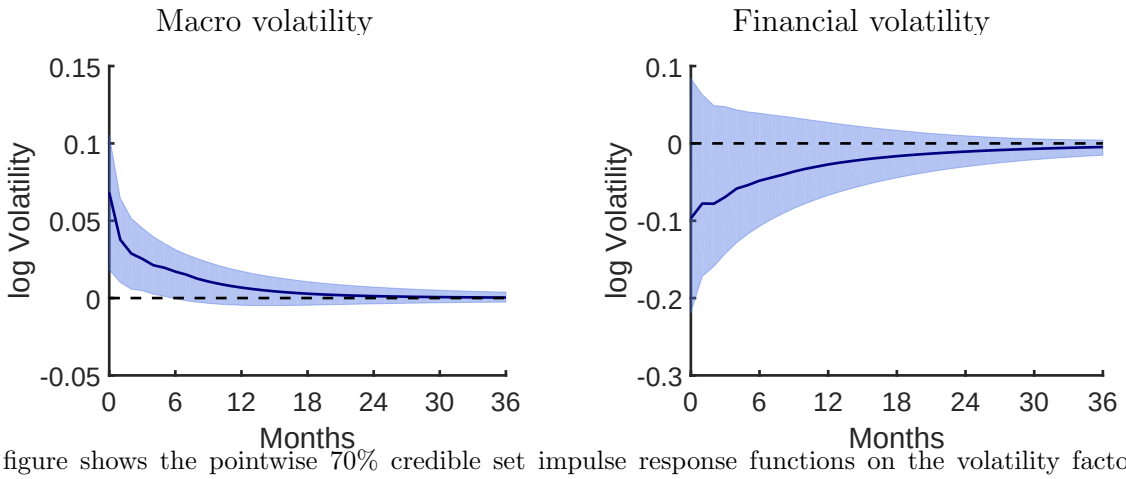

This figure shows the pointwise 70% credible set impulse response functions on the volatility factors to a 1 standard deviation macro uncertainty shock for the Carriero et al. (2017) model. The reduced-form parameters are drawn from their posterior distributions. We assume a Haar prior over the rotation matrices. We only keep the impulse response functions that satisfy Assumptions $\mathcal{A}^2_{uf}$ and $\mathcal{A}^2_{um}$. The dark blue line is the impulse response function drawn from a single Q^* that is closest to the pointwise median in a sum of squares sense (median target method of Fry and Pagan (2007)).

a macro uncertainty shock.

Finally, figure A-48 shows the volatility responses to the two uncertainty shocks. With this

Figure A-46 **Posterior results:**
Financial uncertainty shock on level variables (Haar/S&P500 identification)

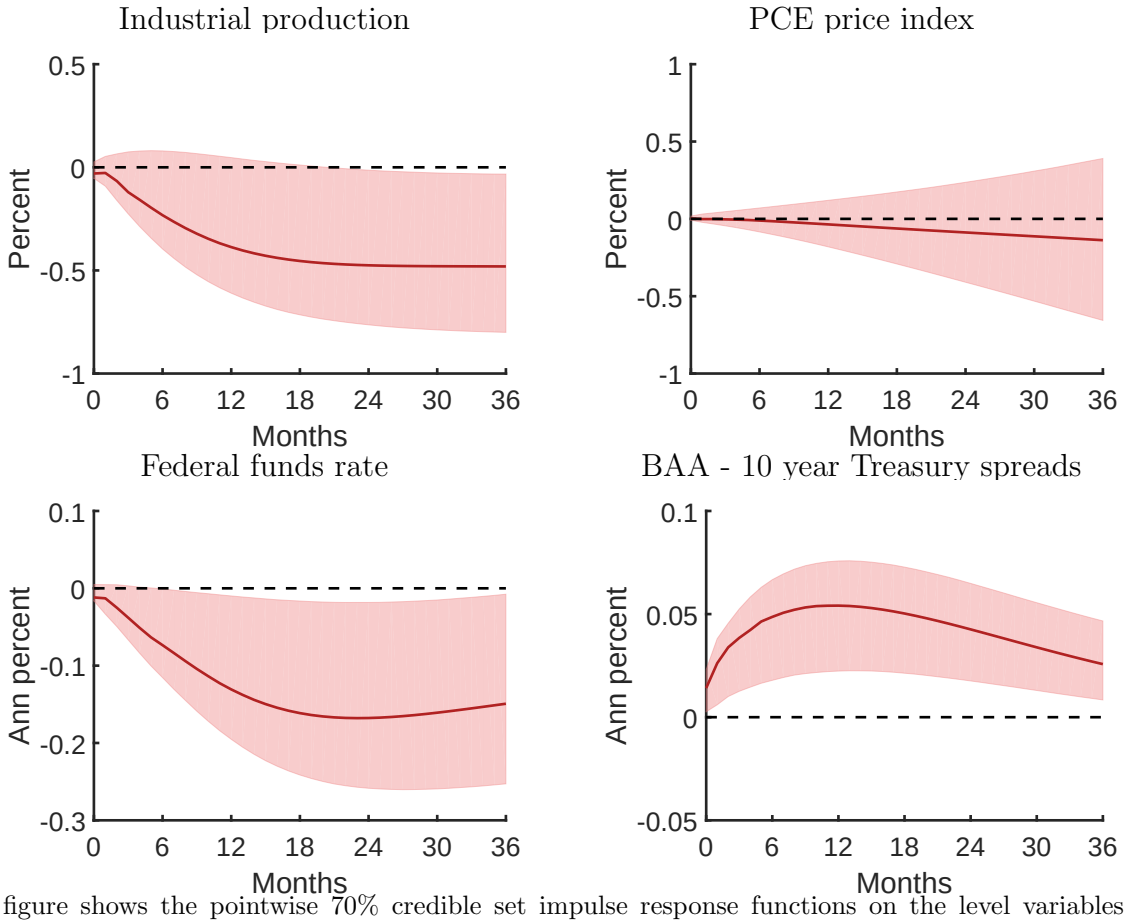

This figure shows the pointwise 70% credible set impulse response functions on the level variables to a 1 standard deviation financial uncertainty shock for the Carriero et al. (2017) model. The reduced-form parameters are drawn from their posterior distributions. We assume a Haar prior over the rotation matrices. We only keep impulse response functions that satisfy Assumptions $\mathcal{A}^2_{u'f}$ and $\mathcal{A}^2_{u'm}$. The dark red line is the impulse response function drawn from a single Q^* that is closest to the pointwise median in a sum of squares sense (median target method of Fry and Pagan (2007)).

alternative identification, a financial uncertainty shock no longer leads to increases in both macro and financial volatility factors. The persistence of the increase in financial volatility after the financial uncertainty shock is still higher than the persistence of the increase of macro volatility to a macro uncertainty shock.

Figure A-47 **Posterior results:**
Macro uncertainty shock on level variables (Haar/S&P500 identification)

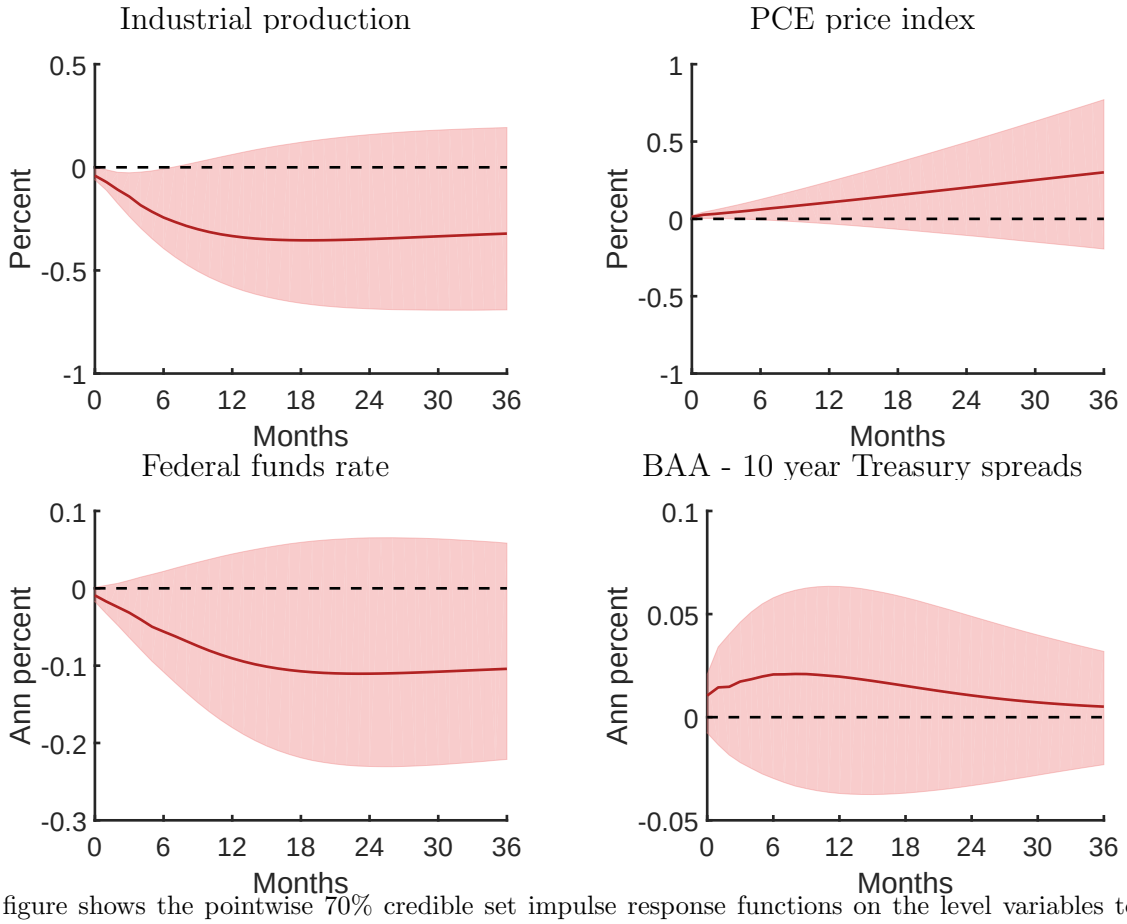

This figure shows the pointwise 70% credible set impulse response functions on the level variables to a 1 standard deviation macro uncertainty shock for the Carriero et al. (2017) model.The reduced-form parameters are drawn from their posterior distributions. We assume a Haar prior over the rotation matrices. We only keep impulse response functions that satisfy Assumptions $\mathcal{A}^2_{u'f}$ and $\mathcal{A}^2_{u'm}$. The dark red line is the impulse response function drawn from a single Q^* that is closest to the pointwise median in a sum of squares sense (median target method of Fry and Pagan (2007)).

Figure A-48 **Posterior results:**
Financial uncertainty shock on volatility factors (Haar/S&P500 identification)

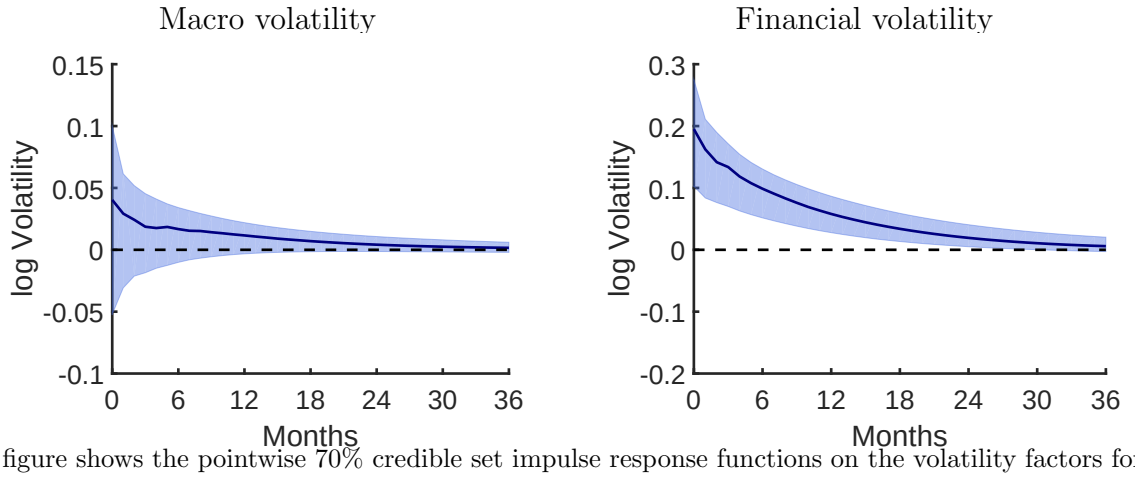

This figure shows the pointwise 70% credible set impulse response functions on the volatility factors for the Carriero et al. (2017) model. We assume a Haar prior over the rotation matrices using the sign restriction on the S&P500. The dark blue line is the impulse response function drawn from a single Q^* that is closest to the pointwise median in a sum of squares sense (median target method of Fry and Pagan (2007)).

Figure A-49 **Posterior results:**
Macro uncertainty shock on volatility factors (Haar/S&P500 identification)

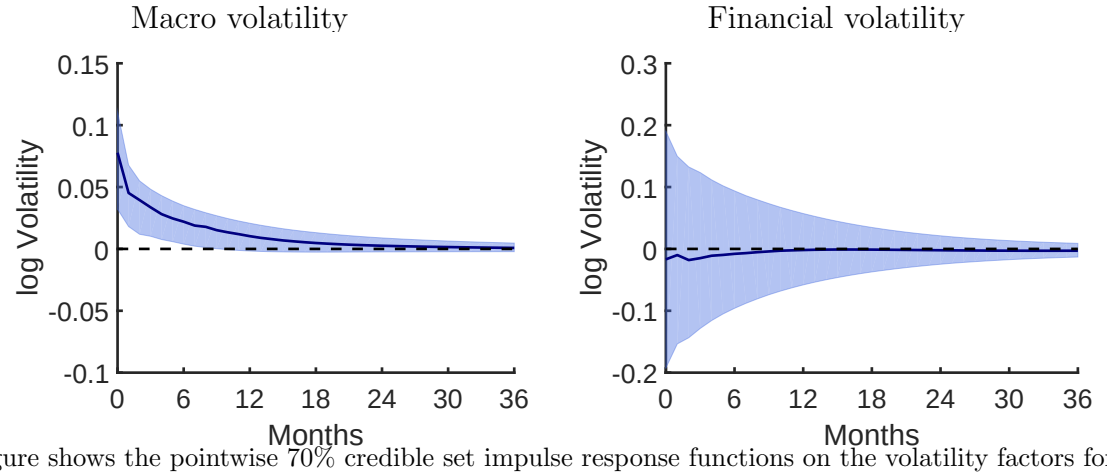

This figure shows the pointwise 70% credible set impulse response functions on the volatility factors for the Carriero et al. (2017) model. We assume a Haar prior over the rotation matrices using the sign restriction on the S&P500. The dark blue line is the impulse response function drawn from a single Q^* that is closest to the pointwise median in a sum of squares sense (median target method of Fry and Pagan (2007)).

D Supporting results

In this section, we present some additional results that supplement our main fin. First, we discuss an analysis of the relationship between periods of high financial uncertainty and the macroeconomy. We aim to show that financial uncertainty indeed is correlated with downturns in the macroeconomy. Second, we discuss empirical exercises using international data (Germany, France, Italy, and Spain) that support our spread identification restriction.

D.1 The relationship between financial uncertainty and the macroeconomy

We provide evidence on how the economy behaves around periods of high financial uncertainty.

To identify these periods, we turn to two different indices that purport to measure financial uncertainty. The first is the posterior mean of the financial volatility factor of Carriero et al. (2017). This index measures financial uncertainty as the common movements in volatilities across a broad range of financial variables. It runs from $1960M9-2014M7$. The second is the US equity uncertainty index of Baker et al. (2013).[12] This index searches all US newspapers in the NewsBank service. The index is constructed as the fraction of newspaper articles including the words "uncertainty" or "uncertain," the terms "economic" or "economy," and one or more of the following terms: "equity market", "equity price", "stock market", or "stock price." The index is constructed at a daily frequency, so we take an intermonth average to form a monthly index. It runs from $1985M1 - 2017M12$.

[12]The index can be found on www.policyuncertainty.com

D.1.1 Results

We identify time periods of either high broad-based financial uncertainty, as measured by the Carriero et al. (2017) or Baker et al. (2013) indices. We are only interested in time periods of extreme financial uncertainty, so we consider time periods of the index that are greater than 2 standard deviations above the mean of each index, respectively.

Carriero et al. (2017) index We identify 9 dates of high financial volatility according to the index. These dates correspond to the peaks of the financial uncertainty index during periods of heightened financial volatility.

Baker et al. (2013) equity uncertainty index We identify 7 dates with the Baker et al. (2013) index. We find evidence of a strong linear time trend, which we remove before working with the index. The dates we use when identifying peaks of heightened equity uncertainty correspond to the highest points of the index.[13]

Response of macroeconomy Now we look at how the macroeconomy responds following the peaks of high financial uncertainty. We combine the two sets of events identified by our two financial uncertainty indices. In effect, this adds three events to those already identified from the Carriero et al. (2017) index: October 1987 (Black Monday), November 2000 (Dot Com Bubble), and August 2011 (Black Monday). For the events that both uncertainty indices pick up, we use as the peak date the timing from the Carriero et al. (2017).[14]

We focus on industrial production growth, PCE inflation, the federal funds rate, and the BAA-10 year Treasury bond spread. We take an event study type approach and look at the 5 months before and after the financial uncertainty peak in question. For IP growth and PCE inflation, we plot the data, whereas for the federal funds rate and the spreads, we

[13]The index has a large value in Jan 1985, which is the first period of the data. We exclude this observation when detecting uncertainty events because we do not know the date of the peak.

[14]The results are robust to using the Baker et al. (2013) index timing as well.

Figure A-50 **Financial uncertainty indices and identified periods of high financial uncertainties**

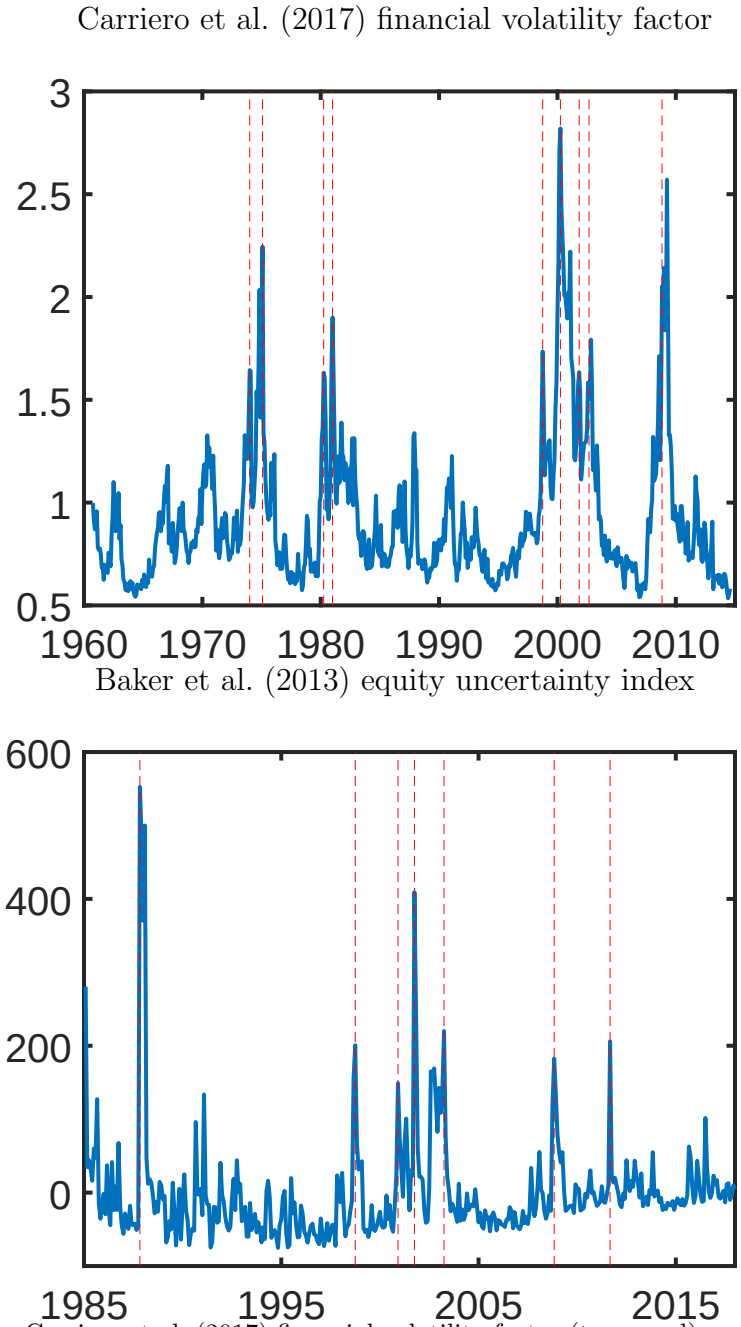

This figure shows the Carriero et al. (2017) financial volatility factor (top panel) and the Baker et al. (2013) equity uncertainty index (bottom panel). The blue lines are the indices themselves whereas the dotted red lines are the identified peaks of the financial uncertainty events that lead the indices to jump more than 2 standard deviations above its historical mean. Note that the Baker et al. (2013) index is first regressed on a constant and linear time trend.

Figure A-51 **Behavior of macroeconomy around periods of high financial uncertainty**

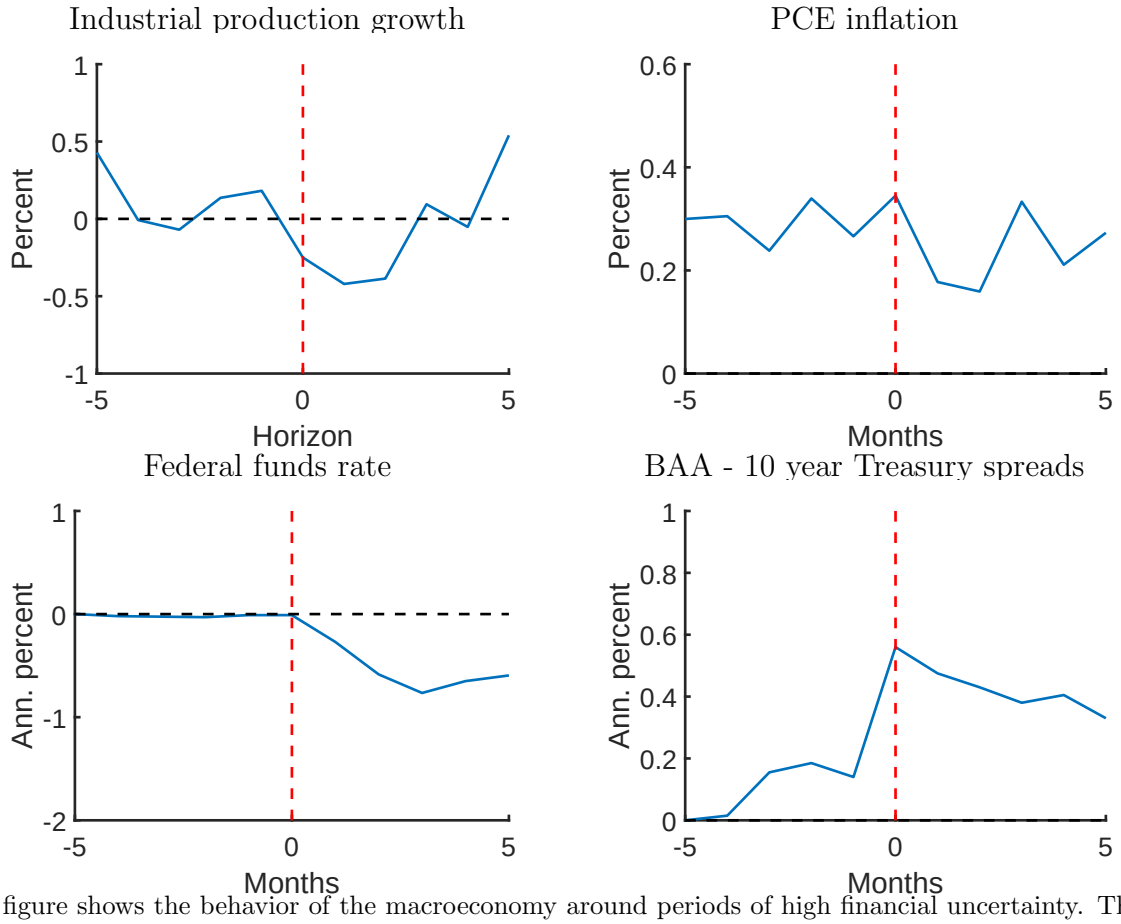

This figure shows the behavior of the macroeconomy around periods of high financial uncertainty. The red dotted line shows the time period of the peak of financial uncertainty, as measured by the Carriero et al. (2017) and Baker et al. (2013) indices. We look at a period of 5 months before and after the peak of the indices. For IP growth and PCE inflation, we plot the data, whereas for the federal funds rate and the spreads, we normalize the time period -5 to be equal to 0%.

normalize the time period -5 to be equal to 0%. We look at the median responses across these 12 identified episodes of high financial uncertainty.

Figure A-51 shows the results from the exercise. We find evidence that IP growth declines the period of the financial uncertainty peak. This decline is persistent, with below average growth for 4 months after the peak of financial uncertainty (average IP growth in our sample is 0.24%) and a trough of -0.42% 1 month after the period of high financial uncertainty. There is also some evidence of a persistent decline in PCE inflation after the financial uncertainty event, with a trough of below 0.2% 2 months after the financial uncertainty event.

The federal funds rate begins to decline as well, with a long run decline of around 60 basis points 5 months after the peak.

Importantly for our results, there is strong evidence of a sharp increase in spreads the month of the financial uncertainty peak. The median response is for spreads to rise by 42 basis points the month of the financial uncertainty peak. Spreads are persistently high for the 5 months after the financial uncertainty event. An additional point to note is that spreads begin rising in the months before the financial uncertainty peak. However, the largest spike in spreads occurs in the period of the financial uncertainty peak. This may be due to the fact that we are taking as the event date the peak of the financial uncertainty index. Indeed, financial uncertainty begins increasing in the months before the peak is reached.[15]

We would like to mention a caveat to these results. We believe that they provide evidence that suggests heightened financial volatility or uncertainty are associated with declines in IP growth, inflation, the federal funds rate, and a rise in spreads. This puts the explanation of a financial uncertainty shock as a potentially important factor in macroeconomic fluctuations on the table, but it by no means rules out other potential explanation. A proper identification scheme would be necessary to disentangle the various structural sources, which is the focus of our paper.

D.2 Assessing the spread identification assumption

A common theme across these two examples is the identifying power of spread behavior in separating the two uncertainty shocks. Specifically, in both examples, a key assumption is that a one standard deviation positive financial uncertainty shock leads to a larger increase in spreads than a one standard deviation macro uncertainty shock. We provide some evidence supporting this identification assumption.

[15] Importantly, the Carriero et al. (2017) model we use for our second example also controls for any possible effects of time $t-1$ level shocks on time t volatility, so the effects of any changes in spreads in the periods before a financial uncertainty shock would be properly accounted for.

D.2.1 Structural model simulations

First, we take a model-based approach. Motivated by the work of Basu and Bundick (2015) and Gertler and Karadi (2011), we consider a New Keynesian model with financial frictions. We look at two structural volatility shocks: a capital quality volatility shock (financial uncertainty) and a total factor productivity (TFP) volatility shock (macro uncertainty) and find support for our identification assumption that a financial uncertainty shock leads to a larger increase in spreads relative to a macro uncertainty shock.

The intuition for this result is straightforward. An increase in TFP volatility encourages agents to decrease consumption, supply more labor, and increase investment. The reason is with increased future uncertainty about TFP, working more and investing in a higher capital stock helps agents smooth out consumption.[16] On the other hand, a capital quality volatility shock increases the riskiness of holding capital, thereby discouraging investment relative to the TFP volatility shock. In these models, investment demand is a key determinant of spread behavior, as stronger investment demand increases the price of capital, thereby improving the intermediary's net worth position and decreasing spreads.

This fundamental difference in the nature of risk means that it indeed is quite difficult to find a parameterization where a TFP volatility shock leads to a higher movement in spreads relative to a capital quality volatility shock. We show the robustness of this result to changes in the persistence and standard deviations of the two volatility shocks, the amount of nominal price rigidities in the model, and the household's risk aversion.[17]

Details on the structural model To motivate our sign restriction assumptions on the spread, we consider the implications of a financial uncertainty shock (capital quality volatility) and a macro uncertainty shock (TFP volatility) for spread behavior in a dynamic equi-

[16] This is the heart of the comovement problem between consumption and investment that plagues TFP volatility shocks in real business cycle models.

[17] As in Basu and Bundick (2015), nominal rigidities do restore the comovement between consumption and investment.

librium model with financial frictions. Specifically, we are interested in deriving some robust predictions on the relative movements in spreads following the two structural volatility shocks. We start with a baseline parametrization of the model as shown in table A-7. We then vary the relative persistence and standard deviations of the two structural shocks, the level of nominal price rigidities, and the risk aversion of the households. The results are clear: for all parameterizations, the capital quality volatility shock produces a larger positive movement in spreads when compared to the TFP volatility shock. Moreover, for all parameterizations, the capital quality volatility shock leads to an increase in the spreads.

The dynamic equilibrium model emphasizes the mechanism highlighted in Gertler and Karadi (2011). The setup is quite similar to the baseline Gertler and Karadi (2011) model, but with three main differences: agents have Epstein-Zin utility, the government does not follow any credit policy, and price setters face Rotemberg (1982) as opposed to Calvo adjustment costs. Please refer to Gertler and Karadi (2011) for a discussion of model details.[18] This exposition will be a general sketch of the model.

There are two types of households: workers and bankers (financial intermediaries). Households have Epstein-Zin utility over consumption and leisure. Workers maximize consumption (C_t), labor (L_t), one period real deposit holdings (B_t), and one period nominal deposit holdings (B_T^n). P_t is the price level, W_t is the real wage rate, R_t is the real return on one period risk free deposits, ir_t is the nominal risk free rate on one period deposits, Π_t are profits from firms, and T_t are transfers.

$$U_t = \max_{C_t, L_t, B_t} \left[\left(C_t^{\eta} (1 - L_t)^{1-\eta} \right)^{\frac{1-\sigma}{\theta_U}} + \beta \left(E_t U_{t+1}^{1-\sigma} \right)^{\frac{1}{\theta_U}} \right]^{\frac{\theta_U}{1-\sigma}} \tag{A.36}$$

subject to

$$C_t = W_t L_t + \Pi_t + T_t + R_t B_t - B_{t+1} + ir_{t-1} \frac{B_t^n}{P_t} - \frac{B_{t+1}^n}{P_t}$$

Financial intermediaries obtain deposits from households and use the funds raised as well

[18] The appendix of Foerster (2015) also contains a useful discussion of the derivations.

as their own net worth to lend to non-financial firms. An intermediary j has the following balance sheet constraint, where Q_t is the price of a claim on non-finanical firms, $S_{j,t}$ is the quantity of claims, $N_{j,t}$ is the net worth, and $B_{j,t+1}$ is the amount of deposits:

$$Q_t S_{j,t} = N_{j,t} + B_{j,t+1} \tag{A.37}$$

Intermediary net worth has the following law of motion, where $R_{k,t+1}$ is the realized return to capital in period $t+1$:

$$N_{j,t+1} = R_{k,t+1} Q_t S_{j,t} - R_{t+1} B_{j,t+1} = \left(R_{k,t+1} - R_{t+1}\right) Q_t S_{j,t} + R_{t+1} N_{j,t} \tag{A.38}$$

Intermediary j's objective function is to maximize expected terminal wealth adjusted by the household stochastic discount factor ($\beta^i \Lambda_{t,t+i}$)

$$V_{j,t} = \max E_t \left(\sum_{\tau=1}^{\infty} (1-\theta)\theta^\tau \beta^\tau \Lambda_{t,t+\tau} \left[\left(R_{k,t+\tau} - R_{t+\tau}\right) Q_{t+\tau-1} S_{j,t+\tau-1} + R_{t+\tau} N_{j,t+\tau-1} \right] \right) \tag{A.39}$$

A banker has the following incentive compatibility constraint, motivated by a desire to divert assets, only $1-\lambda$ of which can be recovered by the households

$$V_{j,t} \geq \lambda Q_t S_{j,t} \tag{A.40}$$

Now we discuss the non-financial side of the macroeconomy. Intermediate goods firms are competitive and produce the goods that are sold to retail firms. They issue S_t claims to capital K_{t+1}. The following arbitrage relation holds between the value of claims and the value of capital:

$$Q_t K_{t+1} = Q_t S_t \tag{A.41}$$

The production function of the intermediate goods firms is Cobb-Douglas and perturbed by

a permanent TFP shock (A_t) and capital quality shock (ζ_t):

$$Y_t = (U_t \zeta_t K_t)^{\alpha} (A_t L_t)^{1-\alpha} \tag{A.42}$$

where U_t is capacity utilization.

Before selling previously purchased capital back on the competitive market, intermediate goods firms also pay a unit cost per unit to repair depreciated capital. Therefore, the realized return to capital K_{t+1} is

$$R_{k,t+1} = \frac{\left[P_{m,t+1}\alpha \frac{Y_{t+1}}{\zeta_{t+1}K_{t+1}} + Q_{t+1} - \delta(U_{t+1})\right]\zeta_{t+1}}{Q_t} \tag{A.43}$$

where $P_{m,t+1}$ is the price of intermediate goods. In addition to purchasing capital, intermediate goods firms also decide on a capital utilization rate and labor supply.

Competitive capital producing firms purchase capital from intermediate goods firms. They repair depreciated capital, build new capital, and sell it on the competitive market. In line with Gertler and Karadi (2011), we assume that adjustment costs are on investment net of depreciated capital. Therefore, capital producing firms only pay a unit cost to repair depreciated capital. Their profits are as follows:

$$prof_t = \delta(U_t)\zeta_t K_t - Q_t\zeta_t K_t + Q_t K_{t+1} - (K_{t+1} - (1-\delta(U_t))\zeta_t K_t) - S\left(\frac{I_{n,t} + I_{ss}A_t}{I_{n,t-1} + I_{ss}A_{t-1}}\right)(I_{n,t} + I_{ss}A_t) \tag{A.44}$$

We define net investment as

$$I_{n,t} = I_t - \delta(U_t)\zeta_t K_t \tag{A.45}$$

Rewriting the profits of capital producing firms in terms of net investment, the maximization problem is as follows:

$$\max_{I_{n,t}} E_t \left(\sum_{\tau=0}^{\infty} \beta^{\tau} \Lambda_{t,t+\tau} \left[(Q_\tau - 1) I_{n,\tau} - S\left(\frac{I_{n,\tau} + I_{ss}A_\tau}{I_{n,\tau-1} + I_{ss}A_{\tau-1}}\right)(I_{n,\tau} + I_{ss}A_\tau) \right] \right) \tag{A.46}$$

The function S is quadratic with respect to changes in net investment. I_{ss} is the trend-adjusted steady state level of investment. Capital good producers choose net investment levels $I_{n,\tau}$ to maximize the expected future discounted value of firm profits.

Retail firms are monopolistically competitive. They buy inputs from intermediate goods firms. The final output is a CES aggregate of each retail firm f product:

$$Y_t = \left[\int_0^1 Y_{ft}^{\frac{\epsilon-1}{\epsilon}} df\right]^{\frac{\epsilon}{\epsilon-1}} \tag{A.47}$$

Retail firms face quadratic price adjustment costs and have the objective function

$$\max E_t \sum_{\tau=0}^{\infty} \beta^\tau \Lambda_{t,t+\tau} \left(\left(\frac{p_{f,t+\tau}}{p_{t+\tau}} - P_{m,t+\tau} \right) \left(\frac{p_{f,t+\tau}}{p_{t+\tau}} \right)^{-\epsilon} y_{t+\tau} - \frac{\phi_p}{2} \left(\frac{p_{f,t+\tau}}{\Pi p_{f,t+\tau-1}} - 1 \right)^2 y_{t+\tau} \right) \tag{A.48}$$

Monetary policy follows a standard Taylor rule with interest rate smoothing that reacts to inflation and output growth deviations from steady state.

$$\frac{ir_t}{ir} = \left(\frac{ir_{t-1}}{ir} \right)^{\rho_R} \left(\left(\frac{\Pi_t}{\Pi} \right)^{\rho_\pi} \left(\frac{\Delta \log Y_t}{\Lambda_A} \right)^{\rho_Y} \right)^{1-\rho_R} \tag{A.49}$$

The Euler equation for nominal bonds holds:

$$\beta E_t \left(\Lambda_{t,t+1} \frac{ir_t}{\Pi_{t+1}} \right) = 1 \tag{A.50}$$

The government fiscal policy is Ricardian. Goods market clearing implies, where G is a fixed, exogenous level of government spending:

$$Y_t = C_t + I_t + \frac{\phi_p}{2} \left(\frac{\Pi_t}{\Pi} - 1 \right)^2 Y_t + S \left(\frac{I_{n,t} + I_{ss} A_t}{I_{n,t-1} + I_{ss} A_{t-1}} \right) (I_{n,t} + I_{ss} A_t) + G \tag{A.51}$$

The capital accumulation equation is:

$$K_{t+1} = (1 - \delta(U_t)) \zeta_t K_t + I_t \tag{A.52}$$

Table A-7 Baseline parameter values of the dynamic equilibrium model

Parameter	Value	Parameter	Value	Parameter	Value
α	0.33	ρ_A	0.2	S''	3
β	0.994	σ_A	0.007	ϕ_p	160
Λ_A	0.004	ρ_ζ	0.66	ρ_R	0.75
Π	0.0092	σ_ζ	0.01	ρ_π	1.5
ϵ	6	$\rho_{h,A}$	0.5	ρ_y	0.5
δ	0.025	$\sigma_{h,A}$	0.5	θ	0.972
η	0.32	$\rho_{h,\zeta}$	0.5	λ	0.381
σ	10	$\sigma_{h,\zeta}$	0.5		
ψ	36	G	$0.19Y_{ss}$		
γ_2	0.01	$R_{k,ss} - R_{ss}$	$0.01/4$		

Depreciation $\delta(U_t)$ is a function of the amount of utilization

$$\delta(U_t) = \delta + \gamma_1 (U_t - 1) + \gamma_2 (U_t - 1)^2 \tag{A.53}$$

The two exogenous shocks and their stochastic volatilities follow autoregressive processes:

$$\begin{aligned}
\Delta \log A_t &= \rho_A \Delta \log A_{t-1} + \epsilon_{A,t}, \epsilon_{A,t} \sim N(0, h_A^2) \\
\log h_{A,t} &= (1 - \rho_{h,A}) \log \sigma_A + \rho_{h,A} \log h_{A,t-1} + \epsilon_{h_A,t}, \epsilon_{h_A,t} \sim N(0, \sigma_{h,A}^2) \\
\log \zeta_t &= \rho_\zeta \log \zeta_{t-1} + \epsilon_{\zeta,t}, \epsilon_{\zeta,t} \sim N(0, h_\zeta^2) \\
\log h_{\zeta,t} &= (1 - \rho_{h,\zeta}) \log \sigma_\zeta + \rho_{h,\zeta} \log h_{\zeta,t-1} + \epsilon_{\zeta,t}, \epsilon_{\zeta,t} \sim N(0, \sigma_{h,\zeta}^2)
\end{aligned} \tag{A.54}$$

We are interested in the model's implications for bond spreads, which in the model is defined as $E_t [R_{k,t+1}] - R_t$.

To justify our sign restrictions, we are specifically interested in whether a capital quality volatility shock leads to a larger movement in bond spreads relative to a TFP volatility shock. Also, we are interested in whether a capital quality volatility shock leads to a positive movement in spreads.

For our baseline calibration, we take many of the parameter values from Gertler and Karadi (2011) and Basu and Bundick (2015). We choose a value of 0.5 for the persistence

of both volatility shocks. The parameter values are also well within the range of those often used in the literature. As this is a quarterly model, such a persistence implies that volatility is 25% that of its height after half a year, which is broadly consistent with our empirical results. We take a third order perturbation of the model with pruning (Kim et al., 2008; Andreasen et al., 2018).

We would like our result to be robust. Therefore, we vary several key parameters of interest around our baseline calibration. First, we vary the persistence and standard deviations of the volatility shocks. Specifically, we vary $\rho_{h,i}$ on a grid of [0.1 0.5 0.99] for $i = A, \zeta$. We vary $\sigma_{h,i}$ on a grid of [0.1 0.5 1]. Note that we consider all possible parameter combinations for $\rho_{h,A}, \rho_{h,\zeta}, \sigma_{h,A}, \sigma_{h,\zeta}$, for a total of 81 possible parameters. This means that we allow for parameterizations with a persistent and large TFP volatility shock combined with a transitory and small capital quality volatility shock. For all parameterizations that we consider, a capital quality volatility shock leads to a larger movement in spreads relative to a TFP volatility shock. A capital quality volatility shock also always leads to an increase in the spreads.

Next, we vary the level of price rigidities. Basu and Bundick (2015) show that a high enough price rigidity can restore comovement between consumption and investment following volatility shocks, so it is of interest for us to vary this parameter. Fixing other parameters at the baseline calibration, we consider a variety of ϕ_p on a grid of [0 160 250 500 750 1000]. Nominal price rigidities do indeed lead to declines in consumption and investment to TFP volatility shocks. For no parameterization considered, however, does a TFP volatility shock lead to a larger increase in spreads relative to a capital quality volatility shock. Furthermore, a capital quality volatility shock continues to always increase the spreads.

Finally, we test robustness to the level of risk aversion in the household utility function. We set household risk aversion to 10, which is well within the range of reasonable parameter values. For robustness, we lower risk aversion to values on the grid [1.01 3 5 7 10]. Our results continue to stay the same.

We conclude from this exercise that our baseline sign restrictions that a financial uncertainty shock leads to a larger increase in spreads than a macro uncertainty shock appears quite robust in a theoretical model. We also find robust evidence that a financial volatility shock leads to an increase in spreads.

In closing this discussion, we would like to discuss a caveat with regards to the relationship between our empirical model and a structural model. It is hard to find a case where our model exactly maps into a fully structural model. Insofar as our econometric model is flexible and the economic restrictions we impose are limited, however, we believe our toolkit can aid in the discovery of important comovements in the data that more structural models with uncertainty shocks should be able to match. Moreover, by focusing on the identification problem in the volatility equation, we can also apply our methodology to models that do not neatly fit into the structural VAR framework, such as factor volatility models.

D.2.2 Evidence from European data

In addition to the model based evidence, we also provide empirical evidence to support our identification strategy. We turn to international data from Germany, France, Italy, and Spain to investigate the relationships between financial and macro uncertainty on corporate bond spreads. We conduct two exercises. First, we estimate bivariate versions of our CAIW model on quarterly EBP and labor productivity data. We use this model to analyze the relationships between productivity volatility, EBP volatility, and the EBP level. Our second exercise identifies financial and macro uncertainty shocks using volatility proxies and a proxy VAR approach.

Productivity volatility, EBP volatility, and the EBP level Our first exercise investigates the relationships between the EBP level and the volatilities of productivity and EBP. We take quarterly EBP and labor productivity data from $1999Q1 - 2013Q3$ for Germany,

France, Italy, and Spain. We use labor productivity data as it is the closest quarterly proxy for total factor productivity that we could find.[19]

We estimate bivariate versions of our volatility-in-mean model assuming the CAIW volatility process. Our model specifies 4 lags in the VAR, a contemporaneous volatility-in-mean effect, and 1 lag in the volatilities.[20] We take $500,000$ draws from the posterior distribution and use the first $300,000$ as burn-in. We use 500 of these final $200,000$ reduced-form parameters (evenly-spaced) and 30 draws of the rotation matrices for each reduced-form parameter draw. We assume a Haar prior on the rotation matrices.

We begin by identifying a productivity (*prod*) uncertainty shock.

Assumption $\mathcal{A}_p^4$ (Productivity uncertainty shock). The uncertainty shock satisfies $\mathcal{A}_p$:

$$\mathcal{A}_{p,1}^4 : IRF\left[\Sigma_{prod,t+h}\middle|v_t^* = e_1; R_t\right] > 0 \text{ for } h = 0.$$

$$\mathcal{A}_{p,2}^4 : IRF\left[\Sigma_{prod,t+h}\middle|v_t^* = e_1; R_t\right] > IRF\left[\Sigma_{prod,t+h}\middle|v_t^* = e_i; R_t\right] \text{ for } h = 0 \text{ and } i \neq 1.$$

This assumption imposes that a productivity uncertainty shock must raise labor productivity volatility contemporaneously and also lead to the largest increase in labor productivity volatility among all second moment shocks. It imposes that the bulk of the fluctuations in labor productivity volatility come from productivity uncertainty shocks.

Figure A-52 shows the responses of the EBP to a productivity uncertainty shock. We find that across these countries, there is little evidence that a productivity uncertainty shock moves EBP. Indeed, the credible sets are wide around 0%, and for Spanish data, the posterior median IRF is negative. We believe that these results support our identification restriction that does not specify the directional response of the EBP to a macro uncertainty shock.

[19] Our EBP data comes from Gilchrist and Mojon (2017) and is monthly. We take interquarter averages to form the quarterly EBP. Our labor productivity is from FRED (Early estimate of quarterly ULC indicators: total labor productivity).

[20] Our priors are the same as those used in Example 1 of the main text.

Figure A-52 **Posterior results:**
Productivity uncertainty shock on EBP for European countries

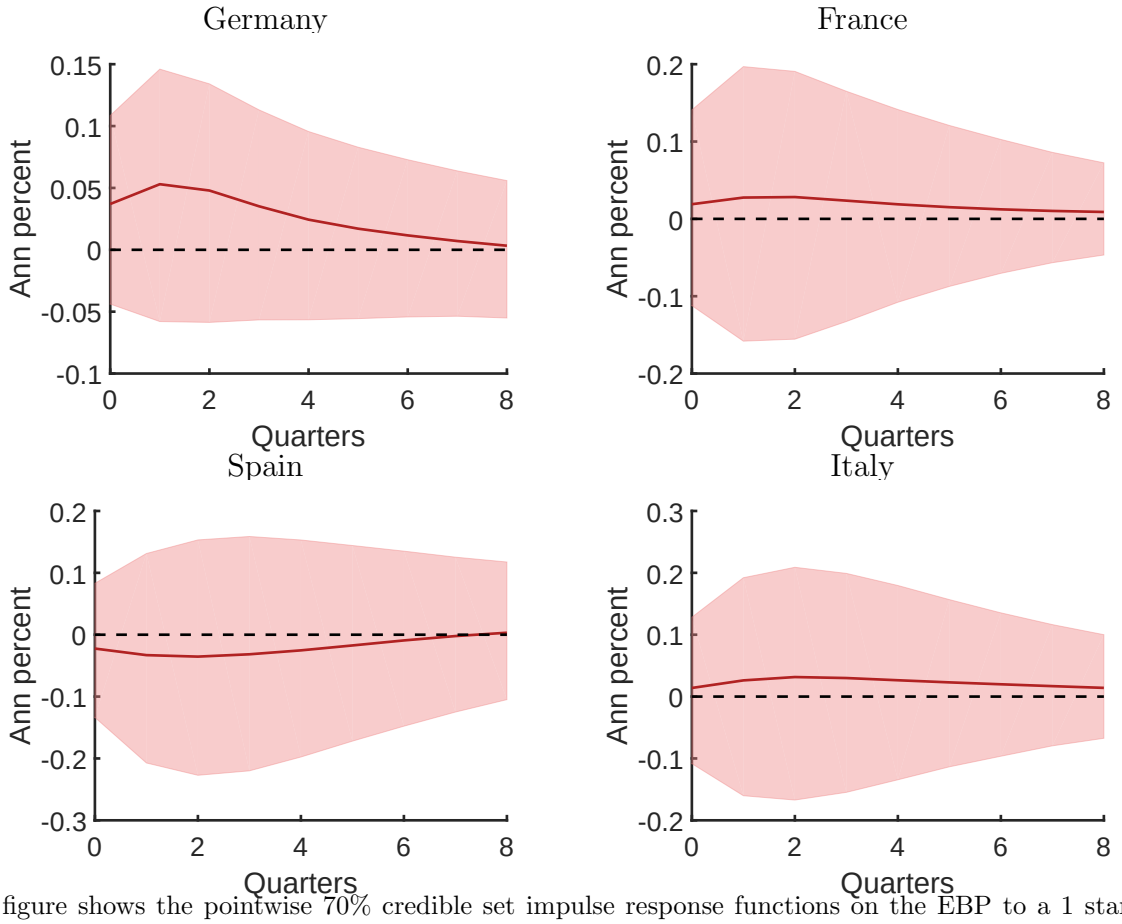

This figure shows the pointwise 70% credible set impulse response functions on the EBP to a 1 standard deviation productivity uncertainty shock for the bivariate CAIW model. The reduced-form parameters are drawn from their posterior distributions. We assume a Haar prior over the rotation matrices. We only keep impulse response functions that satisfy Assumption $\mathcal{A}_p^4$. The dark red line is the impulse response function drawn from a single Q^* that is closest to the pointwise median in a sum of squares sense (median target method of Fry and Pagan (2007)).

A valid concern is that we do not have enough data to properly identify the real effects of any uncertainty shock. We show that this is not the case. We now identify a shock that maximizes EBP volatility:

Assumption $\mathcal{A}^5_{EBPvmax}$ (Uncertainty shock that maximizes EBP volatility). The uncertainty shock satisfies $\mathcal{A}^5_{EBPvmax}$:

$\mathcal{A}^5_{EBPvmax,1}$: $IRF\left[\Sigma_{EBP,t+h}\middle|v_t^* = e_1; R_t\right] > 0$ for $h = 0$.

$\mathcal{A}^5_{EBPvmax,2}$: $IRF\left[\Sigma_{EBP,t+h}\middle|v_t^* = e_1; R_t\right] > IRF\left[\Sigma_{EBP,t+h}\middle|v_t^* = e_i; R_t\right]$ for $h = 0$ and $i \neq 1$.

In imposing Assumption $\mathcal{A}^5_{EBPvmax}$, we do not simultaneously impose Assumption $\mathcal{A}^4_p$, so we are not interested in a joint identification exercise.[21]

Figure A-53 shows the results. We find that this shock indeed does increase the EBP across the four countries. If one were to interpret this shock as financial uncertainty shock, then it would be reasonable to conclude that a financial uncertainty shock increases the EBP by more than the macro uncertainty shock.[22]

Analysis with empirical proxies of uncertainty In this exercise, we compare the reduced-form correlations between the excess bond premium and more financially-related uncertainty proxies versus more macro-based ones. We proxy for financial uncertainty with stock market volatility and macro uncertainty with the common movements in volatility estimated from a large cross section of macro data in the spirit of Jurado et al. (2015).[23] The stock market volatility data is constructed by splicing together volatility measures from daily returns and the implied volatility. The macro volatility factor data is constructed by taking averages of volatility estimates across a large cross section of macroeconomic data. The precise details are in Meinen and Roehe (2017). The data are monthly from $1999M1$ to $2013M10$.

We run country-by-country trivariate Bayesian vector autoregressions with 6 lags using the codes of Giannone et al. (2015). For the variance covariance matrix of the innovations, we put an inverse Wishart prior with degree of freedom 5 and with the mean as a diagonal variance covariance matrix with the variances of the innovations from univariate AR(1) models on the diagonal. Our prior for the VAR parameters is conditional on the variance

[21] Indeed, if one imposes jointly that Assumptions $\mathcal{A}^4_p$ and $\mathcal{A}^5_{EBPvmax}$ hold, then it is not clear how to deal with a second moment shock that simultaneously satisfies both assumptions.

[22] One caveat, of course, that is preventing us from wholeheartedly taking this interpretation is that one should in theory jointly identify the uncertainty shocks within one VAR system. The purpose of this exercise, on the other hand, is not necessarily to jointly identify the two uncertainty shocks. It is to provide supporting evidence to our sign restrictions used in the main text.

[23] We use data provided by Meinen and Roehe (2017).

Figure A-53 **Posterior results:**
Uncertainty shock that maximizes EBP volatility on EBP for European countries

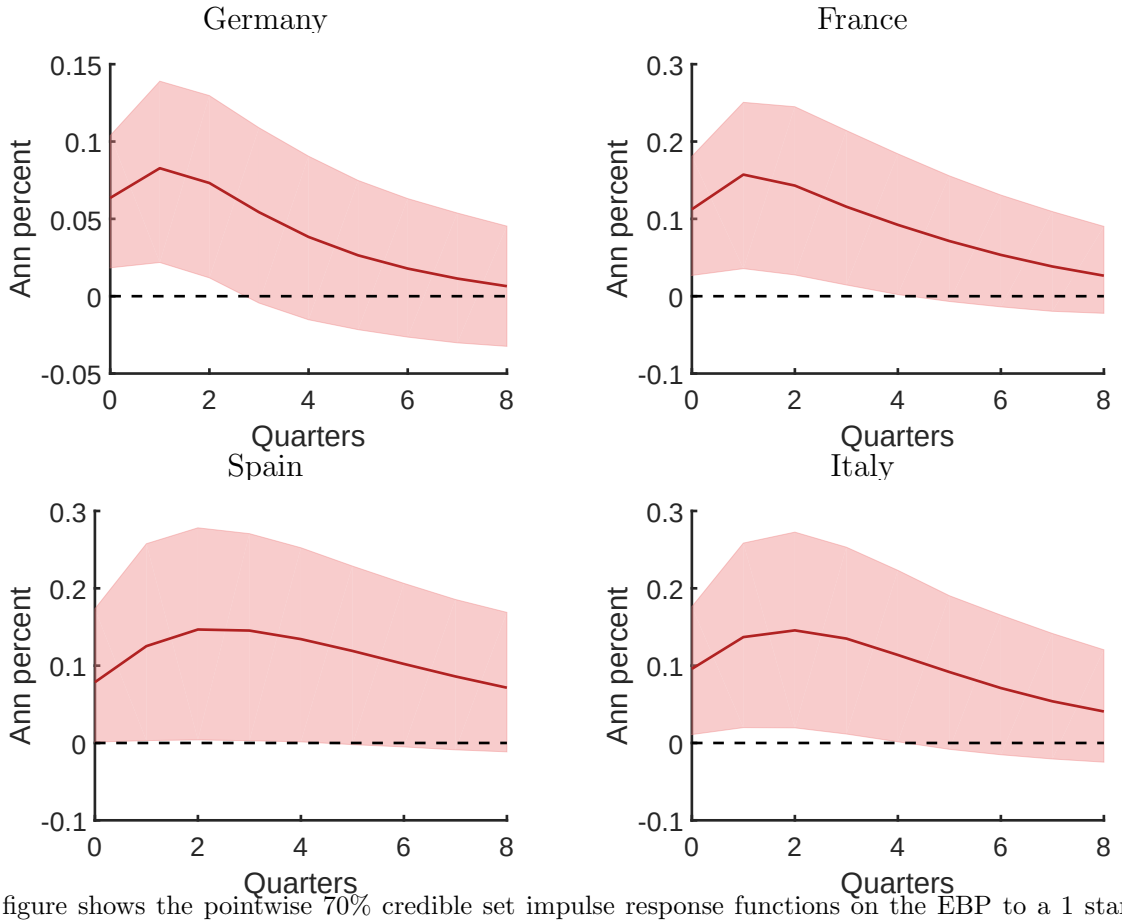

This figure shows the pointwise 70% credible set impulse response functions on the EBP to a 1 standard deviation uncertainty shock that maximizes the EBP volatility increase for the bivariate CAIW model. The reduced-form parameters are drawn from their posterior distributions. We assume a Haar prior over the rotation matrices. We only keep impulse response functions that satisfy Assumption $\mathcal{A}_p^4$. The dark red line is the impulse response function drawn from a single Q^* that is closest to the pointwise median in a sum of squares sense (median target method of Fry and Pagan (2007)).

covariance matrix of the innovations (Σ). Specifically, we put a Minnesota prior on the VAR parameters with variance covariance matrix:

$$cov\left((\Phi_s)_{ij},(\Phi_r)_{hm}|\Sigma\right)=\begin{cases}\lambda^2\frac{1}{s^2}\frac{\Sigma_{ih}}{\widehat{\sigma}_j^2} & \text{if } m=j \text{ and } r=s\\ 0 & \text{otherwise}\end{cases} \tag{A.55}$$

r and s are the lags of the VAR parameters while i is the equation and j is the variable. This prior allows for correlation between the same variables at the same lags in different

Figure A-54 **Posterior results:**
Generalized IRFs of VIX versus macro vol factor for European countries

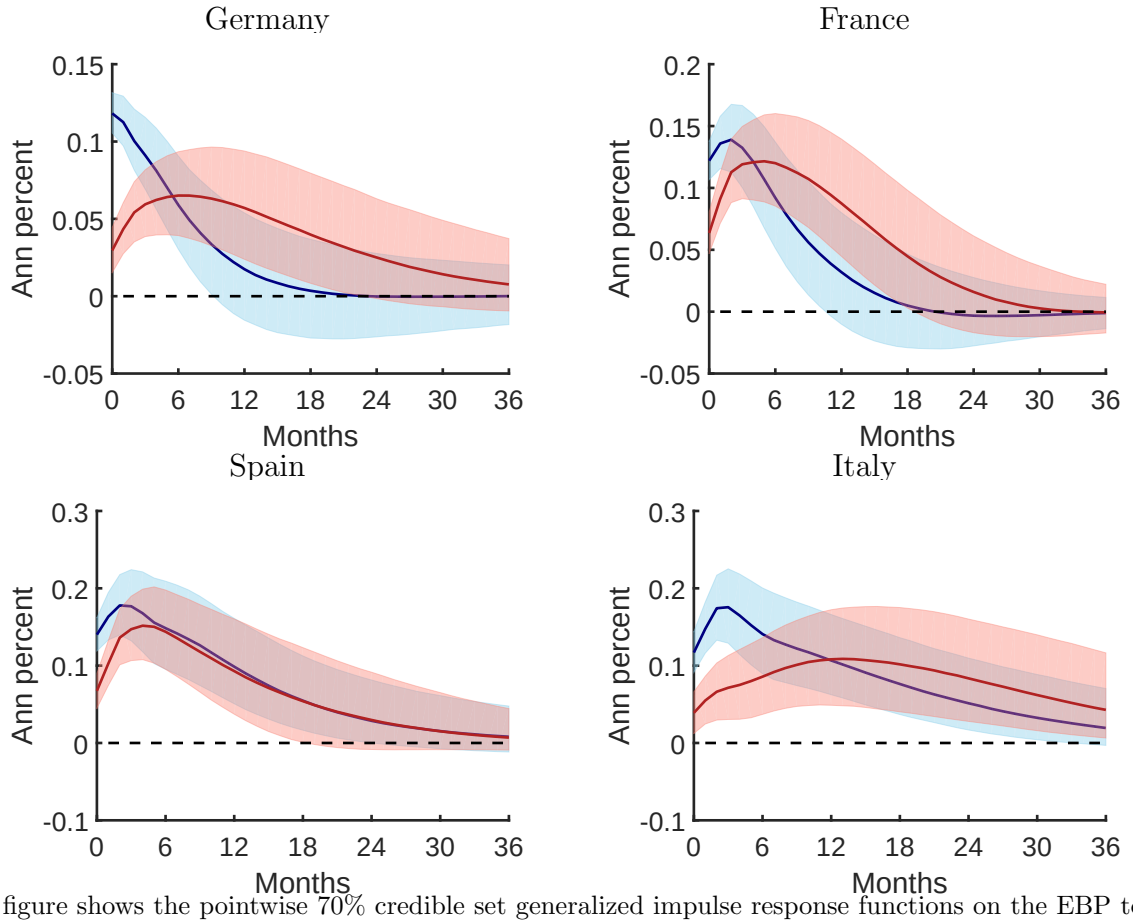

This figure shows the pointwise 70% credible set generalized impulse response functions on the EBP to a 1 standard deviation VIX shock (blue) and macro volatility factor shock (red). The dark blue and red lines are the respective pointwise posterior medians. The parameters are drawn from their posterior distributions.

equations. λ is the prior tightness parameter. We follow Giannone et al. (2015) and put a hyperprior on this parameter, which is a Gamma distribution with a mean of 0.2 and standard deviation of 0.4.[24]

We are interested in characterizing the dynamic relationships between our financial and macro uncertainty measures. To do so, we use generalized impulse response functions of Pesaran and Shin (1998), which give the expected movements in EBP from a one standard deviation innovation to the financial uncertainty and macro uncertainty proxies. Figure A-54 shows the responses of the EBP to shocks to the stock market volatility equation (blue and

[24]We use the codes provided by Giannone et al. (2015).

red lines) and macro volatility factor equation (green and magenta lines). Across the four countries, we see a consistent result that innovations to stock market volatility are associated with higher movements of the excess bond premium on impact relative to innovations to the macro volatility factor. While the purpose of this exercise is not to identify financial and macro uncertainty shocks, we find the relationships between the excess bond premium and the two different uncertainty proxies across many countries as suggestive evidence in support of our bond spread sign restriction assumption.

E Applying our methodology on data simulated from the Gertler and Karadi (2011) model

We now apply our methodology to data simulated from the Gertler and Karadi (2011) model discussed in section D.2 of the appendix. In total, there are 4 shocks hitting the system: TFP and capital quality level shocks, and TFP and capital quality volatility shocks. We simulate data of length 550 from the model (burn-in of 1000). We then estimate our VAR model with the inverse Wishart volatility process on output growth and spread data.

There are two challenges with regards to this exercise. First, the DSGE model is solved by a third order perturbation method. Therefore, the data come from a nonlinear state space model. As our VAR is linear conditional on the volatility estimate Σ_t, we are neglecting some higher-order terms in our empirical model. This is an important caveat to our results to keep in mind. Second, as was pointed out by Born and Pfeifer (2014), it is quite difficult for dynamic equilibrium models to generate large fluctuations in response to second moment shocks without producing unreasonably large responses to first moment shocks. This makes the identification of the real effects of volatility shocks quite difficult. In a data simulation, the effects of level shocks generally dominate. In general, we follow our parameterization in A-7. We make a few parameter changes, with the goal of boosting the importance of the real effects of volatility shocks. We change the persistence of the capital quality and TFP volatility shocks to 0.95, decrease the standard deviations of the volatility shock innovations to 0.1, and set the risk aversion of the agents to 30. The increased persistence of the volatility shock amplifies its real effects, as agents expect the heightened volatility to last longer. The smaller volatility shock innovations prevents unreasonably large swings in the volatility of the data, which may make identification of any level responses to uncertainty shocks difficult to detect. Finally, the increased risk aversion amplifies the agents responses to changes in volatility. Even with this calibration, a one standard deviation capital quality level shock, for example, leads to around a 10 times larger response in spreads and output relative to the

two volatility shocks, making the econometric exercise still quite difficult.

In addition to these first three changes, we also set the price adjustment cost parameter $\phi_p = 0$. This change is so that a TFP volatility shock will lead to an increase in output growth and decrease in spreads whereas a capital quality volatility shock will lead to a decrease in output growth and increase in spreads. This qualitative difference in output movements from the two different types of volatility shocks gives us a clear benchmark on which we can evaluate our sign restrictions identification strategy.

We take $25,000$ draws from the posterior distribution using our inverse Wishart model and treat the first $12,500$ as burn-in. We use the same priors as those used in our empirical exercise in the paper (section C.1.3 of the appendix).

We impose the "traditional sign restrictions" of section C.1.11 of the appendix to identify the two shocks (these were the sign restrictions from our original draft). For convenience, they are reproduced here, with the only change being that the VAR system contains 2 variables instead of 4:

Assumption $\mathcal{A}_{uf}^{3,DSGE}$ (Financial uncertainty shock). The uncertainty shock satisfies $\mathcal{A}_{uf,1}^{3,DSGE}$ and $\mathcal{A}_{uf,2}^{3,DSGE}$:

$$\mathcal{A}_{uf,1}^{3,DSGE} : IRF[\Sigma_{ii,t+h}|v_t^* = e_1; R_t] > 0 \text{ for } h = 0 \text{ and } i = 1, 2.$$

$$\mathcal{A}_{uf,2}^{3,DSGE} : IRF[EBP_{t+h}|v_t^* = e_1; R_t] > 0 \text{ for } h = 0,\ 1,\ 2.$$

Assumption $\mathcal{A}_{um}^{3,DSGE}$ (Macro uncertainty shock). The uncertainty shock satisfies $\mathcal{A}_{um,1}^{3,DSGE}$ and $\mathcal{A}_{um,2}^{3,DSGE}$:

$$\mathcal{A}_{um,1}^{3,DSGE} : IRF[\Sigma_{ii,t+h}|v_t^* = e_2; R_t] > 0 \text{ for } h = 0 \text{ and } i = 1, 2.$$

$$\mathcal{A}_{um,2}^{3,DSGE} : IRF[EBP_{t+h}|v_t^* = e_2; R_t] < 0 \text{ for } h = 0,\ 1,\ 2.$$

Assumption $\mathcal{A}_{o}^{3,DSGE}$ (Other second moment shocks).

Figure A-55 **Capital quality volatility shock**

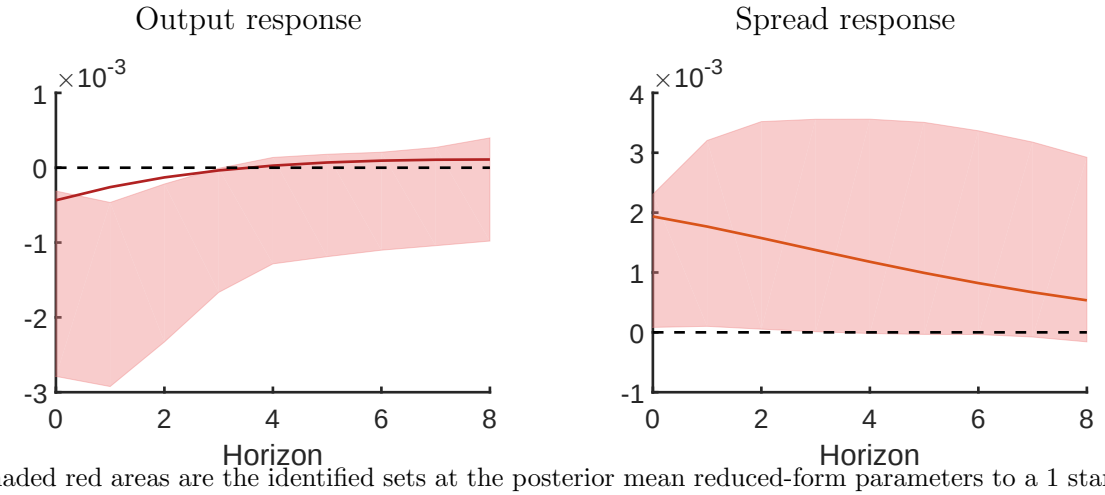

The shaded red areas are the identified sets at the posterior mean reduced-form parameters to a 1 standard deviation financial uncertainty shock. The dark red line is the impulse response produced by the theoretical model to a 1 standard deviation capital quality volatility shock. We only keep impulse response functions that satisfy Assumption $\mathcal{A}_{uf}^{3,DSGE}$.

Figure A-56 **TFP volatility shock**

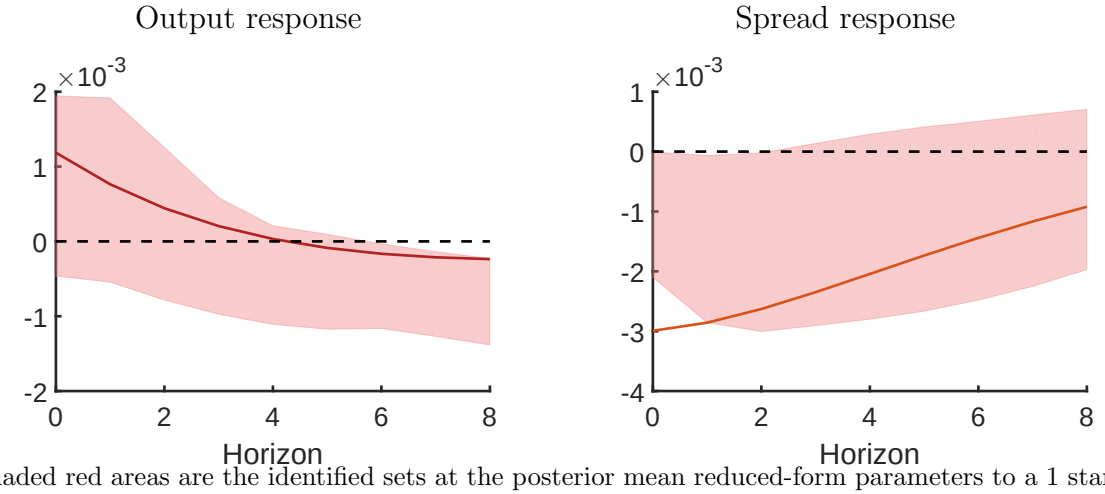

The shaded red areas are the identified sets at the posterior mean reduced-form parameters to a 1 standard deviation macro uncertainty shock. The dark red line is the impulse response produced by the theoretical model to a 1 standard deviation TFP volatility shock. We only keep impulse response functions that satisfy Assumption $\mathcal{A}_{um}^{3,DSGE}$.

$\mathcal{A}_{0}^{3,DSGE}$: For each $j \neq 1, 2$, at least one of the conditions specified in

$\mathcal{A}_{uf,1}^{3,DSGE}, \mathcal{A}_{uf,2}^{3,DSGE}$ and at least one in $\mathcal{A}_{um,1}^{3,DSGE}, \mathcal{A}_{um,2}^{3,DSGE}$ does not hold.

Figures A-55 and A-56 compare the identified sets at the posterior mean reduced-form

parameters to the theoretical impulse response functions produced by the DSGE model.[25] The identified sets at the posterior mean are objects of interest because they are consistent estimator of the true identified sets from a frequentist perspective. The results show that our sign restrictions are indeed able to recover the patterns in output and spreads following a capital quality and TFP volatility shock. Specifically, our estimation finds that a capital quality volatility shock decreases output, as in the theoretical model, and a TFP volatility shock increases output. Our model does a reasonable job estimating the magnitudes of the impulse response functions as well. Therefore, overall, we believe our sign restrictions identification strategy does a good job in capturing the theoretical responses from a DSGE model, despite the fact that our empirical model does not exactly nest the DSGE model.

References

Amir-Ahmadi, P. and T. Drautzburg (2017): "Identification through Heterogeneity," Tech. rep.

Andreasen, M. M., J. Fernndez-Villaverde, and J. F. Rubio-Ramrez (2018): "The Pruned State-Space System for Non-Linear DSGE Models: Theory and Empirical Applications," *The Review of Economic Studies*, 85, 1–49.

Atchadé, Y. F. and J. S. Rosenthal (2005): "On Adaptive Markov Chain Monte Carlo Algorithms," *Bernoulli*, 11, 815–828.

Baker, S., N. Bloom, and S. Davis (2013): "Measuring Economic Policy Uncertainty," Tech. rep., policyuncertainty.com.

Basu, S. and B. Bundick (2015): "Uncertainty Shocks in a Model of Effective Demand," Boston College Working Papers in Economics 774, Boston College Department of Economics.

Baumeister, C. and J. D. Hamilton (2015): "Sign Restrictions, Structural Vector Autoregressions, and Useful Prior Information," *Econometrica*, 83, 1963–1999.

Bloom, N. (2009): "The Impact of Uncertainty Shocks," *Econometrica*, 77, 623–685.

——— (2014): "Fluctuations in Uncertainty," *Journal of Economic Perspectives*, 28, 153–176.

[25] We compute these identified sets by taking the maximum and minimum responses to 1000 proposals from a Haar distribution.

Born, B. and J. Pfeifer (2014): "Policy Risk and the Business Cycle," *Journal of Monetary Economics*, 68, 68–85.

Caldara, D., C. Fuentes-Albero, S. Gilchrist, and E. Zakrajsek (2016): "The Macroeconomic Impact of Financial and Uncertainty Shocks," *European Economic Review*, forthcoming.

Carriero, A., T. Clark, and M. Marcellino (2017): "Measuring Uncertainty and Its Impact on the Economy," *Review of Economics and Statistics*.

Clark, T. E. and F. Ravazzolo (2015): "Macroeconomic Forecasting Performance under Alternative Specifications of Time-Varying Volatility," *Journal of Applied Econometrics*, 30, 551–575.

Creal, D. D. and R. S. Tsay (2015): "High dimensional dynamic stochastic copula models," *Journal of Econometrics*, 189, 335–345.

Creal, D. D. and J. C. Wu (2017): "Monetary Policy Uncertainty and Economic Fluctuations," Tech. Rep. 4.

Foerster, A. T. (2015): "Financial Crises, Unconventional Monetary Policy Exit Strategies, and Agents' Expectations," *Journal of Monetary Economics*, 76, 191–207.

Fry, R. and A. Pagan (2007): "Some Issues in Using Sign Restrictions for Identifying Structural VARs," NCER Working Paper Series 14, National Centre for Econometric Research.

Gertler, M. and P. Karadi (2011): "A Model of Unconventional Monetary Policy," *Journal of Monetary Economics*, 58, 17–34.

Giacomini, R. and T. Kitagawa (2015): "Inference for VARs Identified with Sign Restrictions," Tech. rep.

Giannone, D., M. Lenza, and G. E. Primiceri (2015): "Prior Selection for Vector Autoregressions," *The Review of Economics and Statistics*, 97, 436–451.

Gilchrist, S. and B. Mojon (2017): "Credit Risk in the Euro Area," *The Economic Journal*, n/a–n/a.

Golosnoy, V., B. Gribisch, and R. Liesenfeld (2012): "The Conditional Autoregressive Wishart Model for Multivariate Stock Market Volatility," *Journal of Econometrics*, 167, 211–223.

Jurado, K., S. C. Ludvigson, and S. Ng (2015): "Measuring Uncertainty," *American Economic Review*, 105, 1177–1216.

Kim, J., S. Kim, E. Schaumburg, and C. A. Sims (2008): "Calculating and using second-order accurate solutions of discrete time dynamic equilibrium models," *Journal of Economic Dynamics and Control*, 32, 3397 – 3414.

Leduc, S. and Z. Liu (2012): "Uncertainty Shocks Are Aggregate Demand Shocks," Working Paper Series 2012-10, Federal Reserve Bank of San Francisco.

Meinen, P. and O. Roehe (2017): "On measuring uncertainty and its impact on investment: Cross-country evidence from the euro area," *European Economic Review*, 92, 161–179.

Moon, H. R., F. Schorfheide, and E. Granziera (2017): "Inference for VARs Identified with Sign Restrictions," Tech. rep.

Pesaran, H. H. and Y. Shin (1998): "Generalized impulse response analysis in linear multivariate models," *Economics Letters*, 58, 17–29.

Ritter, C. and M. A. Tanner (1992): "Facilitating the Gibbs sampler: the Gibbs stopper and the griddy-Gibbs sampler," *Journal of the American Statistical Association*, 87, 861–868.

Rotemberg, J. J. (1982): "Sticky Prices in the United States," *Journal of Political Economy*, 90, 1187–1211.

Rubio-Ramirez, J., D. F. Waggoner, and T. Zha (2010): "Structural Vector Autoregressions: Theory of Identification and Algorithms for Inference," *Review of Economic Studies*, 77, 665–696.

Uhlig, H. (2005): "What Are the Effects of Monetary Policy on Output? Results from An Agnostic Identification Procedure," *Journal of Monetary Economics*, 52, 381–419.